Analytical approaches for the separation of deferiprone from its iron (III) complex and the investigation of its interactions with different essential metal ions and targeted proteins

Von der Fakultät für Lebenswissenschaften

der Technischen Universität Carolo-Wilhelmina zu Braunschweig

zur Erlangung des Grades eines

Doktors der Naturwissenschaften

(Dr. rer. nat.)

genehmigte

D i s s e r t a t i o n

von Mufarreh Mohammed Mufarreh Asmari

aus Khamis Mteir / Saudi Arabien

1. Referent: PD. Dr. Sami El Deeb
2. Referent: Professor. Dr. Hermann Wätzig
eingereicht am: 30.09.2019
mündliche Prüfung (Disputation) am: 12.11.2019

Druckjahr 2020

Vorveröffentlichungen der Dissertation

Teilergebnisse aus dieser Arbeit wurden mit Genehmigung der Fakultät für Lebenswissenschaften, vertreten durch den Mentor der Arbeit, in folgenden Beiträgen vorab veröffentlicht:

Publikationen

1. M. Asmari, L. Michalcová, H.A. Alhazmi, Z. Glatz, S. El Deeb, Investigation of deferiprone binding to different essential metal ions using microscale thermophoresis and electrosprayionization mass spectrometry, Microchem.J. 137 (2018) 98–104.
2. M. Asmari, R. Ratih, H.A. Alhazmi, Z. Glatz, S. El Deeb, Thermophoresis for characterizing biomolecular interaction, Methods 146(2018) 107–119.
3. M. Asmari, A. M. Abdel-Megied, L. Michalcová, Z. Glatz, S. El Deeb, Analytical approaches for the determination of deferiprone and its iron (III) complexes: Investigation of binding affinity using liquid chromatography-mass spectrometry and capillary electrophoresis-frontal analysis, Microchemical J. 154 (2020) 104556.

Tagungsbeiträge

1. Asmari, M.; Alhazmi, H. A.; El Deeb, S., LC-ESI-MS Study of Iron(III) Complexes with Deferiprone (poster), AT Europe, Vienna, 2016.
2. Uzlu Z., Ule J., Ahmed F., Balaiev I., Asmari M., El Deeb S., Investigation of deferiprone binding to zinc (II) and copper (II) ions for potential chelation effect using capillary zone electrophoresis (Poster), Internship scientific day, Braunschweig, 2016.
3. Asmari M.; Kleusch C.; El Deeb S.; MicroScale thermophoretic investigation of deferiprone interaction with selected biometals, (poster), DphG2016 Munich, 2016.
4. Michalcová L.; Asmari M.; Glatz Z.; El Deeb S.; Capillary Electrophoresis-Frontal Analysis for the characterization of drug-metal binding, (poster), CECE2016, Berno, 2016.
5. Asmari M.; Ratih R.; El Deeb S Label-free microscale thermophoresis for the study of lactoferrin-drug interaction (Poster), Euroanalysis2017, Stockholm, 2017.
6. Kellner J., Bosbach C., Asmari M., El Deeb S., Investigation of Deferiprone Binding to Human Serum Albumin Using Capillary Zone Electrophoresis (Poster), Internship scientific day, Braunschweig, 2018.

ACKNOWLEDGMENT

In the beginning, this work may have not been possible without the support, help and advice of many peoples during the last four years in my life. First and foremost, I would like to thank my supervisor PD. Dr. Sami El Deeb for the guiding with constant following up to achieve my goals. I will never forget his encouragement to me at every moment in which we achieved progress. Also, I would like to thank Prof. Dr. Hermann Wätzig for the continuous support and the scientific discussions through the week meeting or the semester sessions which enlighten my mind to thinking differently. Additionally, many great thanks to Prof. Dr. Ingo Ott and his group for kind support.

And, I shall not forget the past and present group members of Prof. Dr. Hermann Wätzig. Dr. Tobias Rakow, Dr. Markus Nachbar, Dr. Franziska Steinicke, Jorrit, Julia and Matthias Thanks to all of them for their cooperation and the unforgettable moments during the last four years.

A special thanks to my colleague Ratih for her support and collaboration. I will never forget the great moments in talking and sharing of some ideas for experimental design and collaboration in writing some publications.

A special recognition goes to Dr. Lenka Michalcova where, the achievement in CE/FA, was with her collaboration and support. As well as, a special deep thanks to Dr. Christian Kluesch from Nanotemper technologies for his support during the frequent short visits to make MST measurements.

Finally, a huge thanks from deep of my heart to my wife Noorah Al-Asmari, who has sacrificed so much of her life to make my dream come true. As well as my kids Jood, Ghina and Mohammed whom I and their mother waited for nine years to see them shine in our lives.

Dedication

To:

To the soul of my Parents,

Wife, Kids

List of Abbreviations

ACE	Affinity capillary electrophoresis
AD	Alzheimer disease
AGP	α-acid glycoprotein
API	Atmospheric pressure ionization
APCI	Atmospheric pressure chemical ionization
APPI	Atmospheric pressure photoionization
BGE	Background electrolyte
CE/FA	Capillary electrophoresis/frontal analysis
CP20	Deferiprone
CZE	Capillary zone electrophoresis
DFO	Deferoxamine
DFX	Deferazirox
DMSO	Dimethyl sulfoxide
DNA	Deoxyribonucleic acid
EC50	Effective concentration at half maximal effect
EOF	Electroosmotic flow
ESI	Electrospray ionization
FA	Fluorescence anisotropy
FCS	Fluorescence correlation spectroscopy
FDA	United states food and drug administration
FTICR	Fourier transform ion cyclotron resonance
Hb	Hemoglobin
HD	Hummel dryer
HPs	Hydroxypyridinones
HSA	Human serum albumin
i.d.	Internal diameter
IR	Infrared
ITC	Isothermal titration calorimetry
JH	Joule heating effect

kDa	Kilodalton
Kg	Kilogram
Kv	Kilovolt
L	Liter
LC	Liquid chromatography
LC/MS	liquid chromatography mass spectrometry
LED	Light emitting diode
LF	Lactoferrin
LOD	Limit of detection
LOQ	Limit of quantitation
M	Molar
mACE	Mobility shift affinity capillary electrophoresis
MALDI	Matrix assisted laser desorption ionization
Min	Minute
MST	Microscale thermophoresis
MS	Mass spectrometry
m/z	Mass to charge ratio
mL	Milliliter
mM	Millimolar
µL	Microliter
µM	Micromolar
nL	Nanoliter
nM	Nanomolar
PD	Parkinson’s disease
PI	Isoelectric point
QiT	Quadrupole ion trap
QMS	Quadrupole mass spectrometry
RSD	Relative standard deviation
S	Second
SD	Standard deviation
SDS	Sodium dodecyl sulfate
SPR	Surface plasmon resonance

TF	Transferrin
TOF	Time of flight
VP	Vacancy peak
UV	Ultraviolet

List of Symbols

A	Surface area
Al	Aluminum
Bi	Bismuth
C	Molar concentration
Ca	Calcium
Cd	Cadmium
Co	Cobalt
Cr	Chromium
Cu	Copper
c_{hot}	Concentration at heat zone
c_{cold}	Concentration at cold zone
D	Diffusion coefficient
d_i	Capillary internal diameter
E	Applied potential
Fe	Iron
F_{norm}	Normalized fluorescence
F_{hot}	Fluorescence at hot zone
F_{cold}	Fluorescence at cold zone
Hg	Mercury
j	Molecular flow
K_a	Association constant
K_d	Dissociation constant
K'	Capacity factor
k	Binding constant
pK_a	Ionization constant
L	Capillary length
$log\beta$	Collective stability constant in logarithmic function
$LogK_a$	Stability constant in logarithmic function
Mg	Magnisium
Mn	manganese

Ni	Nickle
N	Number of theoretical plates
n	Hill coefficient
O	Oxygen
P	Joule heat
Pb	Lead
pK_a	Ionization constant
R_f	Free ligand response
R_c	Complex response
Rs	Resolution
r	Fraction bound
S_T	Soret coefficient
t_R	Retention time
$t_{1/2}$	Half life
t_0	Dead time
V_D	Volume distribution
V_{eof}	Velocity of electroosmotic flow
W	Peak width
Zn	Zinc
α	Selectivity
ε	Dielectric constant
ζ	Zeta potential
η	Medium viscosity
$[-]$	Molar concentration
ΔR	Normalized system response
ΔT	Temperature change
σ_{eff}	Effective charge
ΔS_{hyd}	Hydration shell
λ_{DH}	Deby-Hückel screening length

1. Introduction

1.1. Deferiprone

Deferiprone (**CP20**), under the chemical name of 1,2-dimethyl-3-hydroxypyrid-4-one (Fig. 1), is the first oral active iron-chelator. CP20 was introduced by Hider and coworkers in 1982 and approved for clinical use in India in 1995. After that, in 2000, the European Medical Agency (EMA) approved CP20 for treatment of iron overload syndrome with comorbid *β-thalassemia* caused by regular blood transfusions [1]. CP20 is only one derivative of 3-hydroxypyridin-4-one (HPs) and has been approved after undergoing extensive chemical, biological, and pharmacological investigation [2–4]. Therefore, CP20 development and administration to patients before fulfilling all of the formal toxicological evaluations obtained from animal data is an unusual pattern in drug development [5]. Although three decades passed before the drug was approved internationally under the trade name (Ferriprox^{TM}), the Food and Drug Administration (FDA) approved CP20 in 2011 after extensive reviews in which approval was based on reduction of serum ferritin levels without observed treatment benefits, such as symptom improvement or an increase in survival time [6]. Moreover, CP20 is effective in reducing cardiac iron more than other approved iron chelators, including deferoxamine (DFO) and deferasirox (DFX) [7,8].

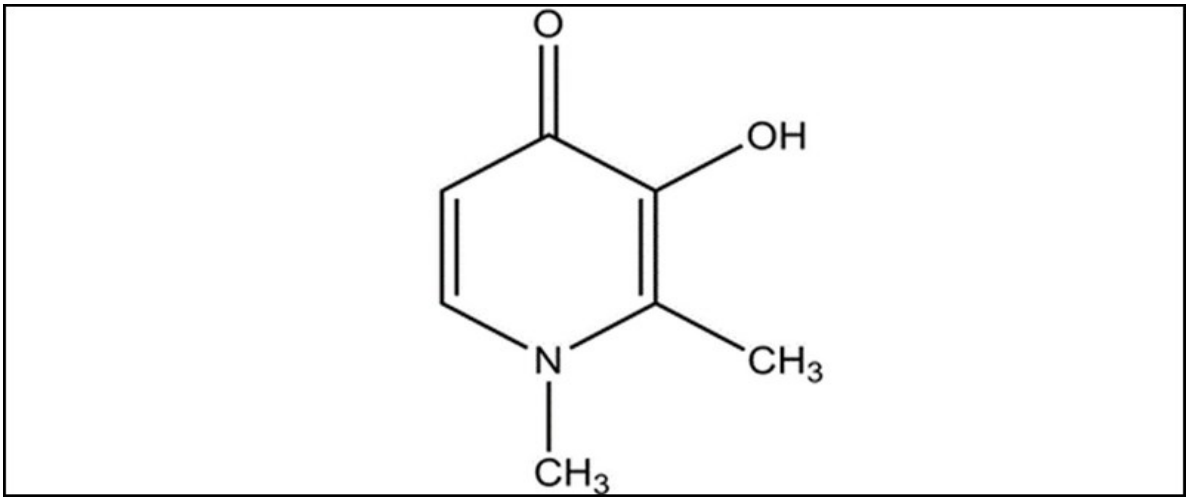

Fig.1. Deferiprone chemical structure.

1.1.1. Deferiprone chemistry

CP20 is a bidentate iron chelator which consisted of alpha hydroxyketone (O, O) chelating groups with high binding capacity. Although HPs were extensively studied as iron chelators, 3-hydroxypyridin-4-one (3,4 HP) derivatives exhibited significant chelation effects against trivalent hard metal ions (such as Fe^{3+}, Al^{3+}, and Ga^{3+}) more than against soft divalent metal ions, such as Zn^{2+} and Cu^{2+} [3,9,10]. This behavior is favored in order to achieve relative selectivity for binding with essential Fe^{3+} ions without disturbing the physiological levels of the other essential metal ions. Hence, these derivatives are successful in treatment of iron overload, which is considered the most prevalent clinical metal overload situation that requires the use of iron chelators [11]. Furthermore, CP20 offers high electron density in the presence of two adjacent functional groups in which the basic properties of the hydroxyl group (pK_a ~ 9.8) and acidic properties of the carbonyl group (pK_a ~ 3.7) make the drug molecule neutral under physiological pH [11,12]. CP20 binds with Fe^{3+} under the physiological conditions to form an $Fe(CP20)_3$ complex in a 1:3 binding ratio in which each Fe^{3+} ion require three molecules of CP20 to form a stable neutral complex as shown in Fig. 2.

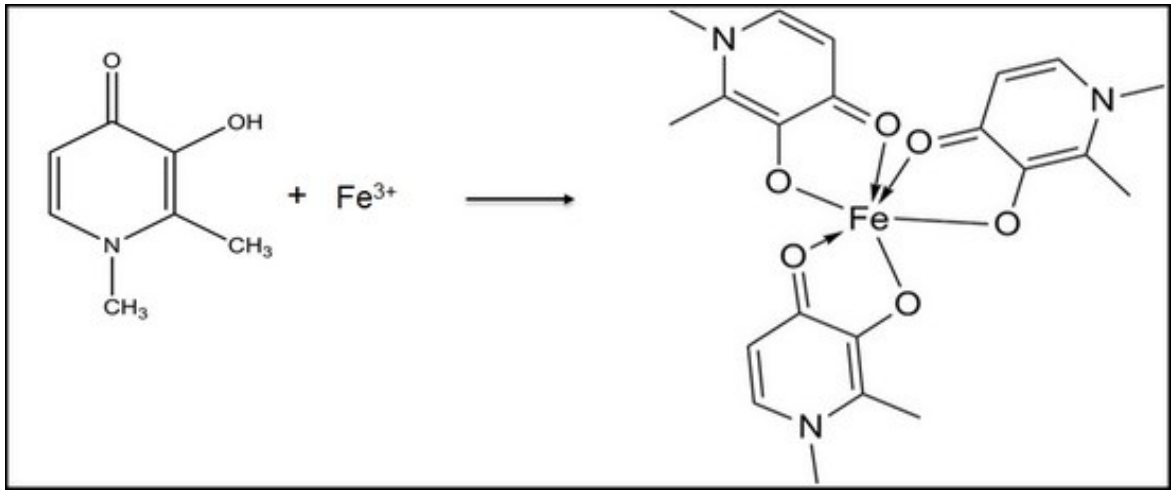

Fig. 2. The chemical reaction scheme for CP20 with Fe3+ to form 1:3 metal-chelate complex.

The resulting complexes in 1:3 binding ratios are stable under wide pH ranges as shown in Fig. 3. In addition, incomplete 1:2 complexes have been observed in dilute solutions $<10^{-6}$ M [12,13]

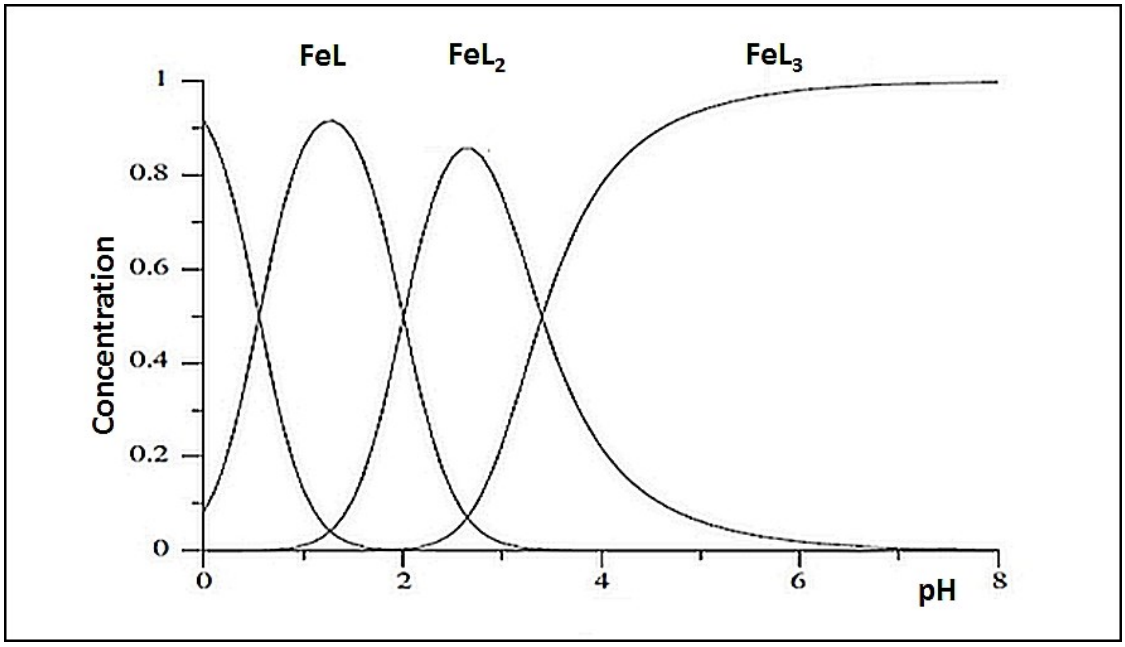

Fig.3. Distribution curve of [Fe(CP20)$_n$] complexes over different pH range [12].

The binding of CP20 with Fe^{3+} is higher than other iron chelators and has an estimated binding constant of logβ ~ 35, which is five orders higher in magnitude than DFO (logβ ~ 30) and eight magnitudes higher than DFX (logβ ~ 27) [12–14]. However, CP20 presents less chelation efficiency than the other iron chelators according to the pFe parameter, which is defined as the negative logarithm of the concentration of free Fe^{3+} in solution at pH 7.4 in which the total Fe^{3+} concentration equals 1 μM, and the total chelator concentration equals 10 μM. The estimated pFe values for iron chelators can be listed in the following order: CP20 pFe ~ 20 <DFX pFe ~ 22 <DFO pFe ~ 27. The pFe values of an effective iron chelator should be ≥20 in order to mobilize iron from transferrin (Tf), which is the main iron storage protein [14,15] although the pFe value takes ligand protonation, denticity, and stoichiometry into account whenever measuring the concentration of free metal ions in solution. However, the *in vivo* drug behavior is quite different from that in solution. There are many factors, including plasma ionic strength, presence of other natural chelators (such as citrate and carboxylate), and physiological temperature that might influence binding events, and these factors are not addressed in the pFe definition. In addition, the iron concentration that is estimated according to the pFe definition is elevated in pathological situations and predicted to be higher than 10^{-6} M. Nevertheless, the

binding constant and pFe parameters at equilibrium can reflect the efficacy of different iron chelators [1,3,12,13,15].

1.1.2. Deferiprone pharmacology

The pharmacology of iron chelators correlates with these drugs' capacities to sequester non-transferrin bound iron within the targeted sites since iron is vital for several biosynthetic and transport pathways due to its characteristic redox chemistry. However, iron overload is a serious health problem in many diseases, such as thalassemia and sickle cell anemia, due to genetic defect in adequate hemoglobin (Hb) synthesis. Patients with these conditions need regular blood transfusions since iron is deposited and accumulate in different body organs, such as liver, spleen, heart, brain, and kidney and can lead to organ dysfunction [14,16]. Herein, chelation therapy is the only strategy for removing excess iron from the body in the absence of the normal physiological mechanism. CP20 is a selective iron chelator that binds to Fe^{3+} to form a complex in a 1:3 binding ratio as shown in Fig. 3. Iron removal via CP20 occurs at the cellular level in which there are two iron deposition pathways for preserving Fe^{3+} in solubilized form and inhibiting metal precipitation in the cell: (1) via transferrin as an iron bound form or (2) non-transferrin bound iron, which is bound to low-molecular-weight chelators, such as intracellular or extracellular citrate or carboxylate (Fig. 4).

Although CP20 is administered in relatively high doses (~ 3.5 g/ day), first pass metabolism deactivates about 85% of CP20 via conjugation with O-glucuronide [17]. However, other pharmacokinetic properties such as half-life ($t_{1/2}$ ~ 1.9h), volume distribution (V_D ~ 1.6 L/Kg), and plasma protein binding (< 10%) are optimal for clinical use as iron chelator in order to avoid drug accumulation in the body fats, especially in the central nervous system during long-term use [5,6,18].

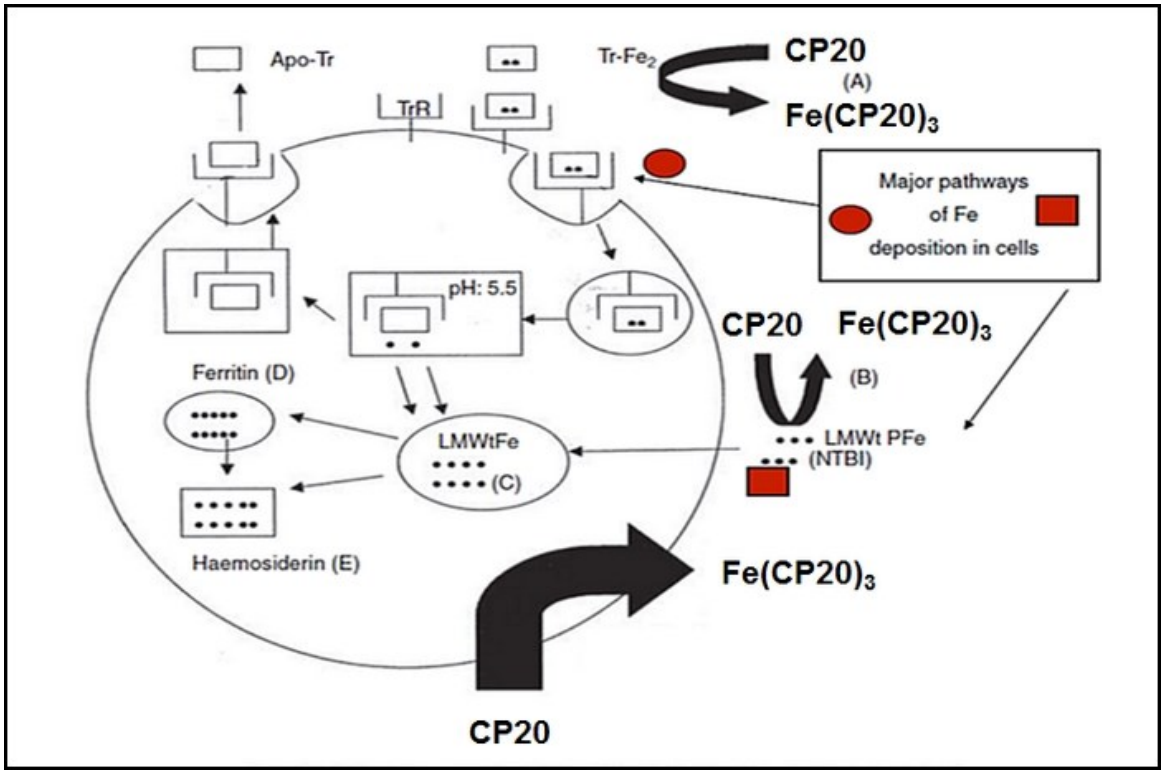

Fig. 4. Schematic illustration of CP20 Mechanism of action where, (A) indicate the chelation of non-transferrin bound iron, (B) indicate the chelation effect to Fe from low molecular weight chelators outside the cell, (C), (D), (E), represent the chelation effect for intracellular iron pool [14].

The side effects of CP20 that have been reported include gastrointestinal abnormalities, such as nausea and vomiting; however, agranulocytosis which was shown to have fatal side effects, has also been reported in about 1.7% of patients who received CP20. The severe drop in the count of white blood cells, especially neutrophils, is concomitant with CP20 administration. This side effect can be resolved with discontinuation of CP20, but the mechanism of CP20-associated agranulocytosis is still unknown [5,6]. Furthermore, arthritis, arthralgia, and Zn-depletion have been reported to a lesser extent as side effects resulting from CP20 treatment. Generally, CP20's safety and efficacy is still questionable due to its drug behavior in biological systems; for example, the Fenton reaction can occur due to dissociation of the $Fe(CP20)_3$ complex [19]. Moreover, it is still not known whether CP20 is secreted into breast milk, especially with respect to evaluating the safety of CP20 during the lactation. The FDA and EMA have stated: "*It is not known whether deferiprone is excreted in human milk*." [5,6]. CP20, similar to many drugs,

might be secreted in breast milk as a protein-bound fraction, in which case it would be harmful to a baby's growth and general health.

In contrast to the previous concerns, CP20 is still promising as an iron chelator in several clinical situations other than iron overload syndrome. These situations include cancers, fungal and viral infections, and renal insufficiency. Although the study of iron chelators as antitumor agents is still in its infancy, there are several trials describing the beneficial use of iron chelators in treatment-specific types of cancers and correlating the findings with iron chelation effects at the cellular level [20]. Overexpression of transferrin (Tf) receptors has been demonstrated in numerous types of cancers, such as leukemia, lymphoma, and breast and prostate cancers; thereby, it clarifies the substantial role of iron in DNA synthesis and repair, which is catalyzed by a key enzyme known as ribonucleotide reductase. Iron chelation therapy can help to slow the overproduction of these enzymes [17]. Moreover, CP20 has been investigated for its effects on inhibiting prostate cancer proliferation via its capability to inhibit the mitochondrial enzyme known as mitochondrial aconitase. This enzyme is sensitive to cellular iron levels and depletion of mitochondrial iron can help to inactivate this enzyme [21]. Additionally, CP20 has been shown to exhibit a blocking effect on eukaryotic initiation factor 5A (eIF5A), which is involved in protein synthesis; overexpression of this initiation factor has been shown to be correlated with cancer [22]. In addition, CP20 as an iron chelator is beneficial for neurodegenerative diseases such as Parkinson's and Alzheimer's diseases (PD and AD, respectively). The role of iron overload has been well defined in disease development through its association with oxidative stress increase [23,24]. Hence, CP20 is presently in phase II clinical trials for treatment of PD [25]. Moreover, CP20 has been reported to be beneficial in treatment of Friedreich's ataxia (FA) [25,26] and diabetic and non-diabetic nephropathies [27]. CP20 also exhibits potent antifungal activity [28,29], and has been proven to induce apoptosis in HIV-infected cell lines through inhibition of deoxyhypusyl hydroxylase, an enzyme involved in the final step of the amino acid hypusine that found in eIF5A protein [30]. CP20 as HPs lead structure, is still promising for several clinical uses as illustrated in Fig. 5.

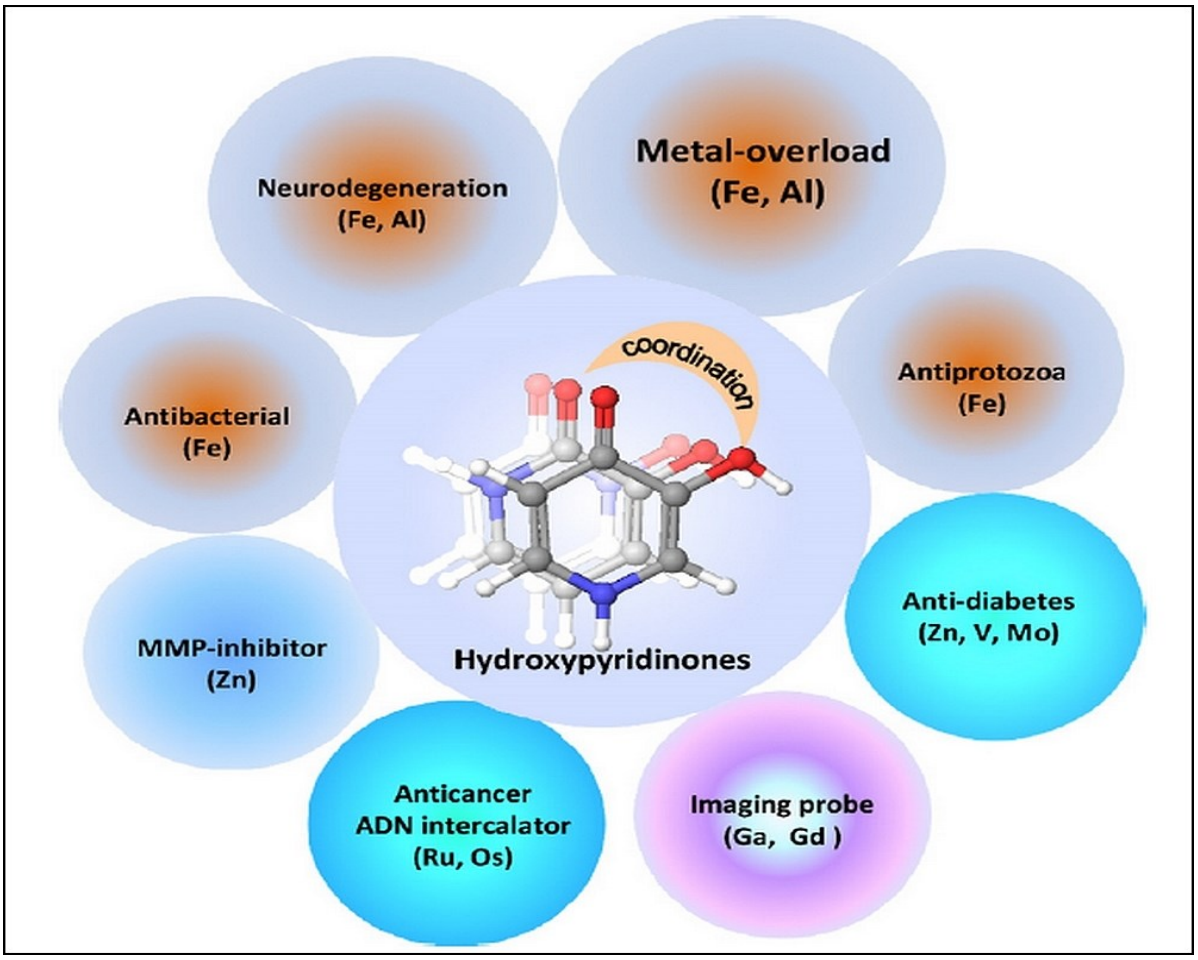

Fig.5. HPs as lead pharmaceutical for different targeted functions [11].

1.1.3. Deferiprone binding

CP20 has been introduced for clinical use due to its high affinity toward Fe^{3+} under physiological conditions. However, its chelation selectivity is incomplete because CP20 is also prone to bind to different polyvalent metal ions such as Al^{3+}, Ga^{3+}, Cu^{2+}, Zn^{2+}, and Co^{2+} [3,9,12,31]. This behavior might be significant when using the drug in metal poisoning, such as in the case of Al^{3+}, or to help in drug design and development [11]. Moreover, CP20 is a small molecule and is capable of penetrating cell membranes in addition to large biomacromolecules. This feature is attractive for studying CP20's binding behavior toward different targeted biomolecules.

1.1.3.1. Deferiprone-metal ions binding

CP20 is mainly an iron chelator, and investigation of its binding affinity to metal ions has been extensively studied. Dobbin and Hider [3] described the advantages of HPs as alternative for hydroxamates and investigated CP20 selectivity for Fe^{3+} and other essential metals including Cu^{2+}, Zn^{2+}, Mg^{2+}, and Ca^{2+}. Moreover, CP20 has been compared to other chelators such as ethylenediaminetetraacetic acid (EDTA), DFO, and catechol. CP20 exhibited greater selectivity toward Fe^{3+} over other essential metals, and the chelation effect has been estimated according to overall binding constant (Logβ) in which Logβ for Fe^{3+} = 37 >>Cu^{2+} = 17 >Zn^{2+} = 12.5 >>Mg^{2+} = 7 >>Ca^{2+} = 4.5. Similarly, Clarke and Martell [9] investigated stabilities of CP20 chelate containing divalent and trivalent metal ions in solution. There are four trivalent metal ions, including Fe3+, Al^{3+}, Ga^{3+}, and In^{3+}, and four divalent metal ions including Cu^{2+}, Zn^{2+}, Co^{2+}, and Ni^{2+} that have been selected for a CP20 binding study. The binding parameters have been estimated as overall binding constant (Logβ) and a 1:3 stability constant as the association constant (LogK_a). CP20 exhibited potent chelation effects toward all trivalent metal ions to the same degree as toward Fe^{3+} and opened the possibility for using CP20 in treatment of metal poisoning. Divalent metal ions displayed various binding affinities toward CP20 but to a lesser extent toward than trivalent metal ions. As shown in Fig. 6, Al^{3+} (among trivalent metal ions) and Cu^{2+} and Zn^{2+} (among other divalent metal ions) are more likely to be chelated by CP20 in addition to Fe^{3+} as a therapeutic target. Thereafter, CP20 has been examined as a chelator for Al^{3+} as described in numerous reports [32–36]. Evaluation of Al^{3+} levels in different organs are difficult to determine due to high variability in the results and the study design; however, CP20 is effective in increasing Al^{3+}urinary excretion.

Moreover, the binding affinity of CP20 toward divalent metal ions has been investigated, and CP20 has a significant effect on Zn^{2+} cellular levels to the point at which Zn^{2+} deficiency has been reported in patients during CP20 treatment [37–39]. The affinity of CP20 towards divalent metal ions indicates that CP20 tends to bind to Cu^{2+} more than Zn^{2+}, but clinical signs, including dry/itchy skin, which is indicative of Zn^{2+} deficiency, are frequently observed [40,41]. Moreover, CP20 was reported to induced thymic atrophy. This effect has been attributed to the direct chelation effect of CP20 on intracellular Zn^{2+}, which is not observed in treatment with DFO, and suggests that CP20 is likely to cause Zn^{2+} depletion from the cellular stores [37]. Meanwhile, CP20 shows a significantly higher affinity for Cu^{2+} over other divalent metal ions [3,10,12]; however, Cu^{2+} deficiency has been reported to a lesser extent than Zn^{2+} deficiency [42]. Zn^{2+} deficiency is more observable and more frequently reported. This difference can be attributed

to the large variations in the total body amounts between Zn^{2+} and Cu^{2+} in which Zn^{2+} concentrations are about 2 gm, which is twenty-five magnitudes higher than Cu^{2+} (80 mg in the human body) [43]; therefore, Zn^{2+} rather than Cu^{2+} monitoring is more clinically relevant.

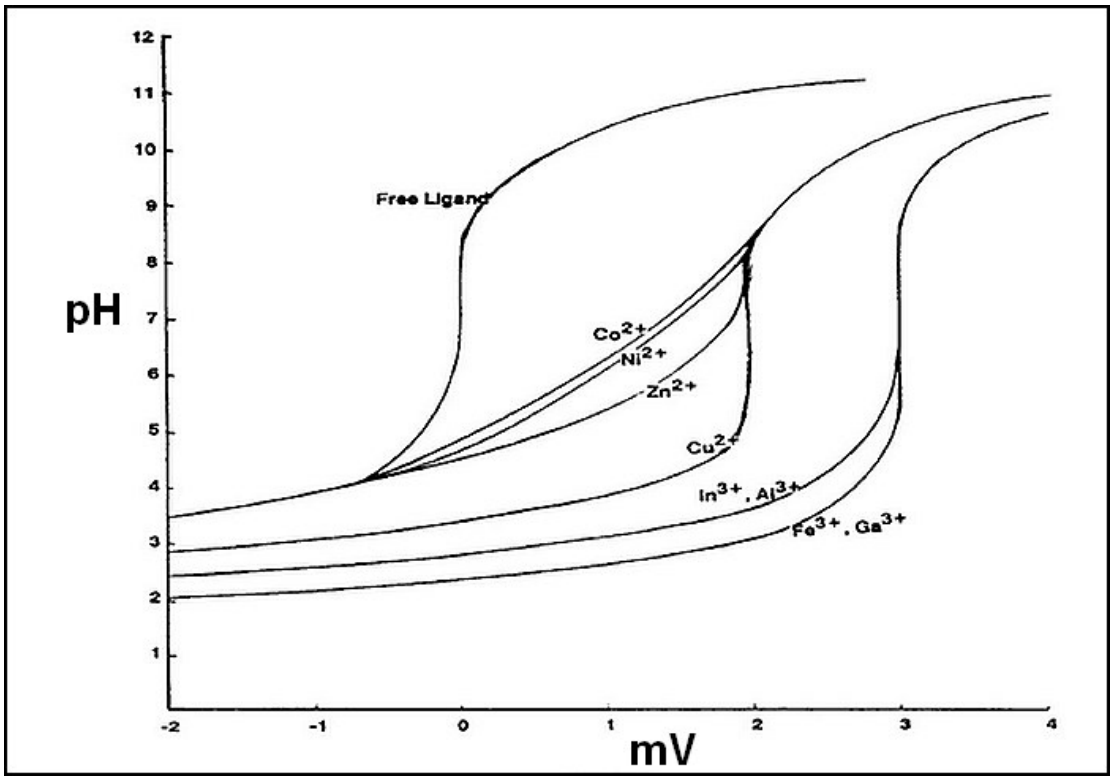

Fig.6. Titration profile of CP20 with different trivalent and divalent metal ions [9].

The binding affinity of CP20 to other trace essential metal ions, such as Co^{2+} and Mn^{2+}, have been reported [9,44]. Although the stability constants of these two metals in solution are approximately similar to Zn^{2+}, the levels of theses essential metal ions were not affected by CP20 as shown in several animal studies [36,45]. On the other hand, Fatemi et al. described the use of iron chelators, including CP20, DFO, and DFX, either as monotherapy or in combination for several toxic heavy metals, including Bi, Hg, Cd, Cr (V and VI) and Pb [46–51]. These studies revealed the possibility of using iron chelators in removing toxic heavy metals from the body.

1.1.3.2. Deferiprone-protein binding

In fact, most of the drug interaction studies are carried out with proteins involved in all physiological and pathological processes. In order to understand these processes at the molecular level, studying drug interactions with the targeted proteins can help understand these processes and provide valuable information. CP20, as a metal chelator, is likely to bind with metals that are involved in biomolecule formation. Several proteins are classified as metalloproteins, and CP20 might be able to penetrate these large biomolecules and induce either desirable or undesirable effects. For instance, CP20 has been reported to interact with Tf, which is the major metal-transporting protein in the blood. This interaction can alter the metabolic pathways of several metal ions, especially those metal ions that possess levels that compete with Fe^{3+} for metal-binding sites [14,52]. Moreover, CP20 is known to be able to remove Fe^{3+} from Tf binding sites as illustrated in Fig. 7 [53].

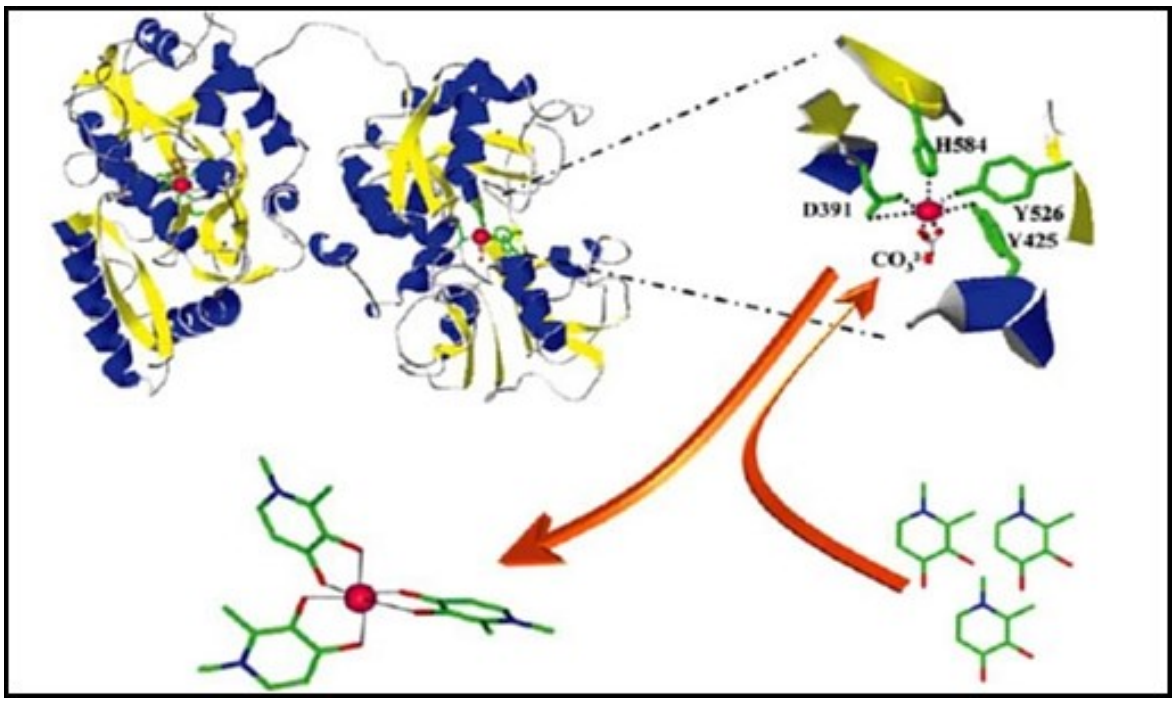

Fig. 7. Fe^{3+} removal mechanism via CP20 from Tf protein [14].

Likewise, human lacoferrin (Lf) is similar to the serum iron binding protein Tf, but is found mainly in milk and other external secretions such as saliva, tears, semen, and mucosal secretions. Lf is described as a multifunctional protein due to its binding capabilities with various metal ions, small molecules, and biomolecules. Biological functions that are attributed to Lf

include antimicrobial, anti-inflammation, iron homeostasis, cell differentiation, and cancer protection [54,55]. In spite of the fact that the versatility of Lf functions are attributed to direct binding with Fe^{3+} ions, which are crucial to various bioactivities, Lf has been described as binding directly with other molecules, such as glycosaminoglycans, lipopolysaccharides, and specific receptors on epithelial and immune system cells. Furthermore, Lf was suggested to bind to and interfere with target cell protein kinase and nuclear factor-kB which related signaling pathways [56]. These salient functions may cast some light on Lf as a targeted protein. According to FDA and EMA reports [5,6], CP20 has not been known to be secreted in breast milk; however, drug secretion as a protein-bound fraction is possible. Lf is most likely a metalloprotein found in breast milk, and studying the binding of CP20 with Lf would be valuable for assessing binding parameters and potential of drug secretion in breast milk as a fraction bound to Lf. Moreover, the chelation synergism for brain iron has been obtained via exploitation of the binding affinity between DFX and Lf as a conjugate, which exhibited more efficacy for iron removal from the brain. This process might be useful in neurodegenerative diseases [57].

Furthermore, the interaction of CP20 with hemoglobin (Hb) has been investigated, and it was found that an interaction occurs via a hydrogen bond and leads to changes in Hb's conformation [58]. These observations open the door for more investigations in order to evaluate the effects of this binding on protein structure and functions. Moosavi-Movahedi et al. [59] investigated the effect of CP20 and DFX on the structure and function of β-Thalassemic Hb using multi-spectroscopic techniques. The effects of CP20 are less than those of DFX with respect to inducing conformational changes in Hb, which cause a reduction in Hb stability in β-thalassemic patients. Another study was implemented by the same research group in order to investigate the effects of CP20 on inhibition of Hb structural changes during the fructation process. CP20 was shown to be capable of preventing the formation of advanced glycation end products that are involved in protein aggregation and lead to loss of heme unit; therefore, Hb assembly can be affected, especially in diabetic patients [60].

Therefore, drug interactions with plasma proteins present the main aspect of this study due to these interactions' direct effects on CP20 pharmacokinetics and pharmacodynamics. There are several plasma proteins, such as human serum albumin (HAS), α1-acid glycoprotein (AGP), lipoproteins, and globulins that are involved in binding to drug molecule; however, the major binding partners to the drugs in plasma are HSA and AGP [61,62]. Principally, HSA is likely to bind with acidic drugs while AGP tends to bind with basic drugs. Both have the same affinity for neutral drug molecules, but this is an oversimplification of the actual situation in which, in comparison to AGP, HAS is more likely to be a universal drug binding agent due to

high concentrations in plasma and possession of more binding sites [63]. In this regard, there is one report in which the interaction between CP20 and HSA is described [64]. CP20 binding parameters have been estimated using multi-spectroscopic techniques, including fluorescence spectroscopy, circular dichroism, and absorption spectroscopy in combination with molecular docking studies (Fig. 8).

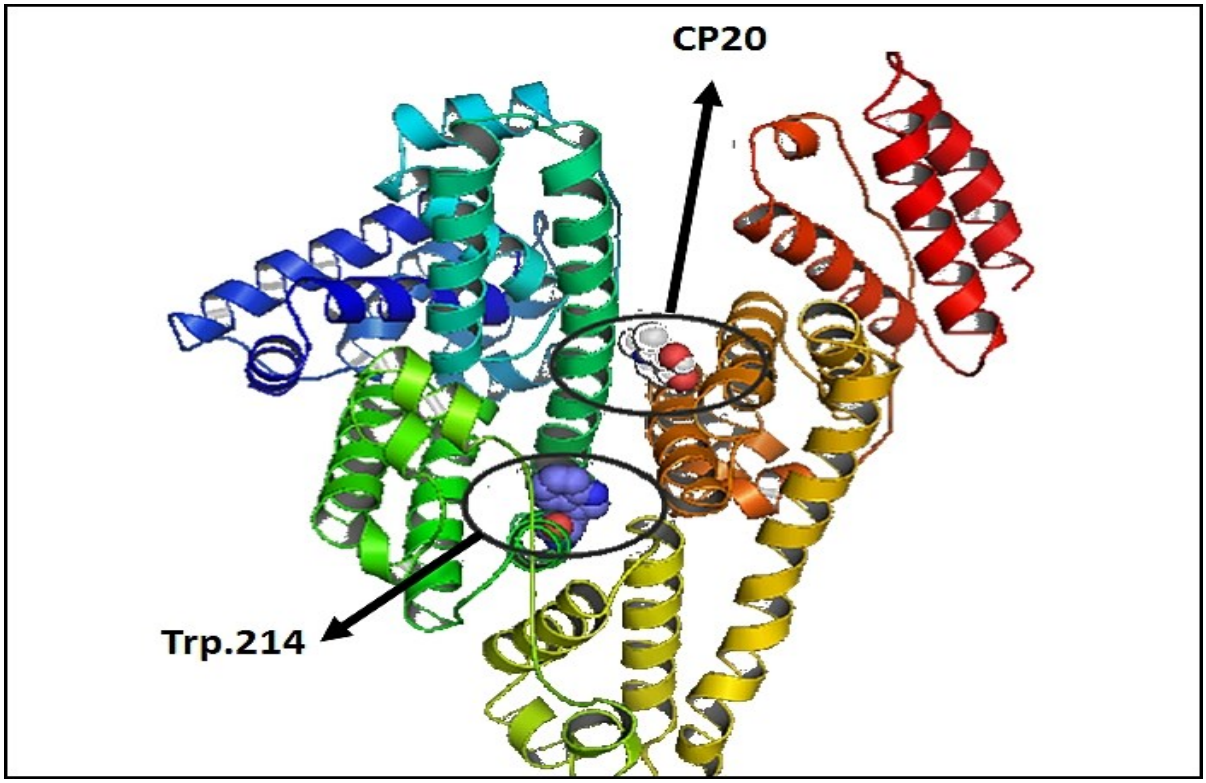

Fig. 8. Docking simulation for CP20-HSA interaction [64].

1.1.4. Deferiprone analytical aspects

Over the past three decades, CP20 has been investigated using different analytical techniques. Goddard and Knotoghiorghes [65] developed the first high-performance liquid chromatography (HPLC) method in order to measure CP20 and other hydroxypyridinone derivatives in serum and urine and achieve good separation of CP20 from other hydroxypyridinones in serum and urine samples. Moreover, challenges in CP20 chromatography at physiological pH, such as peak tailing, have been reported and solved by decreasing the pH to 2 and using ion pair reagents. Klein et al. [66] extracted CP20 from human plasma sample and determined CP20 using the HPLC technique with a carbon-based stationary phase instead of a silica column. However, in this method 2 mM EDTA was added to the acidic mobile phase (pH ~ 3) in order

to achieve good separation for CP20. Similarly, Epemolu et al. [67] tried several chromatographic approaches for separation of seven hydroxypyridinones, including CP20, by using thin-layer chromatography (TLC) and HPLC and found poor chromatographic behaviors on bonded silica stationary phases. Non-silica-based columns with high carbon loaded exhibited good separation for hydroxypyridinone iron chelators. El-Jammal and Templeton [68] determined CP20 and related HP compounds in plasma via addition of Fe^{3+} ions to the acidic mobile phase, which contains 0.04% trifluoroacetic acid and 99.96% H_2O and separates as a 1:1 chelated complex.

Dresow et al. [69] measured CP20 and its iron complex in serum and urine matrices. The iron complex was measured at 450 nm and CP20 at 280 nm; however, no direct separation was achieved between CP20 and the iron complex. In this approach, 10 mM octansulfonic acid as an ion pair reagent has been used at pH 2.5 in the gradient elution mode. The method has been applied to determine the complex in serum and urine samples and then the iron content in urine was estimated by HPLC and atomic absorption spectroscopy. Recently, Song et al. [70] developed a liquid chromatography with tandem mass spectroscopy (LC–MS/MS) method with a pharmacokinetic application for determination of CP20 in human plasma. The resulting method was utilized to recover CP20 in serum samples at a very low concentration range (0.1–20 µg/mL), and in this approach EDTA was used in the mobile phase in order to improve the separation of CP20 in biological samples. The MS/MS detector in product ion mode has been utilized to identify the product ion mass spectra of CP20.

On the other hand, there is only one reported capillary electrophoresis (CE) method for determination of CP20 and DFO in human plasma. Lin et al. [71] developed a new CE method for CP20 and DFO monitoring in patients' plasma. The determination of targeted iron chelators was carried out using a CE stacking strategy and 150 mM sodium dodecyl sulfate (SDS) in micellar form in 100 mM phosphate buffer at pH 3, while BGE was optimized at pH 6.6 using 100 mM phosphate buffer. This method was sensitive enough to monitor DFO and CP20 in real thalassemic patients' plasma samples.

In fact, the aforementioned chromatographic and electrophoretic methods are good approaches for overcoming the challenges of CP20 separation although separation of CP20 from its iron complex was still not achieved using these methods. Some methods used ion pair reagents and some others used competing chelators. CE method used SDS and triethanolamine as buffer additive. Hence, these approaches are intended for analytical use that is aimed at determining CP20 in biological samples. However, the system's complexity is the main drawback, and no reported method that is capable of separating CP20 from iron complex in a single run has been reported.

1.1.5. Aim of the work.

There is a still need to further investigate CP20 and its behavior as a chelator. CP20 capability to chelate essential metal ions, inhibit catalytic enzyme activities, or even directly bind to targeted biomolecules is interesting. Further steps in this direction might be enlightening with respect to new biological activities, which could aid in the development of new pharmacological uses. In this context, this work aims to develop new analytical approaches for investigating CP20 binding behavior to different targets. The first goal is to develop new LC/MS and CE/FA methods for determination of CP20 and separation of the free-form drug from the iron complex in order to investigate its binding affinity. It is well known that the CP20 separation is still a challenge, and no reported method has been able to achieve separation in one single run to date. The second goal is exploitation of MS as a powerful tool for characterizing binding stoichiometry. Furthermore, the binding affinity of CP20 towards essential metal ions in temperature gradient has not yet been studied. Therefore, investigation of CP20 binding affinity to essential divalent metal ions in addition to iron using MST is the third goal. On the other hand, the study of CP20 interaction with proteins is still poor and there is only one publication for characterizing CP20 interaction with HSA using spectroscopic techniques [64]. Therefore, the investigation of CP20 with HSA using MST and ACE techniques is the fourth goal of this work. Subsequently, exploiting MST and ACE to investigate the interaction of CP20 with human lactoferrin as a targeted protein in human breast milk is the fifth goal to predict the possibility of drug secretion as a fraction bound to protein.

2. Analytical techniques

2.1. Separative analytical techniques

2.1.1. Liquid Chromatography Mass Spectrometry

LC/MS is a hyphenated technique that exploits the power of the two technologies in one combined instrument. The separation power of HPLC was aided by the detection power of MS to produce LC/MS, which nowadays is the technique of choice for a broad range of analytical applications [72].

An HPLC instrument (Fig. 9) consists of several main parts connected in sequence starting from mobile phase reservoirs that are connected to a pumping system for delivering the liquid mobile phase and injecting analyte sample into the stationary phase in which chromatographic separation take place. In between the pump and stationary phase, the sample injector or autosampler is the point at which the analyte sample can be injected and delivered for separation inside the stationary phase. Thereafter, the separated samples are eluted and pass through the detector cell, and signal is then detected and recorded.

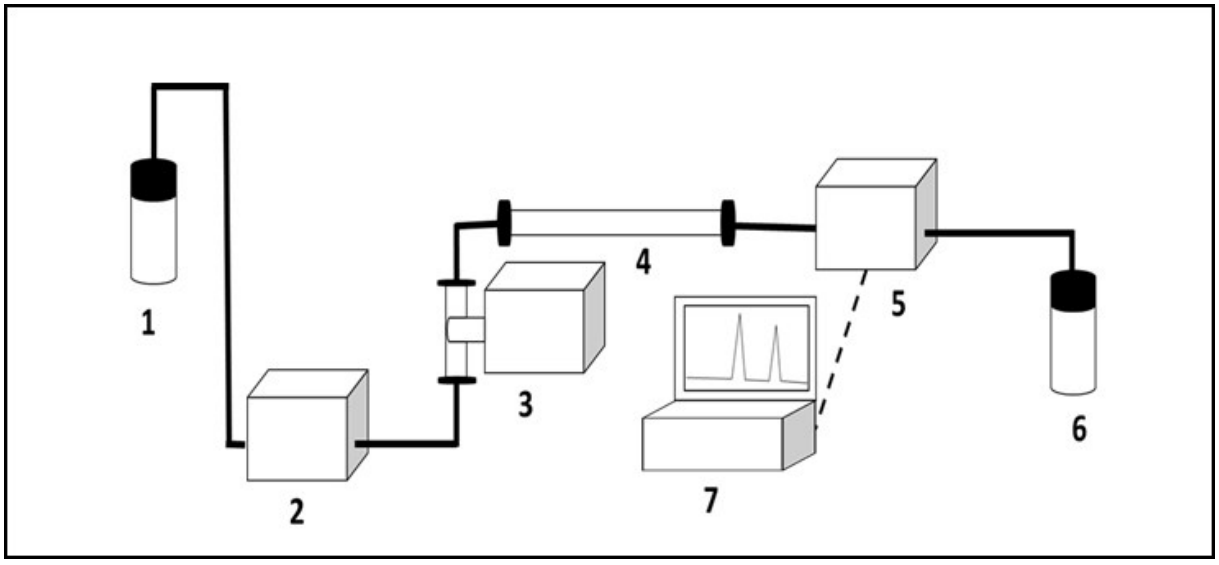

Fig. 9. Scheme of HPLC instrument including the main parts as (1) mobile phase reservoir, (2) pump, (3) sample injector, (4) stationary phase, (5) detector, (6) waste reservoir, and (7) Data records.

HPLC is a well-known separative technique consisting of different separation mechanisms, such as partitioning, size exclusion, and ion exchange. Partitioning mechanisms have been extensively utilized to characterize the analyte molecules that are partitioned between two phases that differ in polarity; one is the stationary phase, and the other one is the liquid phase.

Nevertheless, normal phase liquid chromatography (NPLC) is ideal for analyte partitioning between the polar stationary and non-polar liquid mobile phases, while the opposite mode is known as reversed-phase liquid chromatography (RPLC) in which the phases are reversed. The samples that are partitioned between the two phases are exposed to numerous interactions, such as dipole-dipole and electrostatic interactions, hydrogen bonding, and diffusion. These interactions take place according to the nature of the analyte's physicochemical properties and types of stationary and mobile phases in the LC system [73]. Furthermore, for LC analysis of large molecules, such as proteins, the use of the size exclusion mechanism is ideal due to its capability to separate the analytes depending on their molecular sizes. Moreover, ion chromatography is related to charged molecules and metal ions and has wide applications in environmental analysis [74] and to a lesser extent, in protein purification [75].

The versatility of HPLC is based on several separation phases. However, the RPLC mode is used predominantly in pharmaceutical development and enables researchers to separate a wide range of pharmaceutical compounds depending on their polarities. Therefore, RPLC is the most important mode described in this study.

RPLC separation is achieved by introducing the sample to the polar mobile phase consisting of aqueous solution and organic solvents. The ratio of the mobile phase components can be either in a fixed ratio, which known as isocratic elution, or changeable ratio, which known as gradient elution. Mobile phase solvents, including methanol, acetonitrile, isopropanol, and tetrahydrofuran, are frequently used. Also, different buffer salts and buffer additives can be added in order to achieve the desired separation.

The stationary phase in RPLC is non-polar in which the silica support has been chemically modified with derivatized n-alkyl silane as the hydrophobic ligand. The most common ligands for routine analysis of pharmaceutical and biopharmaceuticals are n-octadecyl (C18), n-octyl (C8), and n-butyl (C4). Thereafter, different types of ligands, such as phenylpropyl, cyanopropyl, and/or aminopropyl silane, could be added to expand the selectivity of the silica support [76].

Furthermore, several experimental parameters should be considered in order to obtain ideal chromatograms, including mobile phase compositions, stationary phase type, flow rate, temperature, and pH, whereas system optimization is the first step in the development of an HPLC method in order to control the effects of these parameters on the separation.

Theoretically, there are a number of parameters for characterizing the chromatographic performance according to the obtained chromatogram as shown in Fig. 10.

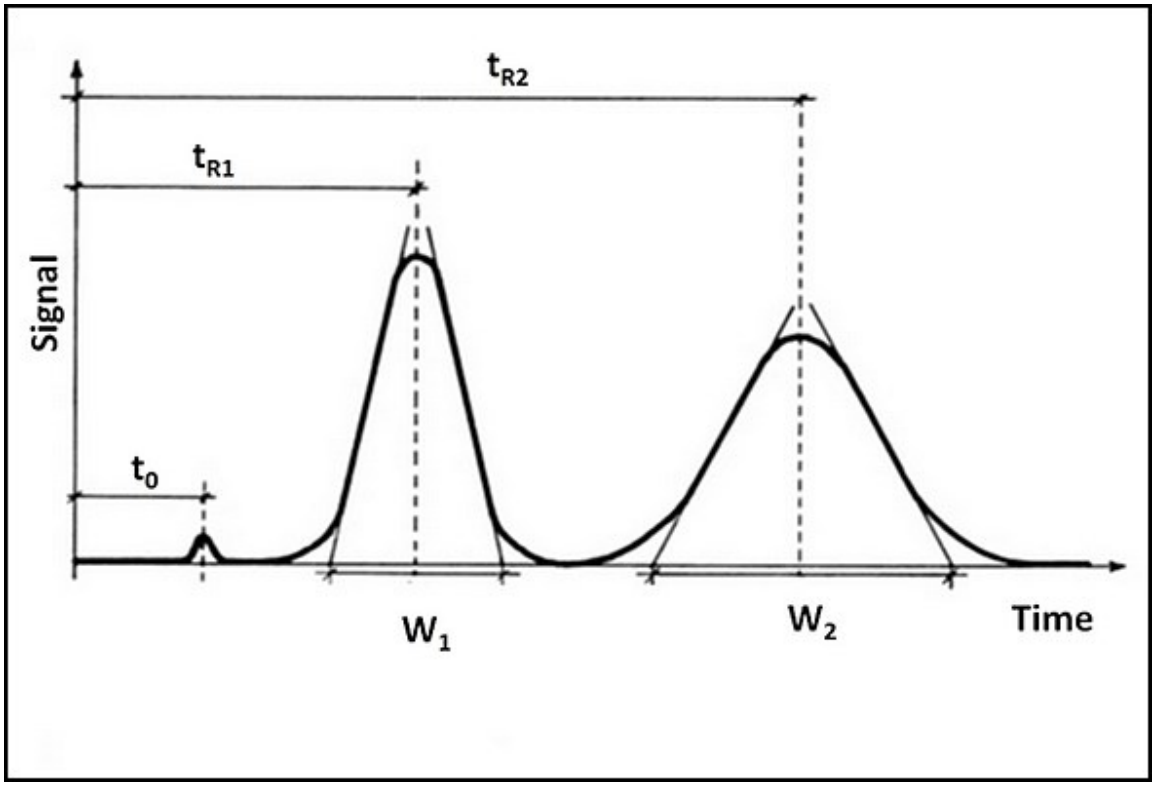

Fig. 10. Illustration for HPLC chromatogram with theoretical parameters.

The retention factor (*K*) is calculated according to the equation:

$$K = \frac{t_R - t_o}{t_o}$$

in which t_o is the dead time, and t_R is retention time.

The retention factor is a unitless value, is considered an independent factor, and is characteristic for analyte under the same conditions in different laboratories [73].

Selectivity (α) is defined as the relative retention between two analytes and is calculated based on the K value of each compounds:

$$\propto = \frac{k_2}{k_1}$$

in which α is dependent on the chromatographic phase and temperature.

Furthermore, the separation efficiency can be calculated with respect to number of theoretical plates (N) and resolution (R_s):

The number of theoretical plates is calculated according to the equation:

$N = 16\ (t_R/w)^2$

in which N = number of theoretical plates, t_R = retention time, and w = peak width at the base.

Resolution (R_s) is defined as a separation measurement between two adjacent peaks and is calculated based on the following equation:

$R_s = 2\ (t_{R2} - t_{R1}/w_2 + w_1)$

Both N and R_s parameters correlate with the stationary phase and indicate the efficiency of the selected column in order to achieve good separation depending on column length, particle size, and flow rate [77].

MS in conjunction with HPLC as detection technique are valuable for yielding information about samples identification. Under a vacuum, MS can be applied to analyze the ionized samples according to their mass to charge ratio (m/z). Therefore, the MS instrument can be used for three consecutive processes: (1) sample ionization; (2) mass analysis; and (3) mass detection. The ionization process is implemented via several ion sources, which are classified as hard ion sources or soft ion sources in which soft ion sources are widely used due to their compatibility with biological samples where, low energy conveyed to conserve the intact biomolecules without occurring further fragmentation [78,79]. The soft ionization including atmospheric pressure ionization (API), which consists of several modes of ion sources such as electrospray ionization (ESI), atmospheric pressure chemical ionization (APCI), and atmospheric pressure photoionization (APPI) are favored for adaption with LC techniques in addition to matrix-assisted laser desorption ionization (MALDI). The second step is the mass analysis process in which mass analyzers are classified according to low- and high-resolution mass analyzers. Low resolution MS analyzers include quadrupole (QMS) and ion trap (QiT) while high-resolution mass analyzers include time of flight (TOF), orbitrap, and Fourier transform ion cyclotron resonance (FTICR) [78,80,81]. However, a single quadrupole mass spectrometer equipped with ESI as ion source (ESI-MS) will be described here (Fig. 11).

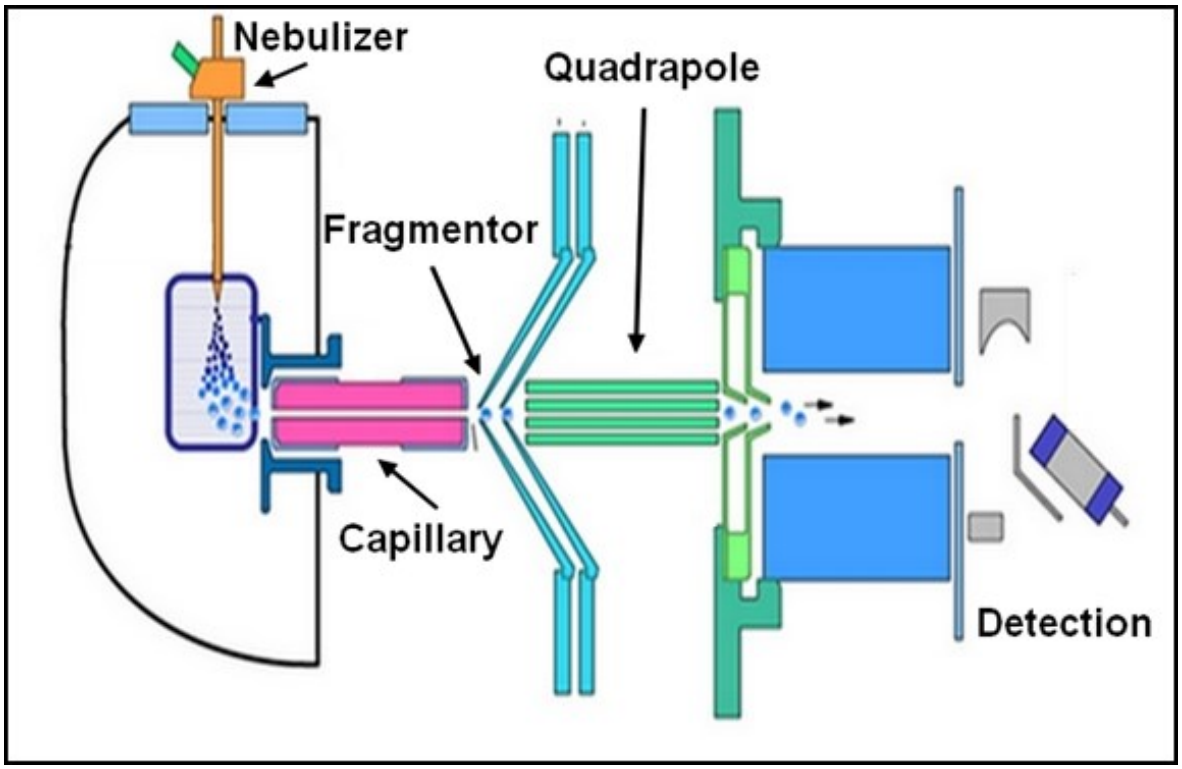

Fig. 11. ESI-MS instrument.

The ESI-MS instrument as shown in Fig. 11 was designed based on three consecutive processes: (1) sample ionization that takes place in the ESI ion source, whereas the liquid sample that comes from the HPLC are pumped into an orthogonal metal capillary called a nebulizer. Under atmospheric pressure, the eluent under the electrical field in the nebulizer is sprayed into a spray chamber to form a droplet. The formed droplets are evaporated via application of dry heated nitrogen gas; thereby, an electrostatic field occurs between the nebulizer and capillary in order to control the movements of ionized molecules into the MS vacuum; (2) mass analysis in which the quadrupole mass analyzer consists of four parallel metal rods, and the ions filter selectively through the oscillating electrical field of radio frequency between the rods according to mass to charge ratio. Therefore, only certain ions can pass through quadrupole track per time unit; and (3) mass detection, after the selected ions pass through the mass analyzer, they can be detected, and signals can be recorded [78,80].

2.1.2. Capillary electrophoresis

Capillary electrophoresis (CE) is an alternative separative technique to LC, and it gained popularity in a wide range of applications. CE and LC are separative techniques, and almost the same parameters are chosen for the analytical method's efficiency and sensitivity; however, CE is different than LC with respect to the separation mechanism. CE separates the charged analytes depending on their size and charge in free solution. The analytes exhibit different velocities within the electrical field [82].

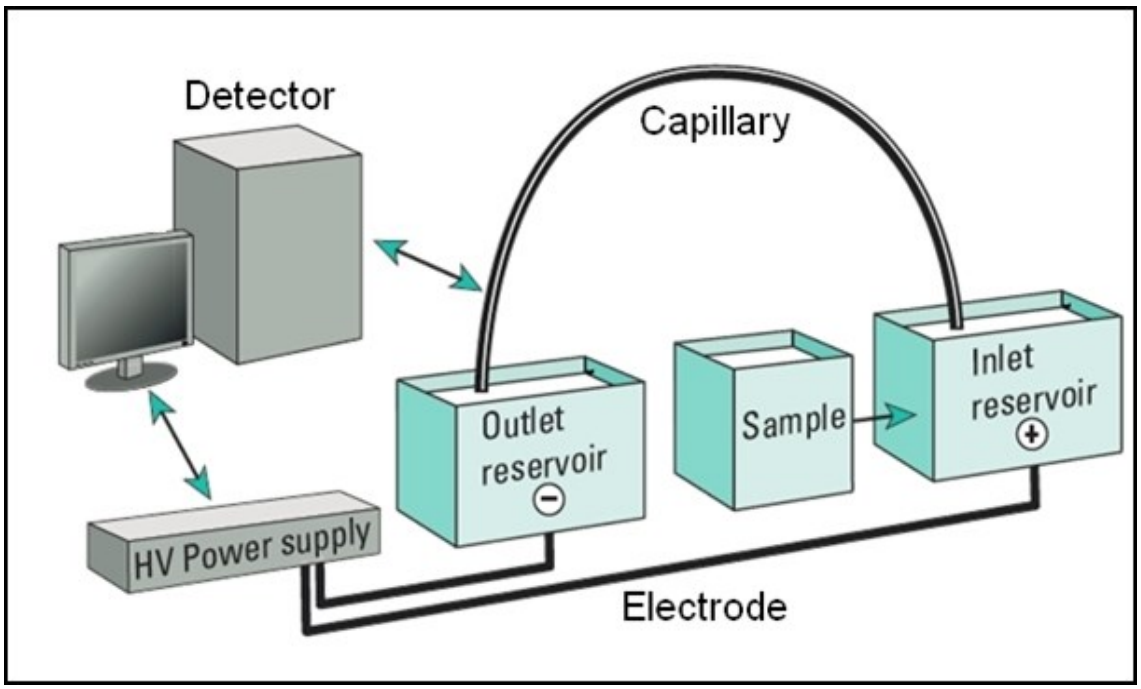

Fig. 12. Illustration for CE instrument.

The instrument (Fig. 12) consists of a fused-silica capillary with an internal diameter range of 25 to 100 μm and an optical detection window. Each end of the capillary was immersed in the buffer reservoir, which was connected to the power supply via two electrodes. The detector is aligned with the detection window in the capillary, and optical detectors, such as ultraviolet–visible (UV–vis) or fluorescence detectors, are attached to the instrument.

Furthermore, the sample was injected hydrodynamically or electrokinetically into either one of the capillary ends; therefore, the capillary is divided into total and effective lengths according to the sampling location, whereas the effective capillary length is the length of the capillary that is used for separation up to the point of the detector. The total capillary length includes effective length plus capillary length after the detection window. Nevertheless, the detection window is

designed with an enclosed electrode (typically the cathode); therefore, the injection could be a long- or short-end injection according to the effective capillary length that is chosen [83].

In principle, the separation in the CE system is dependent on the movements of charged molecules through the narrow bore capillary (usually made of bare fused-silica glass); thereby, these movements occur under the effects of electrophoresis or electroosmosis. Initially, electrophoretic mobility was created due to generation of an electrical field in which the applied voltage (usually 10–30 kV) tends to initiate ion migration toward the opposite electrode (cathode pull the cations while anode pull the anions). However, electroosmotic mobility is greater than electrophoretic mobility, resulting a generation of an additional potential (zeta potential) on the capillary surface. This process leads to flow movements in one direction for the overall movement of running buffer inside the capillary. This phenomenon is known as electroosmotic flow (EOF). Herein, the separation is depending on vector sum of two movements which allows for differentiation between the analytes depending on their charge to mass ratio. EOF, as shown in (Fig. 13), exists in each CE system in which negative charges are generated on the surface of the silica capillary due to ionization of silanol function group at pH >2.5 (Fig 13 A). The hydrolyzed cations that exist in aqueous buffer are attracted to the negative charges on the capillary wall and thus, create a double layer (Fig. 13 B). Subsequently, by applying an electrical voltage, they migrate toward cathode with an action that is similar to the pumping effect in LC (Fig. 13 C) [83,84].

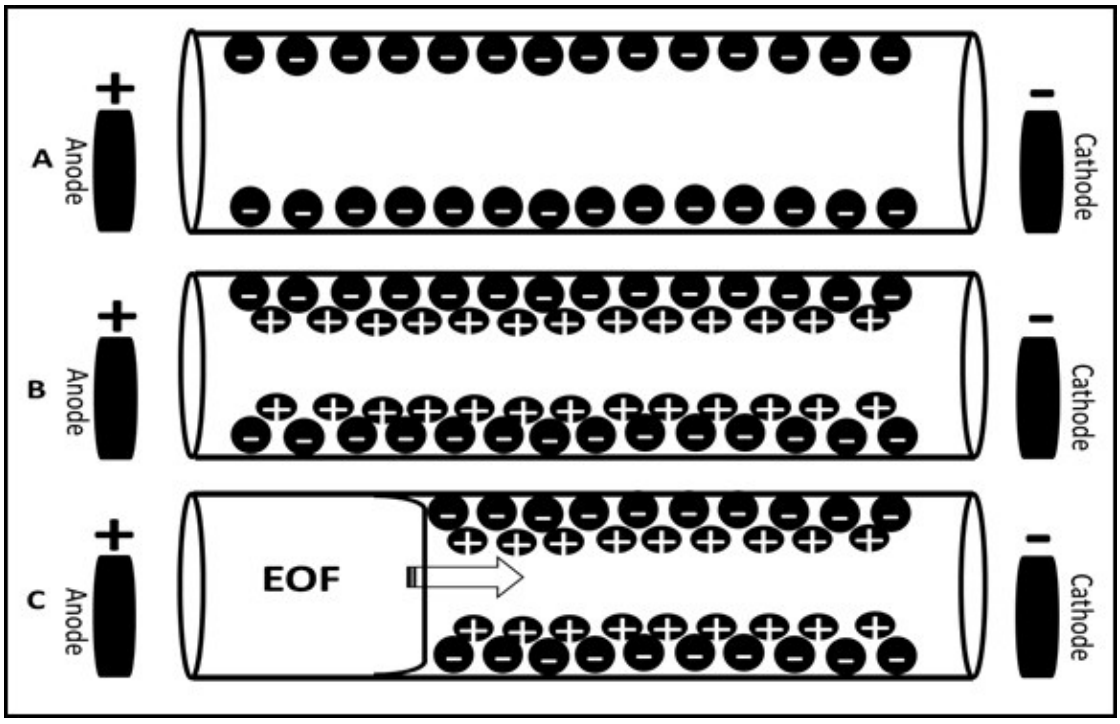

Fig. 13. EOF generation in CE system.

Migration in CE occurs under an electrical field; however, the solution's chemistry is critical for generating charged analytes and exhibiting efficient separation in a CE system in addition to EOF generation. Therefore, an EOF velocity is governed according to the equation [83,85,86]:

$$V_{eof} = -\left(\frac{\varepsilon\zeta}{4\pi\eta}\right)E \quad (1)$$

in which ε is the dielectric constant of electrolytes, ζ is zeta potential (volts) for measuring the charges on the wall of capillary, η is the viscosity, and E is the applied potential. From the equation, EOF velocity is shown to be significantly affected by pH. In an acidic environment (at pH ≤3) EOF effect is minimal due to the silanol group's ionization state, whereas the effect of EOF increasing at neutral pH in which case fused silica behaves as weak acid with a pK_a 6.25 as shown in Fig. 14 [85].

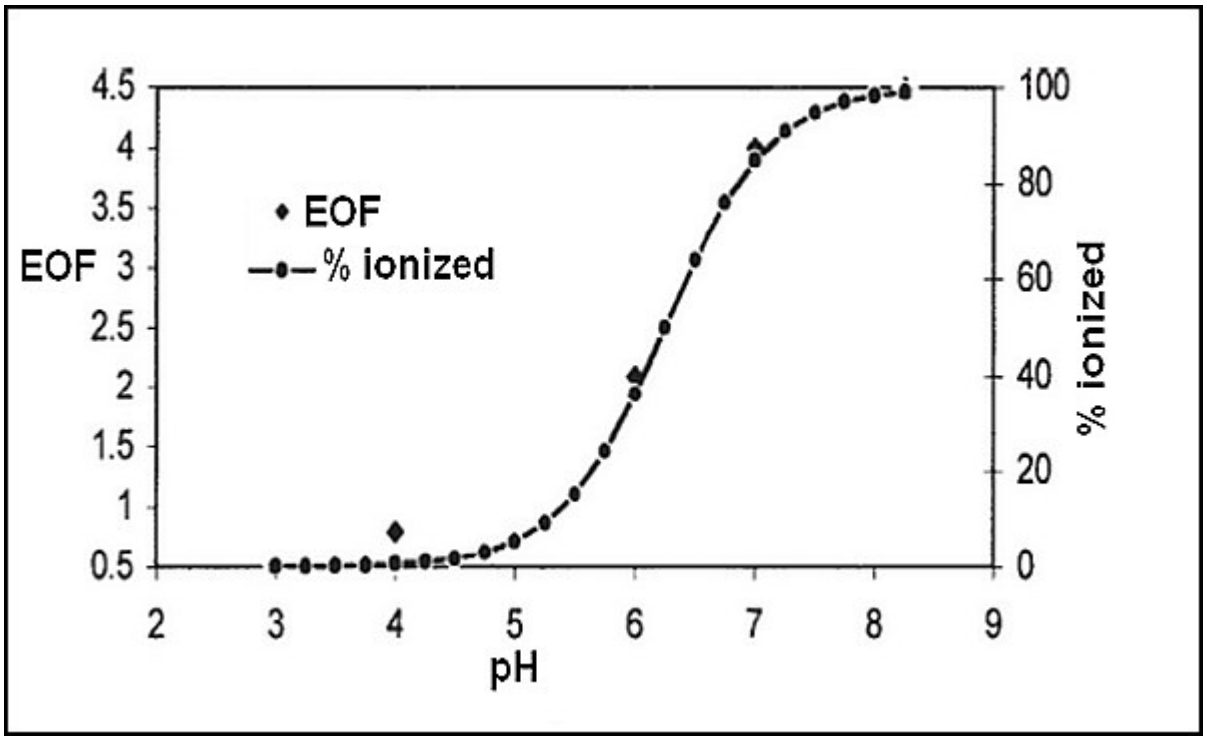

Fig. 14. EOF and silica ionization degree along pH scale [85].

An increase in buffer concentration leads to a decrease in EOF velocity. Charge density as represented by zeta potential (ζ) is directly proportional to EOF velocity. Therefore, the flow in CE capillary is a plug flow in contrast to the parabolic flow in LC as shown in Fig. 15.

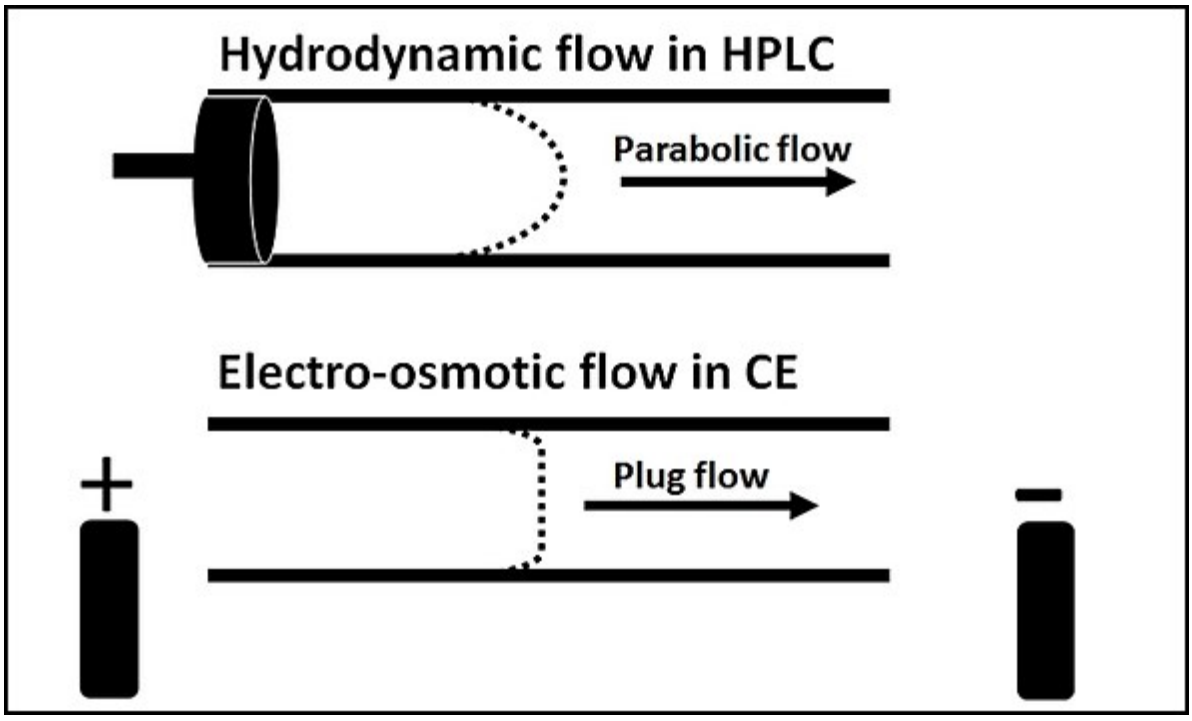

Fig. 15. EOF flow versus hydrodynamic flow.

All of these factors have been taken into account for the use of an uncoated fused silica capillary, which is the most extensively used capillary type in CE methods. However, it could be derivatized with different molecules, such as polyvinyl alcohol, polyacrylamide, or polyethylene glycol. This type of coating might be used for specific applications. For instance, adsorptive substances, such as highly positively charged proteins, are impossible to separate under normal CE conditions. Therefore, the EOF can be altered to suit the application [86].
Furthermore, are other factors such as temperature, applied voltage, capillary length and diameter, and injection volume should be taken in account whenever undertaking CE analyses. However, temperature control is significant for obtaining reproducibility in CE separation, but the temperature is generated from different sources and thereby temperature fluctuation cannot be totally avoided but should be minimized. For instance, the electrical current will generate heat when it passes through the running buffer inside the capillary; this heat is called Joule heating (JH). Actually, JH can be estimated according to the formula [87]:

$$P = \frac{\pi k d_i^2 E^2 L}{4} \qquad (2)$$

in which P is Joule heat that is produced, k is conductivity, d_i is the capillary's internal diameter, E is the electrical field strength, and L is the capillary length. Obviously, the generated heat correlates with several factors, such as capillary dimension, electrolyte conductivity, and electrical current. The electrical current increases directly with the increase in capillary diameter, leading to an increase the resulting JH. Practically, JH might alter EOF via alterations in running buffer viscosity as described in equation (1).

Additionally, applied voltage plays an important role in the analyte's separation via an increase in EOF, leading to an increase in sample migration with a concomitant shortening in analysis time. However, increasing the applied voltage might increase the electrical current, which produces JH as an adverse effect resulting from an increase of applied voltage [84,85].

In CE, the capillary is the heart of system similar to the column in HPLC. The effect of capillary dimensions and properties are described and explained as critical factors that affect both EOF and HJ generation. However, capillary regeneration also is critical in order to exhibit a reproducible result. Capillary regeneration of bare-fused silica is usually achieved using 0.1–1 M sodium hydroxide (NaOH) to hydrolyze the silanol group, which is important for generating EOF. Therefore, washing procedures should be optimized during the CE development method according to the type of analytes and electrolytes in the CE system [85].

2.1.2.1. Affinity capillary electrophoresis

Exploiting CE for binding affinity studies is considered one of the major CE applications. Affinity capillary electrophoresis (ACE) is the CE based methods that allowed the binding investigation in free solutions without the need for immobilizing one partner on the supporting matrix. Moreover, ACE as performing at near physiological conditions, low sample consumption, low cost, short analysis time, and possible adaptation to various detectors. In addition, CE presents a great advantage for miniaturization of instrumental analysis [62,88–91]. ACE can be implemented with several CE-based methods according to several kinetic equilibrium modes:

A. The dynamic equilibrium mode in which this mode is distinguished from other modes by with rapid binding kinetics. In this mode, the equilibrium relaxation time is shorter than migration time. Actually, most of the CE modes, including mobility shift ACE (mACE), Hummel-Dreyer (HD), vacancy peak (VP), and CE frontal analysis (CE/FA) belong to this mode of equilibrium kinetics.
B. The pre-equilibrated mode is distinguished by slow kinetics in which the relaxation time of equilibrium is longer than the migration time. In this mode, equilibration should occur before subjecting the sample to CE analysis. CE modes, which are suitable to be used for this mode of kinetics are CZE and CE/FA in which the dissociation in CE system is negligible due to high binding affinity.
C. The intermediate mode is the kinetic mode which is used to describe the dissociation of binding equilibrium in which the relaxation time is equal to the separation time. In this mode, the co-eluted peak has been observed on electropherograms due to dissociation of the complex. This mode of kinetics might be observed in pre-equilibrated CZE [92].

Therefore, CE exhibits several responses for quantifying the binding event depending on the equilibrium type; thereby, there are different CE-based approaches that might be implemented as described in Table 1 [62,89,93–95].

Table 1. CE modes for binding affinity studies.

	Pre-equilibrated mode		Dynamic equilibrium mode		
	CE/FA	**CZE**	**mACE**	**HD**	**VP**
Setup	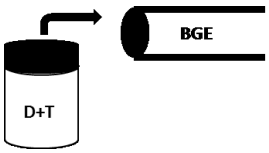		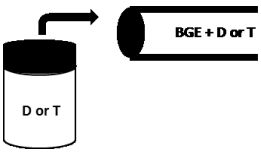		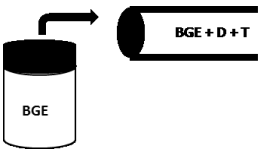
Binding parameters	-binding constant - stoichiometry		-Binding constant	-binding constant -Stoichiometry	- binding constant - stoichiometry
Binding kinetics	Fast and slow	Slow	Fast	Fast	Fast
Electrophoretic response	Peak plateau height or area	Peak area or height	migration time shift	Peak area or height	Peak area or height
CE/FA CE profile	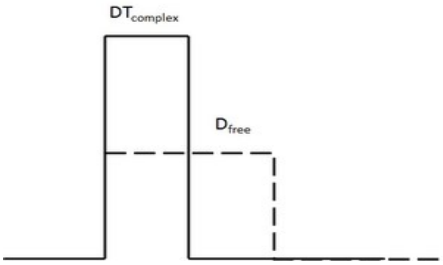				
CZE CE profile	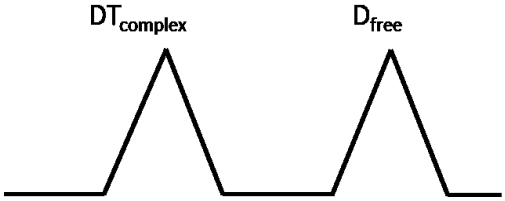				

mACE CE profile	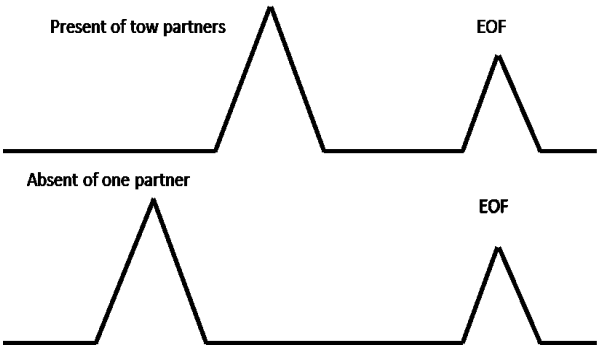
HD CE profile	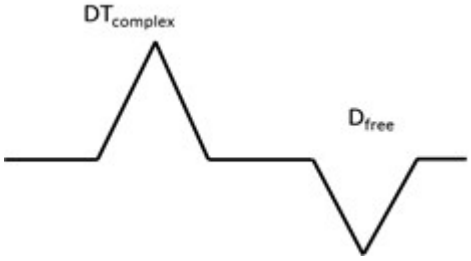
VP EC profile	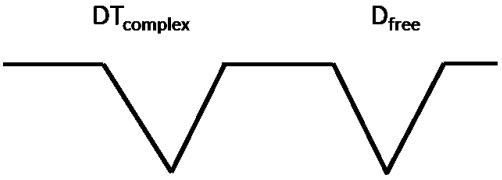
CE/FA	A- Advantages 1. It can be used for Both slow and fast equilibria 2. Multi kinetic equilibrai can be estimated 3. Binding stoichiometry can be estimated 4. The drug bound fraction have been easily obtained B- Diadvantages 1. Not possible for non chromophoric partner 2. Sample might be consumed more than other ACE modes
mACE	A- Advantages 1. Suitable for non-chromphoric interacting partner 2. enantiomeric separation is easy to perform 3. using with sample mixture B- Disadvantages 1. Not used in multi kinetic equilibria. 2. Binding stoichiometry cannot be estimated

2.1.3. Binding fundamentals in the separative techniques

Binding parameters, such as both binding constant and stoichiometry, are the most important parameters that have been used in characterizing the binding events. Although many forms of symbols were assigned to the binding constant, all refer to the association/dissociation rate at equilibrium:

$$[D] + [T] \underset{K_d}{\overset{K_a}{\rightleftharpoons}} [DT] \qquad (1)$$

in which [*D*], [*T*], and [*DT*] are the molar concentrations of free drug, free targeted molecule, and the complex, respectively, and K_a and K_d are the association and dissociation constants, respectively. At equilibrium, the association rate is equal to dissociation rate and the binding constant can be defined using the equation:

$$K_a = {}^{1}/_{K_d} = \frac{[DT]}{[D][T]} \qquad (2)$$

Hence, the total drug and the target concentrations are known, but the complex concentration is unknown and can be calculated as the bound fraction, *r*, which denotes the number of total drugs bound per target at equilibrium in which $K=K_a$:

$$r = \frac{[DT]}{[D][T]} = \frac{K[D]}{1+K[D]} \qquad (3)$$

Based on Equation (3), *r* can be replaced by an experimental response base on the equation:

$$\frac{\Delta R}{\Delta R_{max}} = \frac{R-R_f}{R_c-R_f} = \frac{K[D]}{1+K[D]} \qquad (4)$$

in which *R* is the system response, R_f and R_c are the responses of free target and complex, respectively. The experimental response is expressed according to the selected analytical approach, such as mobility shift in ACE and retention factor in chromatography. In these approaches, the equilibrium kinetics are rapid, and the complex is difficult to stabilize in the system. In addition, the effects of viscosity, ionic strength, and sample adsorption should be taken into account. The binding constant according to Eq. (4) can be estimated using a nonlinear least-squares regression, and the binding stoichiometry was assumed to be a 1:1 binding ratio. Furthermore, several algebraic rearrangements have been addressed for linearizing the relationship [94,96]:

$$\frac{\Delta R}{[D]} = -K\Delta R + K\Delta R_{max} \quad (5)$$

$$\frac{[D]}{\Delta R} = \frac{1}{\Delta R_{max}} + \frac{[D]}{\Delta R_{max}} \quad (6)$$

$$\frac{1}{\Delta R} = \frac{1}{\Delta R_{max} K[D]} + \frac{1}{\Delta R_{max}} \quad (7)$$

Equations 5–7 represent different linear plots for Eq. (4). These algebraic rearrangements have been named x-, y-, and double reciprocal, respectively.

For multiple equilibria systems that occur in biological system, Eq. (3) has been modified to [94,97,98]:

$$r = \frac{[D]}{[T_{total}]} = \frac{n.K[D]}{1+K[D]} \quad (8)$$

in which n is the total number of binding sites per target.

In this system, different binding affinities can be assumed based on the following equation:

$$r = \sum_{i=1}^{m} \frac{n_i \,.\quad k_a \,.\quad [D]_{free}}{1 + \quad k_a \,.\quad [D]_{free}} \quad (9)$$

in which *m* is the independent binding types per target. In this system, binding parameters can be estimated using a nonlinear least-squares regression, and the total number of binding sites can be estimated to yield information about binding stoichiometry.

According to Eq. (9), data can be fitted with fast and slow kinetic equilibrium constants depending on several separative analytical approaches, such as direct LC separation, CZE, and CE/FA. This formula can be used to estimate the binding parameters according to separation of free drug from the complex. Herein, the experimental response can be addressed in order to obtain the concentration of free drug based on an external calibration curve.

2.2. Non-separative techniques

2.2.1. Microscale thermophoresis

Microscale thermophoresis (MST) is a relatively new biophysical technique derived the basic principle from physical phenomenon known as thermophoresis (also defined in other synonyms as thermomigration, Soret effect and thermodiffusion) which describing the movement of the molecules through temperature gradients [99]. The suffix -phoresis indicating the migration of analytes and this migration might be under electrical field as occurs in CE or under temperature gradient as occurs in MST (Fig. 16).

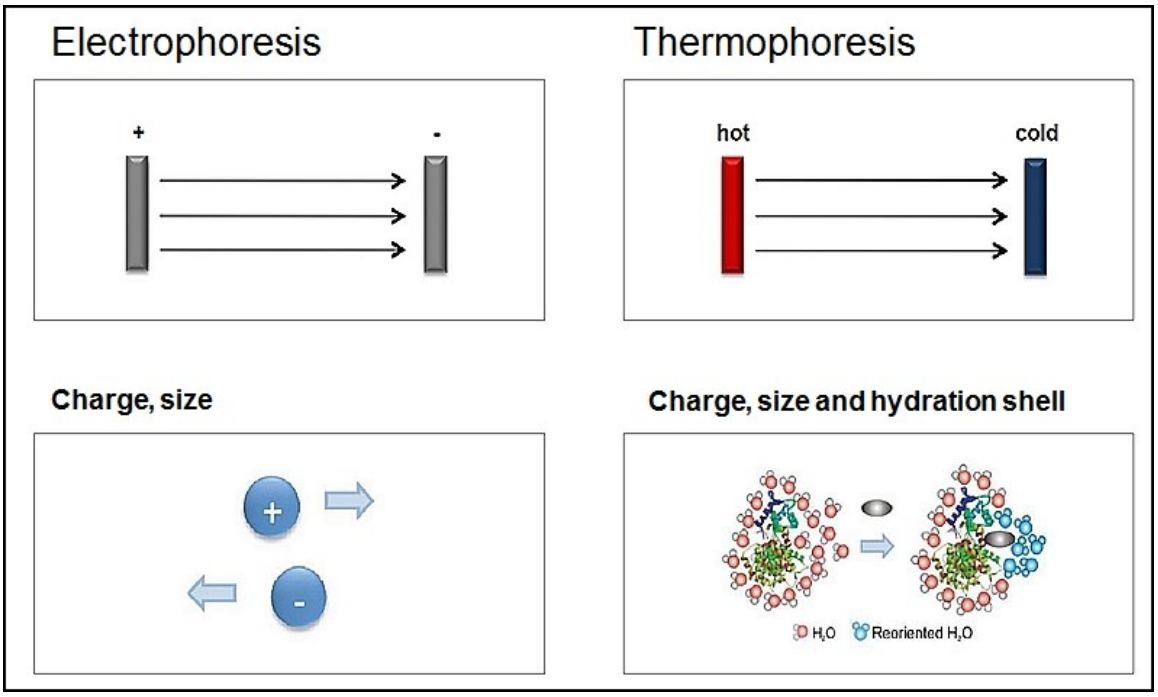

Fig. 16. MST illustration for thermomigration under temperature gradient.

The movement of molecules along temperature gradients is influenced by changes have been induced through molecular binding leading to change of molecular properties as charge, size and hydration shell [99–101]. Thermophoresis can occur in all phases of matter and described at the first time by Carl Ludwig in 1856 [102]. Since then thermophoresis has been exploited in different areas of research such as inorganic polymerization and aerosol mixtures [103,104]. Braun and Libchaber described the first approach of thermophoresis for biomolecule with trapping of DNA and characterizing of thermophoretic depletion. DNA was depleted from heated zone and thermal diffusion constant (D_T) has been quantified for the first time [105,106]. More-

over, Piazza and coworkers reported the effect of thermophoresis in protein solution and provided information's about particle-solvent interactions through studying the effect of protein charge and salt additives on lysozyme Soret coefficient [107,108]. Actually, all of the previous reports have been dealt with theoretical framework of Soret effect for biomolecules in solution however, Duhr and Braun studied all parameters that govern thermodiffusion including particle surfaces, size, effective charge, temperature and salt concentration to measure Soret coefficient (S_T) for DNA and polystyrene beads whereas, postulated the theoretical formula of thermophoresis in solution have been postulated (section 2.2.1.2). Moreover, they stated that "*thermodiffusion can be miniaturized to micrometer scale with all optical fluorescence technique and permit microscopic temperature differences to manipulate molecules based on their surface properties*" [109]. Thermophoresis in microscale units was described by Dieter Braun and coworkers via studying thermophoresis of single strand of DNA in native bulk solution. Where temperature gradients were induced locally using infrared laser focused on rectangular capillary with a 50 μm x 50 μm cross section [110]. Thereafter, the same research group was introduced MST as analytical tool in characterizing the interactions of biomolecules. The experiment was carried out using lab-made MST instrument where temperature gradients were created through using infrared laser diode 1480 nm and microfluidic chambers using fused silica capillary with inner diameter 100 μm. The technique was succeeded in determination of K_d in nanomolar concentration for two different approaches of protein interactions [111]. Nowadays, MST is exploited extensively in characterizing the interaction of several biomolecules such as protein-protein interactions [112–114], protein-nucleic acids interactions [115,116]], protein-small molecules interactions [117–119], protein-metal ions interactions [120,121] and many other molecular interactions that possessed significant applications in life sciences.

Indeed, MST has been introduced to bioanalysis realm with several features to fill the gap between the competing biophysical techniques such as surface plasmon resonance (SPR), isothermal titration calorimetry (ITC), and several spectroscopic techniques [122]. For instance, MST allow to measuring the binding events in free solution by avoiding immobilization of one binding partner that might alter the binding event. Whereas, the surface immobilization process is necessary step in SPR for creation of sensitive sensor to measure the binding kinetics which is the main advantageous of SPR technique however, there are many drawbacks of this artifact such as binding overestimation and concentration depletion [122–124]. Furthermore, MST exhibit high flexibility to use buffers without restrictions unlike ITC which is restricted to buffers with low enthalpy ionization to minimize the overlapping of heated signals although ITC gives affinity, stoichiometry and thermodynamic parameters in free solution and label free system, but it suffers from low sensitivity, slow throughput technique, time consumption and high

amount of sample need to obtain sufficient heat signals [118,123]]. Besides, spectroscopic techniques including fluorescence anisotropy (FA) and fluorescence correlation spectroscopy (FCS) are fluorescence-based methods and similar to MST. Whereas, FCS technique depend on change on diffusion time of fluorescent molecules through detecting of fluorescence fluctuation upon the diffused fluorescent molecules out the focused volume. While, FA almost has the same principle except that measure change in rotational diffusion time thereby, polarized time has been used to excite the fluorescent partner. Both techniques have been dedicated mainly to single molecule applications more than biomolecular interaction as well as time consuming and need to perform more optimization in comparison to other biophysical techniques [100,114,125,126]. Table. 2 compare between SPR, ITC and MST as promising biophysical techniques that are used in biomolecular interaction.

Table 2. Comparison between ITC, SPR and MST techniques

Biophysical technique	Advantages	Disadvantages
ITC	• Several physical parameters can be obtained from one single experiment such as binding constant, binding stoichiometry and binding enthalpy. • Immobilization is not required • Labeling is not required • Inexpensive technique	• Large sample consumption • kinetic data cannot be obtained • Buffer should be with low enthalpy • Low throughput • Low sensitivity • Time consuming
SPR	• Binding kinetic in real time is possible • Label free system • Highly Sensitive technique • High throughput • Low sample consumption	• Expensive technique • Immobilization of one binding partner is required and time consuming • Experiment need to technical skills to perform • Immobilization of one of the binding partners required • Instrument maintenance
MST	• Low sample consumption • Simple handling technique • Immobilization free • Lebel free system is possible • Enabling to wide range of molecules i.e. ions to MDa biomolecules. • High throughput.	• Non-specific binding is possible due to labeling procedures. • Binding kinetics cannot be obtained • Expensive instrument

2.2.1.2. MST principle and theory

Through infrared (IR) laser beam with emission wavelength 1480 nm (Fig. 17 A), the local heating of aqueous solution in diameter of ~ 50 µm and temperature difference ΔT ~ 2-6ºC will generate molecular flow (*j*) which is directly proportional to temperature gradient with proportionality constant D_T. In steady state, thermophoretic flow opposed by mass diffusion and both effects being balanced which are describe in the following equations [109,111,122,127]:

$$j = -cD_T \quad \text{grad } T \qquad (1)$$

$$j = -D \quad \text{grad } c \qquad (2)$$

j: molecular flow; c: molecular concentration; D_T: Thermal diffusion coefficient; T: temperature; D: diffusion coefficient. The Soret coefficient S_T is defined by the ratio:

$$S_T = \frac{D}{D_T} \qquad (3)$$

S_T describes the concentration ratio under steady state conditions and given by:

$$S_T: \frac{C_{hot}}{C_{cold}} = exp(-S_T \Delta T) \qquad (4)$$

where C_{hot} is the concentration of molecules at the hot zone and C_{cold} is the concentration of molecules at the cold zone. S_T is Soret coefficient, which is affected by the factors described in the following equation:

$$S_T = \frac{A}{kT}\left(-\Delta s_{hyd}(T) + \frac{\beta {\sigma^2}_{eff}}{4\varepsilon\varepsilon_0 T} \times \lambda_{DH}\right) \qquad (5)$$

where *A* is the surface area of the molecules, σ_{eff} is the effective charge, Δs_{hyd} is the hydration shell effect, λ_{DH} is the Debye–Hückel screening length, ε is the dielectric constant, and β is temperature derivative of ε. Therefore, any small conformational changes of thermophoretic parameters such as effective charges, hydration entropy or molecular size provide information about binding affinity.

In principle, thermophoresis has been carried out in free solution inside cylindrical capillaries and MST signals that obtained involves of numerous subsequent processes. Initially, MST records fluorescence in the focal of IR-laser zone at ambient temperature without laser heating which called initial state (Fig. 17 B-I). Then, IR-laser turn on for heating of specific focal zone in sample solution and leads to change of fluorescence intensity known as T-jump (Fig. 17 B-II). After T-jump, thermophoretic movements of the molecules start as well as fluorescence intensity will decrease till reach to the steady state depend on molecular depletion to out of heated zone according to the typical thermophoresis which described as the movement of the molecules from hot to cold zone (Fig. 17 B-III). Thereafter, IR-laser switched off to induce mass diffusion of molecules depends on concentration gradient which called back-diffusion state (Fig. 17 B-IV). The total time for each MST signal takes ~35 seconds.

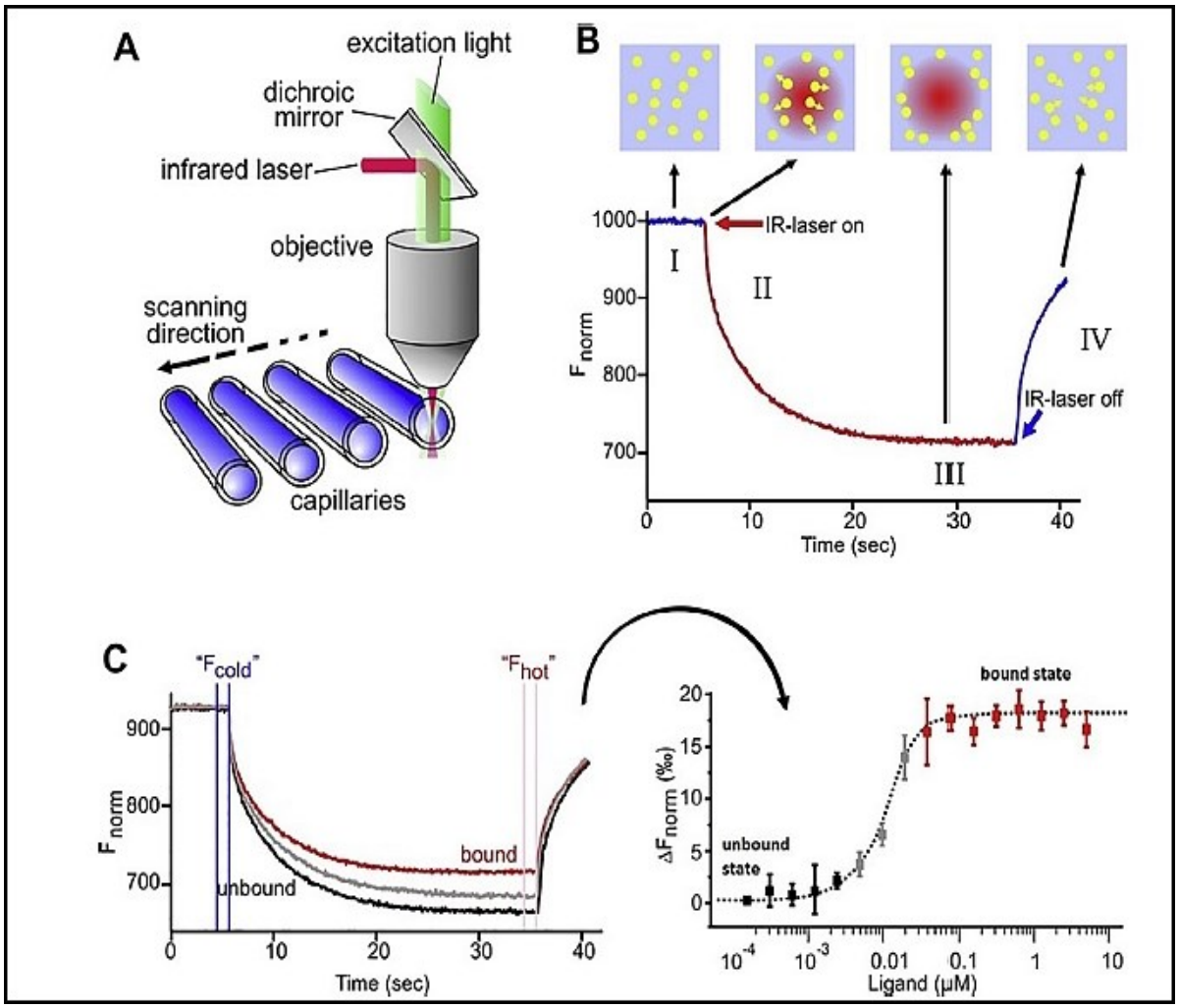

Fig. 17. A) Schematic setup of MST instrument. B) Subsequence stages of thermophoresis. C) Thermophoretic signals for bound/unbound molecules (left), Binding curve (right) [127].

Herein, binding quantifications is taking place by analyzing the change in fluorescence intensity which estimated as relative fluorescence (normalized fluorescence) according to the following equation:

$$F_{norm} = {}^{F_{hot}}/_{F_{cold}} \qquad (6)$$

Whereas, F_{norm}: normalized fluorescence; F_{hot}: fluorescence in heated zone; F_{cold}: fluorescence at initial state or in cooling state. The differences in F_{norm} of the bound and unbound state (depend on the concentration of titrated partner) allow to estimate fraction bound (FB) as shown in (Fig. 17 C) according to the following equation:

$$F_{norm} = (1 - FB)F_{norm}(unbound) + (FB)F_{norm}(bound) \qquad (7)$$

Thus, F_{norm} is used to quantify the concentration of fluorescent molecules which is temperature dependence and governed by the flowing equation:

$$F_{norm} = {}^{F_{hot}}/_{F_{cold}} = 1 + \left(\frac{\delta F}{\delta T} - S_T\right)\Delta T = \frac{C_{hot}}{C_{cold}} + \frac{\delta F}{\delta T}\Delta T \qquad (8)$$

2.2.1.3. MST data analysis

Binding isotherm of MST can be illustrated as shown in (Fig. 17 C right) where x-axis is the molar concentration of the sample against the relative fluorescence % on the y-axis. Actually, there are two binding models that have been implemented to fit MST data. The first, assuming the binding stoichiometry to be 1:1 binding ratio or multiple binding ratios with the same affinities. In this case, the dissociation constant K_d can be estimated as follow [100,111,127]:

$$A + B \rightleftharpoons AB \qquad (1)$$

A: binding partner A; B: binding partner B; AB: complex

The equilibrium dissociation constant K_d as:

$$K_d = \frac{[A]_{free} - [B]_{free}}{[AB]} \qquad (2)$$

Whereas, free concentrations of each partner are not known. Total concentrations are used according to the following formula:

$$[A] = [A]_{free} + [AB] \; and \; [B] = [B]_{free} + [AB] \qquad (3)$$

$[A]_{free}$: free concentration of partner A; $[B]_{free}$: free concentration of partner B; $[AB]$: bound complex concentration.

Hence, K_d is calculated as follow:

$$K_d = \frac{([A] - [AB])([B] - [AB])}{[AB]} \qquad (4)$$

Then, fraction bound FB is calculated as a total concentration of A and B and correlated with K_d parameter as follows:

$$FB = \frac{[\mathrm{A}] + [\mathrm{B}] + K_d - \sqrt{([A] + [B] + K_d)^2 - 4[AB]}}{2[B]} \qquad (5)$$

Where, FB represents linearity with normalized fluorescence form MST measurements.
The second model is implemented when the binding events is more complicated in which more than one binding sites with different affinities or cooperative systems. In these cases, Hill coefficient and EC_{50} have been estimated according to hill equation:

$$FB = \frac{1}{1+(EC_{50}/B)^n} \qquad (6)$$

Where B represent concentration of titrated partner. EC_{50} is defined as half maximal concentration of titrated partner which provide information about affinity of two partner depends on their concentration and n is Hill coefficient which provide information about system cooperativity.

2.2.1.4. Experimental implementation of MST

Implementation of MST experiment require discussing some important issues such as MST instrumentation, samples preparation, and MST optimization.

2.2.1.4.1. MST instrumentation

MST instrument as illustrated in Fig. 17 A consists of visible light passed through an objective to induce fluorescence excitation/emission for fluorescent molecules in specific μm- zone of the sample inside a glass capillary. Afterwards thermophoresis will be generated through switching on the IR laser to pass throughout the same objective and heating specific local zone inside the zone of fluorescence excitation light. The two beams of light are perpendicular whereas, IR light focus beam is switched on and off each 35 S and is reflected via dichroic mirror to couple with visible light. The position of local zone should be fixed in each capillary and can be tested through capillary scanning test (see MST optimization). The capillaries that is used in MST instrument is made of high pure glass with capacity about 4 μl and known as standard capillary. Moreover, coated capillaries are available as a second option for sticky samples, if the sample sticking was occurred. The capillary tray is loaded with16 different samples in each experimental measurement. Virtually, MST detection can be carried out through either label or label free system where, several molecules/biomolecules had native fluorophores in UV region such as presence of tryptophan in protein which have excitation wavelength at 280 nm and emission wavelength at 360 nm. MST label free system can be used whenever the fluorescence signals of intrinsic fluorophores are sufficient to be detected otherwise, labeling is the best choice for MST measurements. Furthermore, if both partners have intrinsic fluorophores, one partner should be distinguished for measuring in specific wavelength range without overlapping from the second [128]. For the experiments that use labels, MST

instrument contains three types of LED filter combinations: blue (excitation 460-480 nm, emission 515-530 nm), green (excitation 515-525 nm, emission 560-585 nm) and red (excitation 605-645 nm, emission 680-685 nm). There are wide range of detection wavelengths depend on the dyes that used for labeling of one partner. Moreover, high-affinity interactions with a sub-Nanomolar scale preferred to carry out in red visible zone using red dyes to improve the sensitivity in low-picomolar concentrations [127].

2.2.1.4.2. Samples preparation

One of MST advantages is the very low sample consumption. The samples might be prepared in microliter of volume range ~20 µl and the capillary volume is about 4 µl while, thermophoresis occurrs in about 2 nl of capillary sample volume. MST measurements is taking place through the titration of serial concentration of nonfluorescent partner against fixed concentration of fluorescent partner. The samples can be prepared through serial dilution procedures as shown in the general scheme (Fig.18).

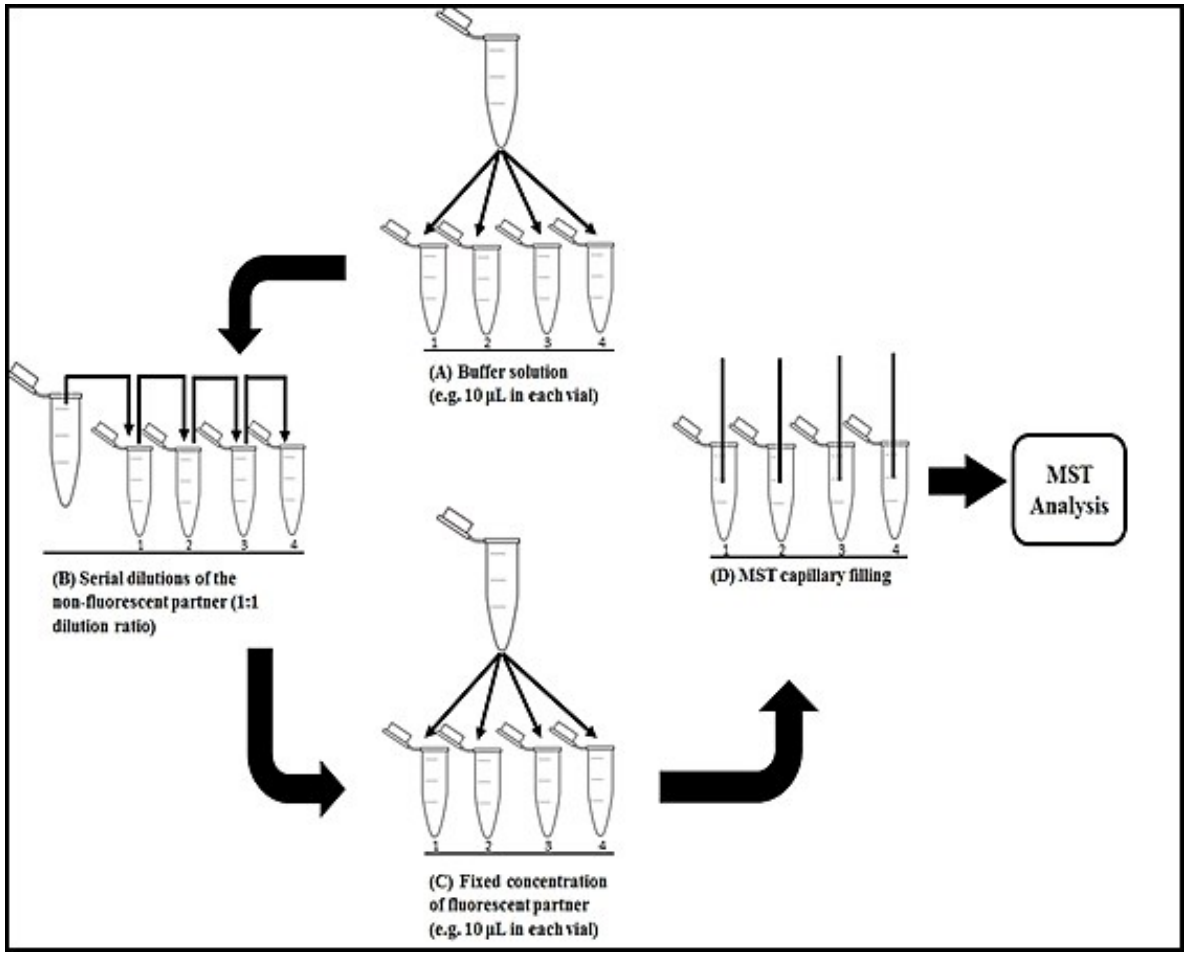

Figure. 18. General scheme for MST sample preparation.

Furthermore, the minimum and maximum sample concentrations are determined according to the titrated partner (nonfluorescent molecule) where the minimal concentration should be sufficiently low to measure unbound state and maximum concentration should be 40-fold above the dissociation constant to reach the saturation [100,127]. MST allow to use buffers without restrictions however, the concentration of the buffer should be kept constant as well as the solvent that is used to dissolve some analytes especially small molecules such as ethanol, methanol, dimethyl sulfoxide (DMSO), etc. Buffer additives such as the detergents and the sample stabilizers might be used as well [122].

By contrast, the labeling procedures is necessary to provide high sensitivity and selectivity in fluid mixture therefor, most MST approaches have been carried out with labeling technique to avoid high background of UV fluorescence that exist in bioliquid samples such as cell lysate and blood serum [100]. Usually, protein labeling can be implemented via using crosslinker reactive group which covalently binds to specific functional group of protein after coupling of fluorescent dye such as N-hydroxysuccinimide and maleimide. This labeling approach is need for the washing step to remove unreacted dyes before MST measurements [129–131]. Alternatively, using of fluorescent protein such as green fluorescent protein via direct fusion to the targeted biomolecules can be applied [132].

The labeling approaches are crucial to obtain highly sensitive and selective measurements although the presence of labels at random position has no influence on thermophoresis [100].

2.2.1.4.3. MST method optimization

The optimization of MST experiment is substantial to produce valuable measurements of binding events. Therefore, MST instrument offers optimization steps before the measurements including fluorescence test and capillary scanning test to minimize experimental errors such as sample pipetting, sample sticking, low/high fluorescence intensity and suboptimal concentration range. Furthermore, MST signals might indicate some problems such as protein aggregation during the assay. Fluorescence scanning test is the first pretest to perform for one time at the beginning of MST experiment because it is important to optimize the fluorescence intensity of fluorescent partner and to avoid such background fluorescence resulted from sample mixture and to select the proper concentration of fluorescent partner which can give sufficient signal. Fluorescence pretest is carried out through selecting three different concentrations of fluorescent partner, buffer sample without any reactant partners, and the non- fluorescent partner.

The second pretest is capillary scanning test which is performed at the beginning of each sample measurement to provide indication about variations in fluorescence intensity between the samples which might be attributed to handling errors or sample sticking to the capillary wall as shown in Fig 19.

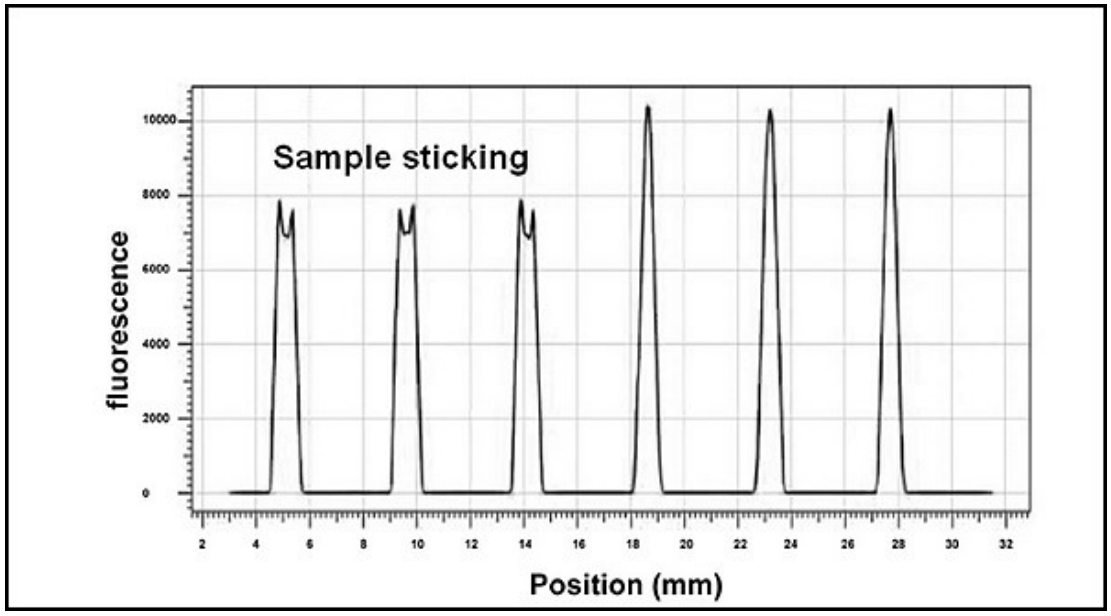

Fig. 19. Capillary scanning test where, sample sticking could be detected through peak shape and intensity [127].

Furthermore, there is one important indicator that can be obtained from MST signals whereas, the signal shape can be distorted due to sample aggregate (Fig.20). In this case new sample preparation is recommended with different buffering system or by adding buffer additives to inhibit sample aggregates.

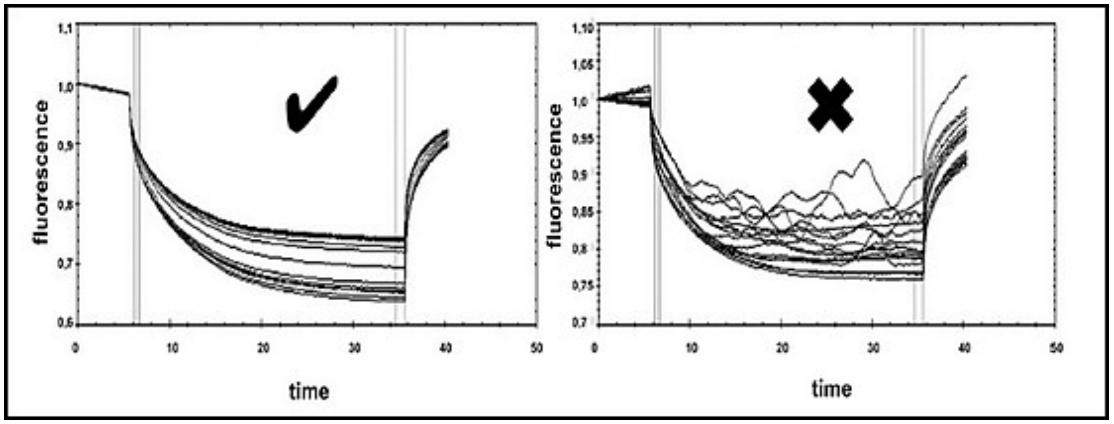

Fig. 20. MST signals for Sample aggregates (left) in comparison with normal MST signals (right) [127].

Therefore, the good sample preparation is a critical factor in MST experiment and many experimental errors are related to poor sample preparation and handling. In this context, troubleshooting of several MST analytical errors and suggested optimum steps are summarized in Table 4 [100,124,127].

Table 4. Troubleshooting of MST analytical errors

Problem	Indication	Optimization
Sample adsorption	- Asymmetric peak in capillary scanning. - Instable fluorescence intensity for the same sample over the runs. - Fluorescence drop along titration curve.	- Using coated capillaries. - Using buffer additives.
Sample aggregation	- MST signals show bumps or waves. - MST signals strongly deviated.	- Spinning down the sample before the experiment. - Using buffer additives. - Buffer optimization.
Concentration error	- No binding saturation has been obtained. - Unable to quantify unbound state.	- Optimize the concentration range to be wider.
Pipetting errors	- Peak intensity in capillary scanning is deviated.	- Use correct pipetting technique.
Low signal to noise ratio	- MST signals not discriminated from background fluctuation.	- Increase IR laser power. - Spinning the sample. - Increase the activity of the fluorescent sample.

3. Materials and methods

3.1. Deferiprone-Iron (III) separation and interaction studies

3.1.1. LC/MS method

3.1.1.1. Chemicals and reagents

Deferiprone, ferric chloride hexahydrate $FeCl_3.6(H_2O)$ were purchased from Sigma Aldrich (Steinheim, Germany). Ammonium hydroxide, methanol, ammonium formate (HPLC grade), and sodium hydroxide (analytical grade) were purchased from Merck (Darmstadt, Germany). PTFE filters (0.2 µm) were obtained from Agilent (Agilent Technologies, Germany). Ultra-pure water (resistivity > 18 $M\Omega.cm^{-1}$ at 25°C and TOC < 5 ppb) was obtained from Arium™ pro ultrapure water system (Sartorius, Goettingen, Germany).

3.1.1.2. Instrumentation

Chromatographic analyses were performed using Agilent 1200 LC/MS system (Agilent Technologies, Waldbronn, Germany) equipped with a quaternary pump, autosampler with controlled tray thermostat, column heater, and photodiode array detector as well as 6120 series single quadrupole mass spectrometer (Agilent Technologies, Waldbronn, Germany). All data processing was carried out using Agilent Chemstation software (Agilent Technologies, Waldbronn, Germany).

3.1.1.3. LC/MS conditions

Chromatographic separation was achieved on high-resolution monolithic column Chromolith™, Speed ROD RP-18e (100 mm x 4.6 i.d.) made from a single rod of high-purity monolithic silica, (Merck, Darmstadt, Germany) equipped at room temperature (25°C). The stationary phase is stable within a pH range from 2.0 to 8.0. The mobile phase was pumped with a gradient elution program using three lines (A- ammonium formate buffer (pH 7.4; 10 mM), B- water, and C- 10% methanol) and was delivered at a flow rate of 1.0 mL min−1 according to the following programs: 0.0–0.5 min (10% A, 80% B), 0.5–2.5 min (10% A, 70% B), 2.5–3.0 min (80% A, 10% B), 3.0–4.5 min (70% A, 20% B), and 4.5–5.5 min (10% A, 80% B). Each component of the mobile phase was degassed before use in an ultrasonic bath for 10 min. Ionization was conducted in the positive mode with a gas temperature of 350°C, a nebulizing gas pressure of 35 psi, a capillary voltage of 3000 V, and a fragmentor voltage of 100 V for each analyte. Nitrogen was used as both nebulizer and drying gas at a flow rate of 10 L min^{-1}. MS identification was performed under mass scanning mode which allows working in a mass range from 10 to 1500 m/z ratio.

3.1.1.4. Samples preparation

In the LC/MS method, the primary stock solution of CP20 (10 mM) was prepared in water by dissolving 0.0139 g in a 10 mL volumetric flask. Further dilutions were conducted to prepare 0.5, 0.7, 0.9, 1.1, 1.3, 1.5, 1.7, and 1.9 mM of standard solutions for calibration measurements. $FeCl_3.6\ H_2O$ (10 mM) stock solution was prepared by dissolving 0.027 g in water. For binding study, Fe/CP20 mixtures of 1:2, 1:2.8, 1:3.6, 1:4.4, 1:5.2, 1:6, 1:6.8, and 1:7.6 were prepared by aliquoted of a proper amount of CP20 (range of 0.5–2 mM) to mix with fixed concentration of Fe^{3+} ion (250 µM) then complete the volume with 10 mM ammonium formate buffer at pH 7.4. All samples were left to stand for 5 min to equilibrate. The working standard solutions were freshly prepared every week and stored in amber bottles at 4°C.

3.1.2. CE/FA Method

3.1.2.1 Chemicals and reagents

Deferiprone, ferric chloride hexahydrate $FeCl_3.6(H_2O)$, and sodium tetraborate decahydrate $Na_2B_4O_7.10(H_2O)$ were purchased from Sigma Aldrich (Steinheim, Germany). Sodium hydroxide (analytical grade) were purchased from Merck (Darmstadt, Germany). Hydrochloric acid (HCl) was obtained from Fluka (Buchs, Switzerland). PTFE filters (0.2 µm) were obtained from Agilent (Agilent Technologies, CA, USA). Ultra-pure water (resistivity > 18 $M\Omega.cm^{-1}$ at 25°C and TOC < 5 ppb) was obtained from Arium™ pro ultrapure water system (Sartorius, Goettingen, Germany).

3.1.2.2. Instrumentation

Electrophoretic analyses were achieved using Agilent G1600AX Capillary Electrophoresis System (Agilent Technologies, Waldbronn, Germany) equipped with a diode-array UV–Vis detection system. The analyses were carried out in a 75 µm I.D., 375 µm O.D. uncoated fused silica capillary with a length of 48.5/8.5 cm (Ltot/Leff) from Polymicro Technologies (Phoenix, AZ, USA) thermostated at 25°C. Data were collected and analyzed using the software ChemStation (Agilent Technologies) and Microsoft Excel.

3.1.2.3. CE/FA conditions

CE analyses were carried out using short-end injection mode. The samples were injected hydrodynamically into the capillary by placing the vial with the sample at the outlet and the vial with the buffer at the inlet and then by applying a negative pressure of 10 mbar for 50 s at the inlet. An operational voltage of 10 kV was applied in negative polarity mode, and the detection wavelength was set to 280 nm. Before the first use, the new capillary was conditioned by rising with 1 M NaOH for 20 min and then BGE for 20 min. At the beginning of each measuring day, the capillary was conditioned by rinsing with 1 M NaOH for 15 min followed by BGE for 15 min;

between runs, the capillary was conditioned by rinsing with BGE for 0.5 min, 1 M NaOH for 2.5 min, and again BGE for 1.5 min. All rinsing steps were achieved with a pressure of 950 mbar at 25°C.

3.1.2.4. Samples preparation

All stock and sample solutions were prepared in 20 mM borate buffer which is also used as BGE. BGE was prepared by dissolving 0.763 gm of sodium tetraborate decahydrate ($Na_2B_4O_7 \cdot 10\ H_2O$) in 80 ml of water then adjust pH to 10.5 with 1 M NaOH. The volume was then completed to 100 ml with water. The primary stock solution of CP20 (10 mM) was prepared in BGE by dissolving 0.0139 g in a 10.0 mL volumetric flask. Thereafter, further dilutions were conducted to prepare different concentrations in the range of 40–240 μM for calibration measurements. $FeCl_3.6(H_2O)$ (100 mM) stock solution was prepared by dissolving 0.27 g into water. Every day, the stock solution was diluted with BGE to obtain 10 mM, which was then used for preparation of the calibration and the mixture samples. The mixed samples contain a final fixed concentration of Fe^{3+} ion (60 μM) and different concentrations of CP20 in the range of 60–400 μM, dissolved in BGE. The complex was left to stand for 5 min to equilibrate and then injected to the CE instrument.

3.2. Deferiprone-essential metal ions interaction studies

3.2.1. MST Method

3.2.1.1. Chemical and reagents

Deferiprone, $FeCl_3.6(H_2O)$, $ZnCl_2$, $NiCl_2.6(H_2O)$, $MnCl_2$, $CuCl_2.2(H_2O)$, $CoCl_2.6(H_2O)$, $MgCl_2$, $CaCl_2$, 2-Amino-2-(hydroxymethyl) propane-1,3-diol (Tris) buffer were purchased from Sigma Aldrich (Steinheim, Germany). Hydrochloric acid (HCl), sodium hydroxide (NaOH) were purchased from Merck (Darmstadt, Germany). Ultrapure water was obtained from Arium^{TM}pro ultrapure water system (Sartorius, Goettingen, Germany).

3.2.1.2. Instrumentation

The Monolith NT.115 LabelFree^{TM} MST instrument (NanoTemper Technologies, Munich, Germany) was used to measure the binding events. MST instrument was equipped with a capillary tray allowing for the successive measurement of 12 samples in each run using standard glass capillaries. The MST instrument was supplemented with NT Analysis software provided by NanoTemper Technologies.

3.2.1.3. MST conditions

The MST experiment was performed on a label-free system, which depends on the intrinsic fluorescence of one interacting partner. MST scanning was conducted first to optimize the MST conditions. During MST optimization, LED intensity was set at 50% excitation intensity and MST power at 20% power. All samples were loaded in the standard MST capillaries and the total analysis time for each experiment was about 10 min. For each measurement, a total laser on/off cycle of 35 sec was set, which involves 30 sec on and 5 sec off. Fluorescence detection has been carried out at excitation wavelength 280 nm and emission wavelength at 360 nm.

3.2.1.4. Sample preparation

Tris buffer (0.1M) was prepared by dissolving 12.114 g of powder in water, and then adjusting pH to 7.4 and completing the volume with water to 1000 ml total volume using volumetric flask. The obtained solution was used as a diluent for further metal ions and CP20 serial dilutions. A solution of 1 mM of each metal ion was prepared first by dissolving a calculated amount of metal salts in water to ensure metal solubility, and then completing the total volume with 0.1 M Tris buffer to 10 ml total volume. CP20 was prepared by dissolving 0.0139 g of the standard powder in water to obtain 10 mM stock solution. All stock solutions were stored in a dark box and refrigerated at 4 ^{o}C.

MST scanning experiment have been carried out using three different concentrations of CP20 (500, 250, and 100 µM) and 500 µM of each metal ion were prepared by dilute aliquoted volumes from stock solutions using 0.1 M Tris buffer, and the obtained solutions were used for

MST scanning to investigate the fluorescence activity of the interacting components. Subsequently, MST titration conducted by preparing 12 different samples for each measurement that contained CP20/metal ion complexes, whereas 100 µM of CP20 titrated against different serial concentrations of intended metal ions in the range from 0.048 to 100 µM. The components were mixed well in PCR vials using 1:1 serial dilution and left for 30 min to equilibrate before measuring in the MST instrument.

3.2.2. ESI-MS method

3.2.2.1. Chemicals and reagents

Deferiprone, $FeCl_3.6(H_2O)$, $ZnCl_2$, $NiCl_2.6(H_2O)$, $MnCl_2$, $CuCl_2.2(H_2O)$, $CoCl_2.6(H_2O)$, $MgCl_2$, $CaCl_2$, and ammonium acetate buffer (CH_3COONH_4) were purchased from Sigma Aldrich (Steinheim, Germany). Ammonium hydroxide solution (NH_4OH) 25% were purchased from Merck (Darmstadt, Germany). PTFE filters of 0.2 µm was obtained from Agilent (Agilent Technologies, Waldbronn, Germany). Ultrapure water was obtained from Arium^{TM} pro ultrapure water system (Sartorius, Goettingen, Germany).

3.2.2.2. instrumentation

ESI-MS analyses were performed on an Agilent 6120 single quadrupole mass spectrometer (Agilent Technologies, Waldbronn, Germany). The instrument was equipped with ESI source and processed in positive ion mode with selected ion monitoring or mass scanning, which allows to work with a mass range from 10 to 1500 m/z ratio.

3.2.2.3. ESI-MS conditions

ESI-MS was used as a complementary technique to confirm the interaction and binding stoichiometry. The samples were directly infused into the ion source through the instrument syringe pump (10 µl min^{-1}). ESI-MS conditions were optimized as follows: Capillary voltage 3000 V (positive polarity), drying gas temperature 300ºC, nebulizer pressure 35 psi, and fragmentor voltage 100 V.

3.2.2.4. Samples preparations

In ESI-MS experiment, metal–CP20 complexes were prepared in a fixed ratio of 1:5 with an excess CP20 concentration to avoid system contamination by metal ions. Moreover, 200 µM of each metal ion was mixed with 1 mM of CP20, and then the volume was completed with ammonium acetate buffer at pH 7.4 to the total final volume of 10 ml. All samples were left in dark for 30 min to equilibrate. Thereafter, the samples were filtrated using PTFE 0.2 µm filter and injected directly to MS.

3.3. Deferiprone-human serum albumin interaction studies

3.3.1. CE based methods

3.3.1.1. Chemicals and reagents

Deferiprone and human serum albumin (HSA) (>97%, essentially fatty acid free, lyophilized powder), Acetanilide were purchased from Sigma Aldrich (Steinheim, Germany). Potassium phosphate buffer as monobasic and dibasic, Sodium phosphate buffer as monobasic and dibasic, were purchased from Merck (Darmstadt, Germany). sodium hydroxide (NaOH) were purchased from Merck (Darmstadt, Germany). Ultrapure water was obtained from Arium^{TM} pro ultrapure water system (Sartorius, Goettingen, Germany).

3.3.1.2. Instrumentation

Electrophoretic analyses were achieved using PrinceCE-C760 Capillary Electrophoresis System (Prince technologies, Netherland) equipped with a diode-array UV-Vis detection system. The analyses were carried out in a 50 µm I.D., 360 µm O.D. uncoated fused silica capillary with a length of 35/25.5 cm (L_{tot}/L_{eff}) (Polymicro Technologies AZ, USA) thermostated at 25°C. Data were collected and analyzed using Microsoft Excel.

3.3.1.3 CE/FA conditions

CE/FA analyses were carried out using long-end injection mode. The samples were injected hydrodynamically into the capillary by placing the vial with the sample at the inlet and the vial with the buffer at the outlet and then by applying a positive pressure of 50 mbar for 80 s at the inlet. An operational voltage of 15 kV was applied in the positive polarity mode, and the detection wavelength was set to 210 nm. Before the first use, the new capillary was conditioned by rising with 1 M NaOH for 20 min and water for 10 min then BGE for 20 min. At the beginning of each measuring day, the capillary was conditioned by rinsing with 1 M NaOH for 10 min, water 5 min, and BGE for 10 min; between runs, the capillary was conditioned by rinsing with 1 M NaOH for 2 min, water for 1 min and BGE for 2 min. All rinsing steps were achieved with a pressure of 1000 mbar at 25°C.

3.3.1.4. CE/FA samples preparations

All stock and sample solutions were prepared in 20 mM potassium phosphate buffer which used as BGE through using of two potassium phosphate salts. By weighting 0.5818 gm of dibasic potassium phosphate buffer (K_2HPO_4) then dissolved in 100 ml of water and 0.0678 gm of mono basic potassium phosphate buffer (KH_2PO_4) has been dissolved 100 ml of water. BGE was prepared in 100 ml volumetric flask by mixing of 23 ml of KH_2PO_4 and 77 ml of K_2HPO_4 and, adjusting the pH to 7.4. This solution has been also used as diluent for the samples. The stock solution of CP20 (10 mM) was prepared in BGE by dissolving 0.0139 g of CP20

in a 10 ml volumetric flask. Thereafter, further dilutions were conducted to prepare different concentrations in the range of 100–800 μM for calibration measurements. HSA 1 mM stock solution was prepared by dissolving 0.664 g of the protein in 10 ml BGE. For binding experiment, different concentrations of CP20 in range of 50-700 μM have been prepared in BGE then 150 μM of fixed concentration of HSA were added and the volume was completed to 1 ml with BGE. The complex was left to stand for 10 min to equilibrate and then injected in the CE capillary.

3.3.1.5 mACE conditions

All samples have been injected through long-end injection hydrodynamically at the inlet with positive pressure of 50 mbar (0.5 kPa) for 5 s. An operational voltage of 10 kV was applied in positive polarity mode, and the detection wavelength was set to 230 nm. Before the first use, the new capillary was conditioned by rising with 1 M NaOH for 20 min and H_2O for 10 min then BGE for 20 min. At the beginning of each measuring day, the capillary was conditioned by rinsing with 1 M NaOH for 10 min, H_2O 5 min, and BGE for 10 min; between runs, the capillary was conditioned by rinsing with 1 M NaOH for 2 min, H_2O for 1 min and BGE for 2 min. All rinsing steps were done with a pressure of 1000 mbar (95 kPa) at 25°C.

3.3.1.6. mACE Samples preparations

All stock solutions have been prepared as described in previous CE/FA methods (See section 3.3.1.4). Additionally, Acetanilide as EOF marker was prepared by dissolving of 0.0135 gm in 10 ml of BGE to obtain 10 mM stock solution.

In mACE binding experiment, different concentrations of CP20 in the range of 50-400 μM have been prepared in BGE and injected to the CE capillary. The injected sample consisted of 75 μM HSA and 1 mM acetanilide as EOF marker.

3.3.2. MST method

3.3.2.1. Chemicals and reagents

See section (3.3.1.1)

3.3.2.2. Instrumentation

The Monolith NT.115 LabelFree^{TM} MST instrument (NanoTemper Technologies, Munich, Germany) was used to measure the binding events. MST instrument was equipped with a capillary tray allowing for the successive measurement of 16 samples in each run using standard glass capillaries. For each measurement, a total laser on/off cycle of 35 sec was set, which involves 30 sec on and 5 sec off. The MST instrument was supported with NT Analysis software provided by NanoTemper Technologies.

3.3.2.3. MST conditions

The measurements have been carried out under the optimized MST conditions with LED power 50% (excitation power) and MST power 20% (laser power to induce thermophoresis). MST signals was obtained thorough 35 S of time scale where set laser on for 30 S to induce thermal diffusion followed by 5 S laser off for back diffusion state. Fluorescence detection has been carried out at excitation wavelength 280 nm and emission wavelength at 360 nm.

3.3.2.4. Sample preparation

Standard stock solutions have been prepared in 0.1 M phosphate buffer. Where, 2.209 gm of dibasic sodium phosphate buffer (Na_2HPO_4) and 0.3394 gm of monon basic sodium phosphate buffer (NaH_2PO_4) have been dissolved in 80 ml of H2O then, adjust pH to desired pH at 7.4 with NaOH and completed the volume with H_2O to obtain 100 ml of sodium phosphate buffer which used as diluent for the stock samples preparations and further serial samples dilution. CP20 10 mM was prepared through weighting of 0.0139 gm of reference standard powder and dissolved in 10 ml of 0.1 M sodium phosphate buffer. While, 100 μM of HSA standard solution has been prepared by dissolving 0.0664 gm of HSA standard powder in 10 ml of 0.1 M sodium phosphate buffer.

The working samples have been prepared according to 1:1 serial dilution of CP20 titrated partner with concentration range of 48 nM to 100 μM then, the fixed concentration of 1μM of fluorescent partner (HSA) has been added to each sample. The mixtures were kept stand for 10 min in dark area to equilibrate before MST measurement.

3.4. Deferiprone-human lactoferrin interaction studies

3.4.1 MST method

3.4.1.1 Chemicals and reagents

Deferiprone, human lactoferrin (Lf) 98% lyophilized powder and 2-Amino-2-(hydroxymethyl) propane-1,3-diol (Tris) buffer were purchased from Sigma Aldrich (Steinheim, Germany). Hydrochloric acid (HCl), sodium hydroxide (NaOH) were purchased from Merck (Darmstadt, Germany). Ultrapure water was obtained from Arium®pro ultrapure water system (Sartorius, Goettingen, Germany).

3.4.1.2. Instrumentation

The Monolith NT.115 LabelFree^{TM} MST instrument (NanoTemper Technologies, Munich, Germany) was used to measure the binding events. MST instrument was equipped with a capillary tray allowing for the successive measurement of 16 samples in each run using coated capillaries. For each measurement, a total laser on/off cycle of 35 sec was set, which involves 30 sec on and 5 sec off. The MST instrument was supplemented with NT Analysis software provided by NanoTemper Technologies. Fluorescence detection has been carried out at excitation wavelength 280 nm and emission wavelength at 360 nm.

3.4.1.3. MST conditions

The measurements have been carried out under the optimized MST conditions with LED power 40% (excitation power) and MST power 20% (laser power to induce thermophoresis). MST signals was obtained thorough 35 S of time scale where set laser on for 30 S to induce thermal diffusion followed by 5 S laser off for back diffusion state. Fluorescence detection has been carried out at excitation wavelength 280 nm and emission wavelength at 360 nm.

3.4.1.4. Samples preparations

Standard stock solutions have been prepared in 0.1 M tris buffer. Tris buffer was prepared by dissolving 1.2114 g of the powder in water, and then adjusting the pH to 7.4 with HCl and completing the volume to 100 ml with water. The obtained solution was used as a diluent for further stock and samples serial dilutions. CP20 10 mM was prepared through dissolving 0.0139 gm of the reference standard powder in 10 ml of 0.1 M tris buffer. While, 100 μM of Lf standard solution has been prepared by dissolving 0.084 gm of Lf standard powder in 10 ml 0.1 M tris buffer then, further dilution was made to reach 1 μM Lf standard solution.

The working samples have been prepared according to 1:1 serial dilution of CP20 titrated partner in a concentration range of 7 nM to 250 μM then, the fixed concentration of 120 nM of fluorescent partner (Lf) has been added to each sample. The mixtures were kept stand for 10 min in dark area to equilibrate before the MST measurement.

4. Results and Discussion

4.1. Deferiprone-iron (III) separation studies

4.1.1. LC/MS method

Analysis of metal complexes using LC is challenging because of weak system stability and possible dissociation of the complex during separation. This separation is of particular concern for complexes with weak binding affinities. However, the CP20-Fe binding system is relatively stable because Fe^{3+} is a hard Lewis acid that forms stable complexes over a wide pH range. The concentrations of Fe^{3+} and CP20 are critical for system stability because of the low denticity of CP20; therefore, in extremely dilute solutions ($<10^{6}$ M), the $Fe(CP20)_3$ complex is prone to dissociation [12,13]. Thus, the concentrations of the working solutions were kept close to the millimolar range (10^{3} M). Moreover, adding excess amounts of CP20 to the solution is necessary to maintain the equilibrium state. All chromatographic separations were performed at pH 7.4 to ensure that the system resembled physiological conditions as well as the stability of the complex during separation in the LC system. Under chromatographic conditions consisting of a mobile phase (10 mM ammonium formate:methanol 60:40) in isocratic elution, a high-resolution C18 monolithic column as the stationary phase under a controlled temperature at 25°C, and a flow rate of 1 ml/min, CP20 was determined successfully (Fig. 21 A). However, partial separation was obtained for the $Fe(CP20)_3$ complex (Fig. 21 B). Furthermore, mobile phase manipulations involving an increase or decrease in the organic modifier did not yield improvements in resolution between free CP20 and the $Fe(CP20)_3$ complex. Increasing the amount of methanol led to a decrease in separation and the analytes were eluted at the same retention time, whereas decreasing the amount of methanol led to improved separation. However, no complete separation was achieved. Replacement of methanol with acetonitrile as an organic modifier produced co-elution of many relevant peaks with CP20. Therefore, isocratic elution using a binary mixture of NH_4HCO_2 buffer and methanol as an organic modifier could be used to determine CP20, but it was not capable of yielding full separation between CP20 and its $Fe(CP20)_3$ complex.

The relevant peaks for both CP20 and the $Fe(CP20)_3$ complex were confirmed via MS scanning in the positive ion mode. A base peak at m/z 140 represented CP20, whereas a complex was formed at m/z 471.1, which represented the $Fe(CP20)_3$ complex. Furthermore, one significant peak at m/z 332, which represented the $Fe(CP20)_2$ complex, was formed in the medium and detected via the MS detector (Fig. 21 C).

In addition, the UV spectrum pattern was characteristic for the complex, including the presence of a broad absorption band at a maximum intensity of 450 nm. This band did not exist for CP20, confirming that the method achieved satisfactory discrimination between CP20 and its iron complex (Fig. 21 D and E).

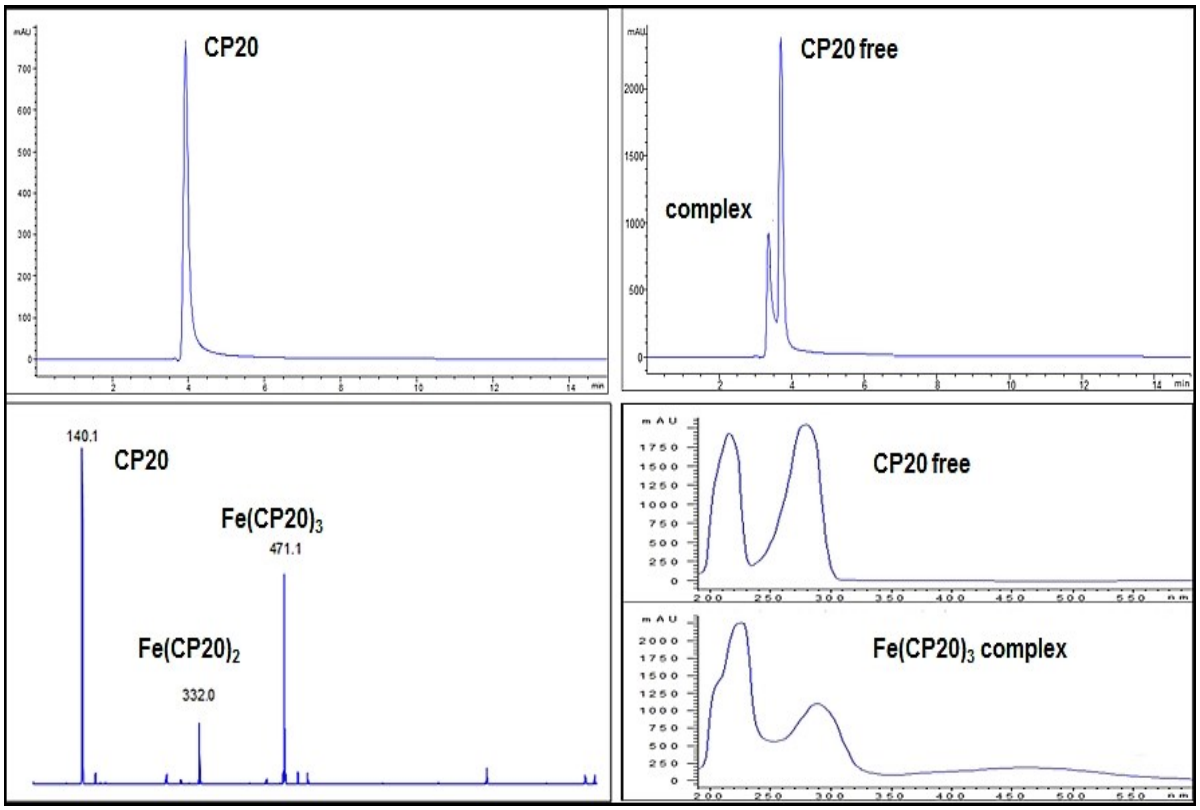

Fig. 21. LC chromatogram of CP20 (A), CP20 and the $Fe(CP20)_3$ complex using isocratic elution order (B). MS spectra of CP20 and its iron (III) complexes (C). UV spectra of free CP20 (D) and the $Fe(CP20)_3$ complex (E).

To improve chromatographic resolution between CP20 and the $Fe(CP20)_3$ complex, LC separation was investigated under different temperatures (25, 30, 37, and 40°C). As shown in Fig. 22, insignificant changes in complex formation were observed in response to temperature increases, whereas CP20 tended to form complexes at physiological temperatures. Conversely, the temperature changes did not improve separation between CP20 and the $Fe(CP20)_3$ complex.

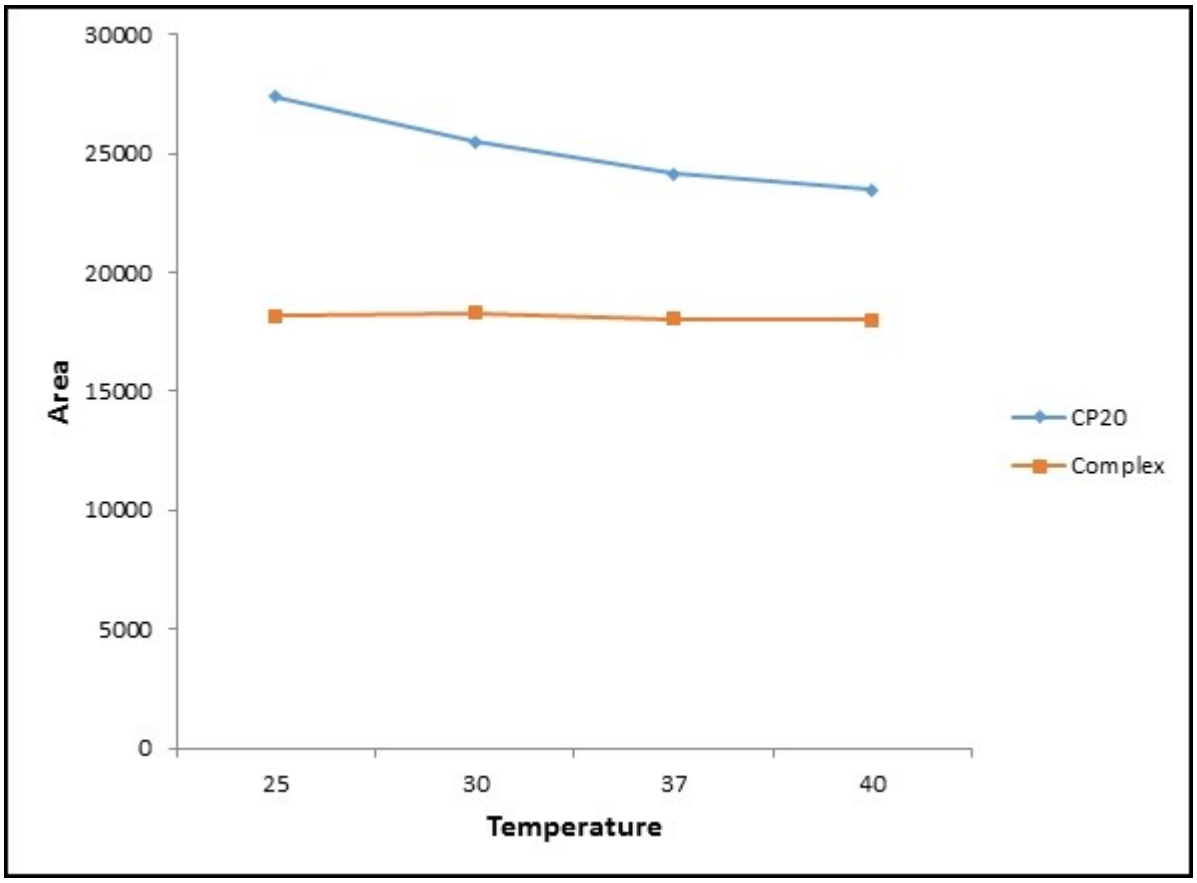

Fig. 22. Effect of temperature on CP20 and $Fe(CP20)_3$ complex formation.

To achieve complete separation between free CP20 and the $Fe(CP20)_3$ complex, isocratic elution was replaced with gradient elution using a mobile phase consisting of three components: (1) 10 mM NH_4HCO_2 buffer; (2) H_2O; and 10% methanol. The successful separation of free CP20 from the $Fe(CP20)_3$ complex might be attributable to the addition of a high water ratio (80%) and decreasing the methanol content to 10% in comparison to the composition of the isocratic elution. Obviously, the gradient system led to changes in the elution order for CP20, which was eluted before the $Fe(CP20)_3$ complex (Fig. 23).

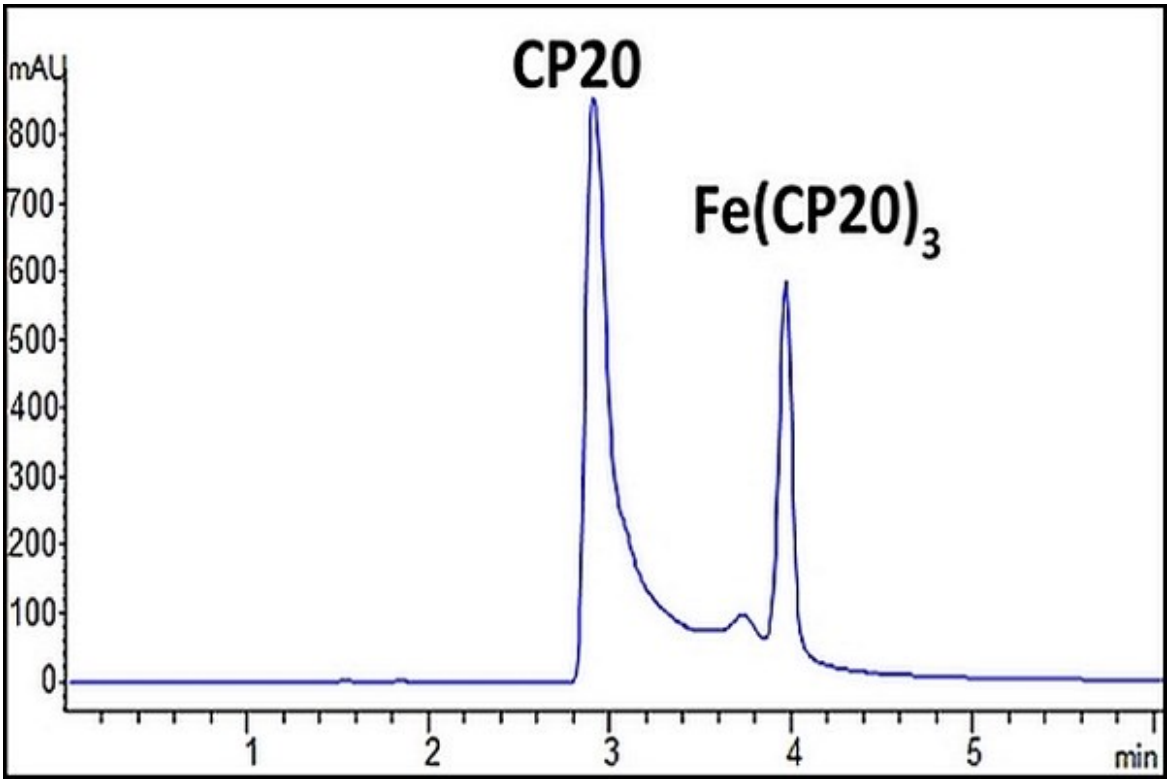

Fig. 23. LC chromatogram for the separation of CP20 and $Fe(CP20)_3$ complex using gradient elution.

Under these optimal conditions, a partial method validation was performed for the sample containing only CP20 without Fe^{3+} for calibration dependencies such as linearity, accuracy, repeatability, limit of detection (LOD), and limit of quantitation (LOQ), which were calculated from the calibration curve. Table 5 lists the parameters used in method validation for the LC/MS systems.

Table 5. Validation parameters of the developed LC/MS method

Detection	**UV detection** 280 nm **MS detection** m/z 140.1 for $[CP20 + H]^+$ m/z 332.1 for $[Fe(CP20)_2]^+$ m/z 471.1 for $[Fe(CP20)_3]^+$
Linearity range	0.5–2 mM
Regression equation	y = 0.3825x − 60.536
Correlation coefficient	0.998
Repeatability (RSD%)	<1.3
****LOD**	17 µM
*****LOQ**	53 µM
*RSD is the relative standard deviation, which is defined as SD/mean × 100 (n = 3). ** LOD is the limit of detection, which is defined as (3.3 × σ/slope). *** LOQ is the limit of quantification, which is defined as (10 × σ/slope).	

4.1.2. CE/FA method

In the CE system, the separation strategy is different from that of LC. The strategy depends on the separation of different ionizable molecules when traveling through the electrical current. Thus, several challenges were encountered when considering the separation of CP20. CP20 is a neutral molecule over a wide pH range (3.5–9.7). Thus, analysis at a physiological pH of approximately 7.4 is not possible using CE/FA techniques without modifying the system and adding additives to the background electrolyte (BGE), which complicates the system and potentially affects complex formation. Moreover, the complex is stable under varying neutral and alkaline pH conditions [12,13]. For this reason, the CE/FA study was performed in a borate buffer at pH 10.5, which permitted the maintenance of a stable complex and simultaneously stabilized the peak plateau of free CP20 (Fig. 24).

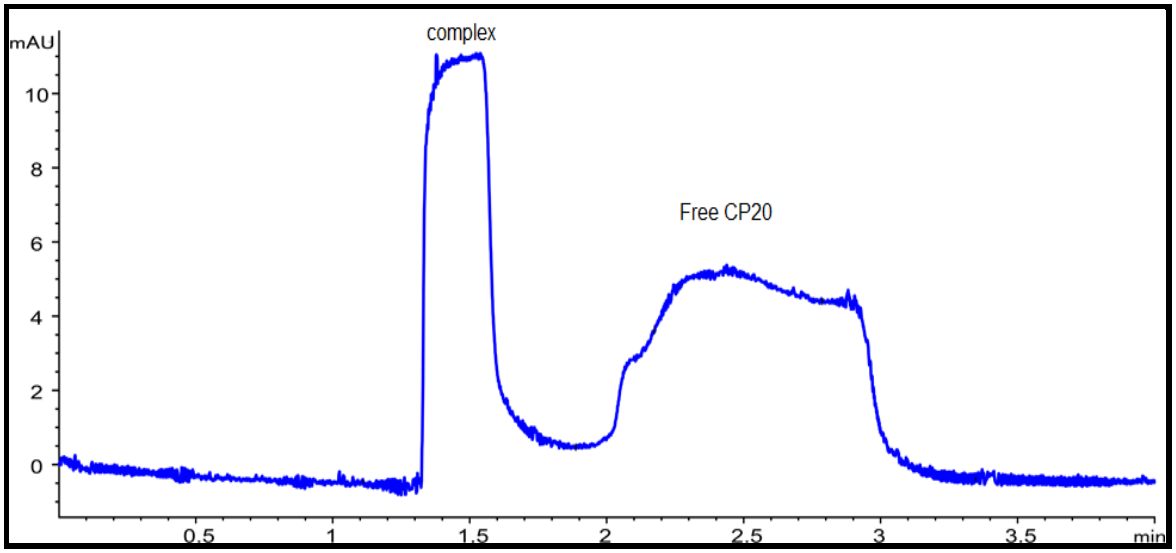

Fig. 24. CE/FA electropherogram of Fe-$(CP20)_3$ complex and free CP20.

Therefore, numerous washing procedures can be implemented to obtain a stable electropherogram with sufficient separation between free drug and the complex, thereby enabling proper estimation of the binding events. The rinsing protocol was performed using 1 M HCl, 0.1 M EDTA, 1 M NaOH, H_2O, and 20 mM borate buffer as a BGE. However, rinsing with EDTA worsened the electropherogram and led to distortion of the complex peak plateau. Moreover, the rinsing protocol using 1 M HCl in addition to NaOH was unsuitable, and lower peak resolution was obtained. Optimized rinsing procedures were obtained using 1 M NaOH for 2.5 min

followed by BGE for 1.5 min as a pre-run conditioning procedure and then flushing with BGE for 0.5 min as a post-run rinsing procedure (Fig. 25).

Pre-flushing	Post-flushing	Electropherogram
2.5 min 1M NaOH 1.5 min BGE	0.5 min BGE	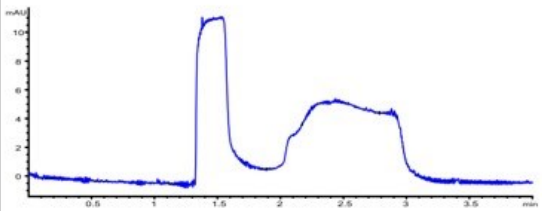
1.0 min 1M HCl 0.5 min H_2O 2.5 min 1M NaOH 1.5 min BGE	0.5 min BGE	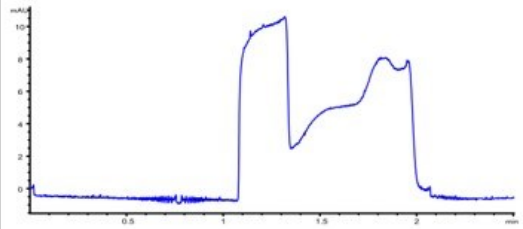
2.5 min 1M NaOH with 0.1M EDTA 1.5 min BGE	0.5 min BGE	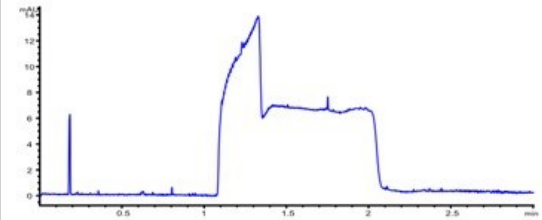
1.0 min 1M HCl 0.5 min H_2O 2.5 min 1M NaOH with 0.1M EDTA 1.5 min BGE	0.5 min H_2O	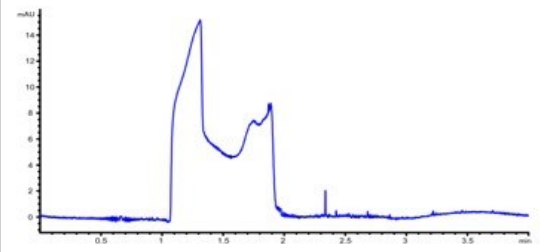

Fig. 25. CE/FA electropherograms for different capillary flushing procedures.

Moreover, a large plug injection using 10 mbar for 50 s is sufficient to keep the system in equilibrium in comparison to a small plug injection using 10 mbar for 5 s, which caused a decrease in the system's stability and affected the result's reproducibility. A short-end injection was applied using negative polarity, which proved sufficient for achieving peak separation with a short surface contact (~8.5 cm) in the CE/FA separation mode. The optimal applied voltage was 10 kV, which was obtained through manipulation at several applied voltages (5–15 kV) in the negative polarity mode. Because of the increase in applied voltage, the migration time and resolution decreased for the free drug and complex peaks (Fig. 26).

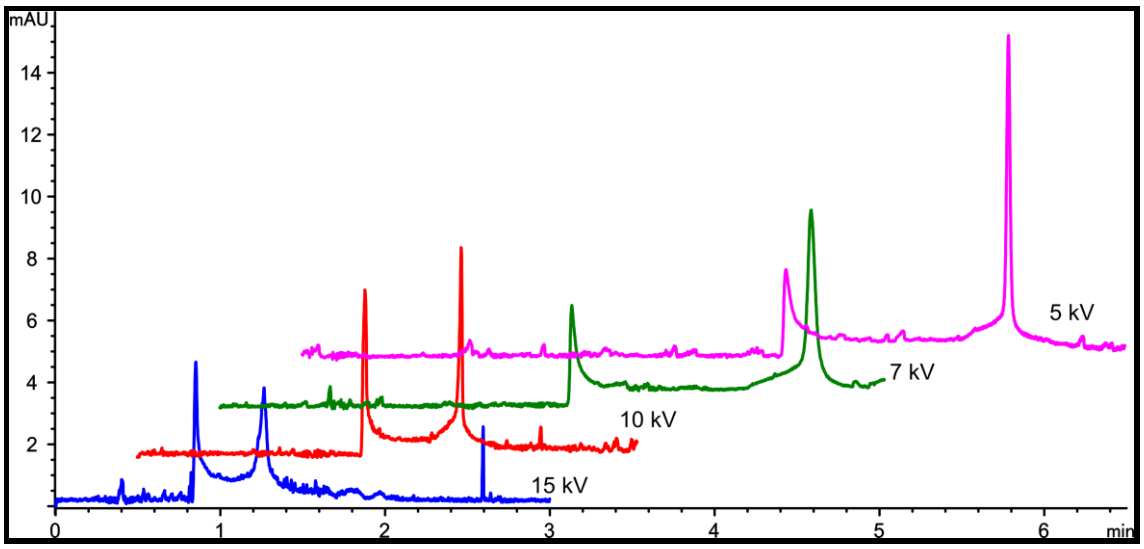

Fig. 26. Effect of different applied voltages on the separation of free CP20 from the $Fe(CP20)_3$ complex.

The developed method was partially validated for linearity, accuracy, and repeatability. Method linearity and accuracy were assessed using samples containing only CP20 without Fe^{3+}. Moreover, the repeatability test result was estimated as RSD%, whereas LOD and LOQ were calculated from the calibration curve. Table 6 lists the parameters under which the method was validated for the CE/FA systems.

Table 6. Validation parameters of the developed CE/FA method

Detection	**UV detection** 280 nm
Linearity range	40–240 µM
Regression equation	y = 0.0175x + 0.3774
Correlation coefficient	0.9986
Repeatability (RSD%)	<4.33
****LOD**	7.9 µM
*****LOQ**	24.0 µM
*RSD is the relative standard deviation, which is defined as SD/mean × 100 (n = 3). ** LOD is the limit of detection, which is defined as (3.3 × σ/slope). *** LOQ is the limit of quantification, which is defined as (10 × σ/slope).	

4.1.3. Estimation of binding events from separative methods

Estimation of the binding events for LC/MS and CE/FA data was performed using the same principle used to determine the free CP20 concentration. Both LC/MS and CE/FA successfully achieved good separation of free CP20 from the $Fe(CP20)_3$ complex with good reproducibility. The binding events were determined as the association constant (K_a), and all binding param-

eters were calculated using a nonlinear least-squares analysis (see section 2.1.3). Furthermore, the LC/MS method was performed using a binding constant of $LogK_a$ = 8.3 ± 0.17 and precision of RSD% <2.06 (Fig. 27 A). Meanwhile, the CE/FA method was optimized to estimate the binding constant as $LogK_a$ = 10.48 ± 0.12, which was in agreement with the reported values in the literature [12,13] with good precision as RSD% of <1.17 (Fig. 27 B).

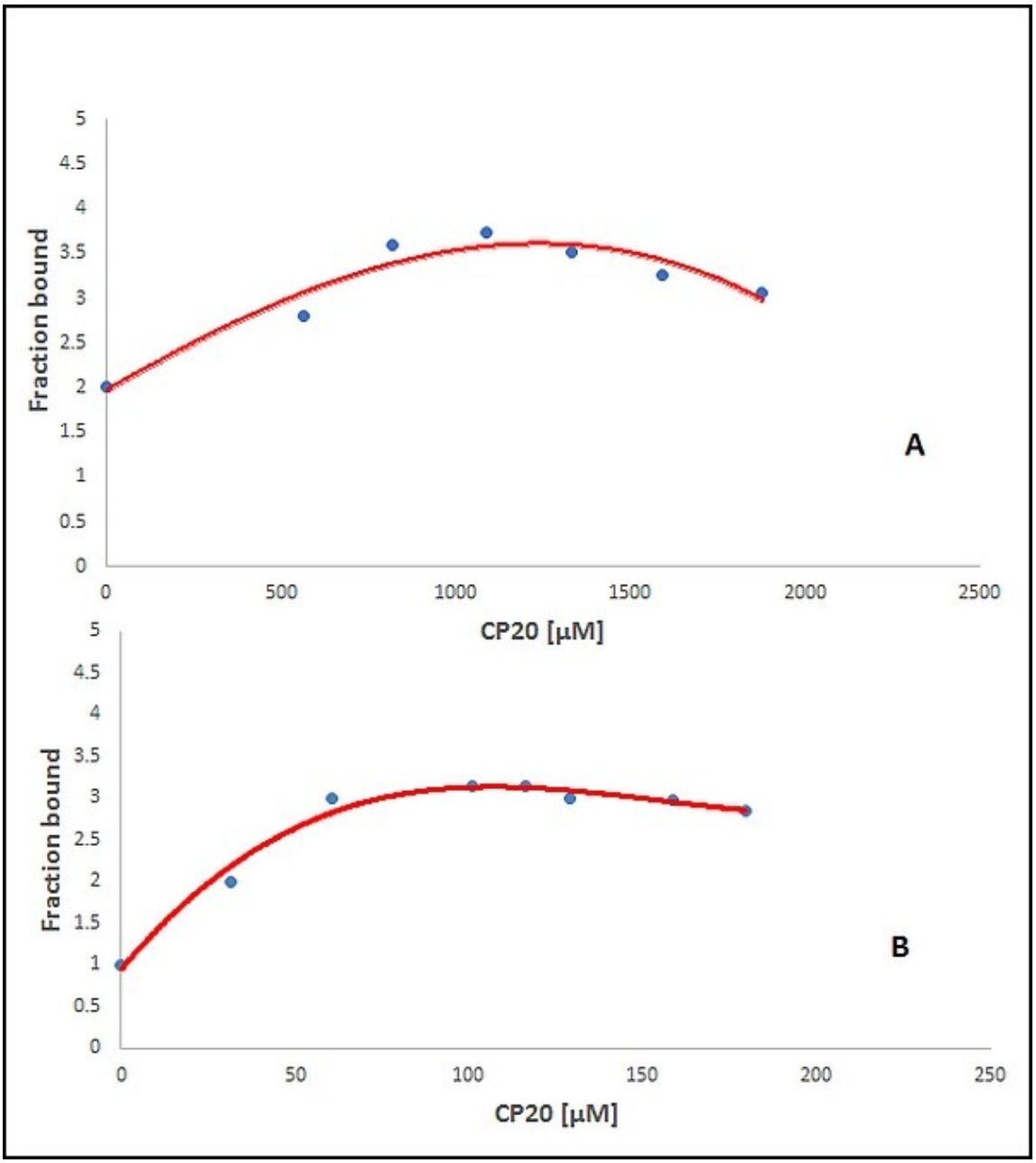

Fig. 27. Binding curves for the Fe-CP20 interactions, (A) Representative data obtained from the LC/MS, (B) Representative data obtained from the CE/FA.

Furthermore, the numbers of binding sites, n_i, were estimated to be 3.40 ± 0.65 and 3.04 ± 0.10 for the LC/MS and CE/FA systems, respectively. This finding approximately reflects the binding ratio in 1:3 Fe:CP20 stoichiometry, as confirmed using the MS detector in the LC/MS method. The estimated values of $LogK_a$ and n_i are summarized in Table 7.

The variations in the estimated binding constants between the two methods might be attributable to the use of different methods; thereby, numerous parameters, such as pH, the buffering system, and separation mechanism, could affect the binding. Although LC/MS is an attractive technique that provides direct information about the binding stoichiometry, it is not ideal for estimating the binding events because of the lack of complex stability during LC separation. Moreover, the method was less sensitive because a millimolar concentration range was used in comparison to micromolar range for the CE/FA method.

Table 7. Summary of the binding parameters for CP20 and its iron complex obtained using LC/MS and CE/FA methods

Methods	$LogK_a$ ± SD	$LogK_a$ repeatability (RSD%)	n_i ± SD	Literature values
LC/MS	8.31 ± 0.17	2.06	3.40 ± 0.65	10.11 [12,13]
CE/FA	10.48 ± 0.12	1.17	3.04 ± 0.10	

4.2. Deferiprone-essential metal ions interaction studies

4.2.1. MST and ESI-MS methods

The chelation selectivity is considered a major concern in chelation therapy. Thus, the ideal chelator should selectively bind with the targeted metal without affecting other essential metals [15]. In this regard, an additional step was included to evaluate the interaction of CP20 with the most important essential metal ions. However, this type of interaction is weak, and it cannot be achieved via using the separation techniques. Therefore, this study was designed to evaluate the use of MST for the rapid screening of the interaction of CP20 with essential metal ions. It is worth noting that the presence of the intrinsic fluorescence of CP20 has not been previously reported. Meanwhile, the intrinsic fluorescence of CP20 allowed the use of label-free MST. The pre-test MST scan indicated that CP20 was fluorescent at concentrations ≥100 μM; therefore, the fixed concentration of the fluorescent partner was 100 μM, which produced a sufficient fluorescence signal. Different concentrations of essential metal ions were prepared and titrated against the fixed concentration of CP20. The binding affinity of CP20 for essential metal ions varies widely. CP20 exhibited significant binding to Fe^{3+}, Cu^{2+}, Zn^{2+}, Co^{2+}, and Ni^{2+} (Fig. 28).

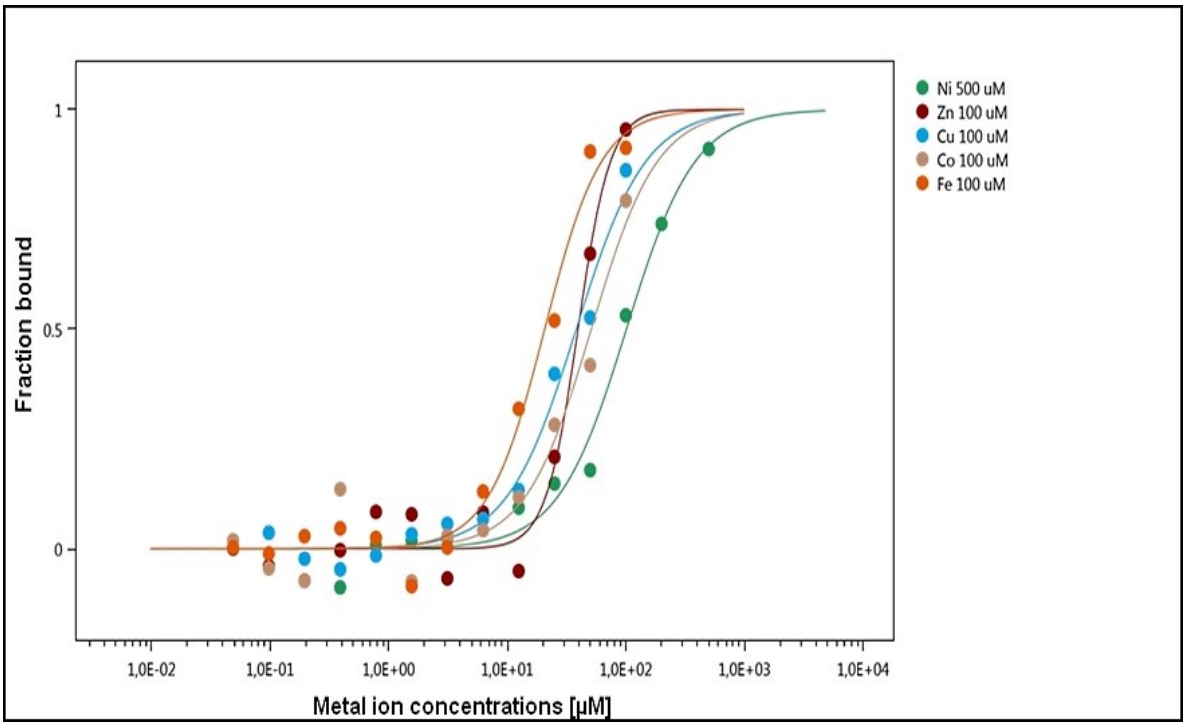

Fig. 28. Saturation curves for CP20 with different metal ions. The green curve represents Ni^{2+} ions, the brown curve represents Zn^{2+} ions, the blue curve represents Cu^{2+} ions, the gray curve represents Co^{2+} ions, and the red curve represents Fe^{3+} ions.

In this study, Fe^{3+} (Fig. 28 red) was more likely to bind to CP20 because of the higher oxidation state, which featured a hard Lewis acid, in comparison to other divalent metal ions, and the estimated EC_{50} of this interaction was the lowest among the metal ions (20 ± 3.34 μM). Table 8 presents a summary of the MST results for CP20 with the tested essential metal ions.

Table 8. MST binding parameters for CP20 with essential metal ions

Metal ion	EC_{50}± SD [a]	Hill Coefficient [b]
Fe^{3+}	20.6 ± 3.34	1.50
Cu^{2+}	38.1 ± 3.39	3.19
Zn^{2+}	39.5 ± 4.90	1.48
Co^{2+}	51.1 ± 6.86	1.56
Ni^{2+}	101.1 ± 22.70	1.81
Mn^{2+}	-	-
Mg^{2+}	-	-
Ca^{2+}	-	-

[a] EC_{50} is defined as the concentration of the half-maximal response.

[b] Hill coefficient was calculated using equation (6) in section 2.2.1.3.

Meanwhile, the ESI-MS results indicated that theCP20 alone displayed a 100% base peak at m/z 140 (Fig. 29 A) while, the $Fe(CP20)_3$ complex was formed at m/z 471, confirming the binding stoichiometry for the complex in a 1:3 Fe:CP20 ratio with a significant relative abundance of 25%. Concomitantly, another molecular ion peak with a relative abundance of 10% was noted at m/z 332. This peak represented the $Fe(CP20)_2$ complex, and minor dissociation might have occurred under MS condition (Fig. 29 B).

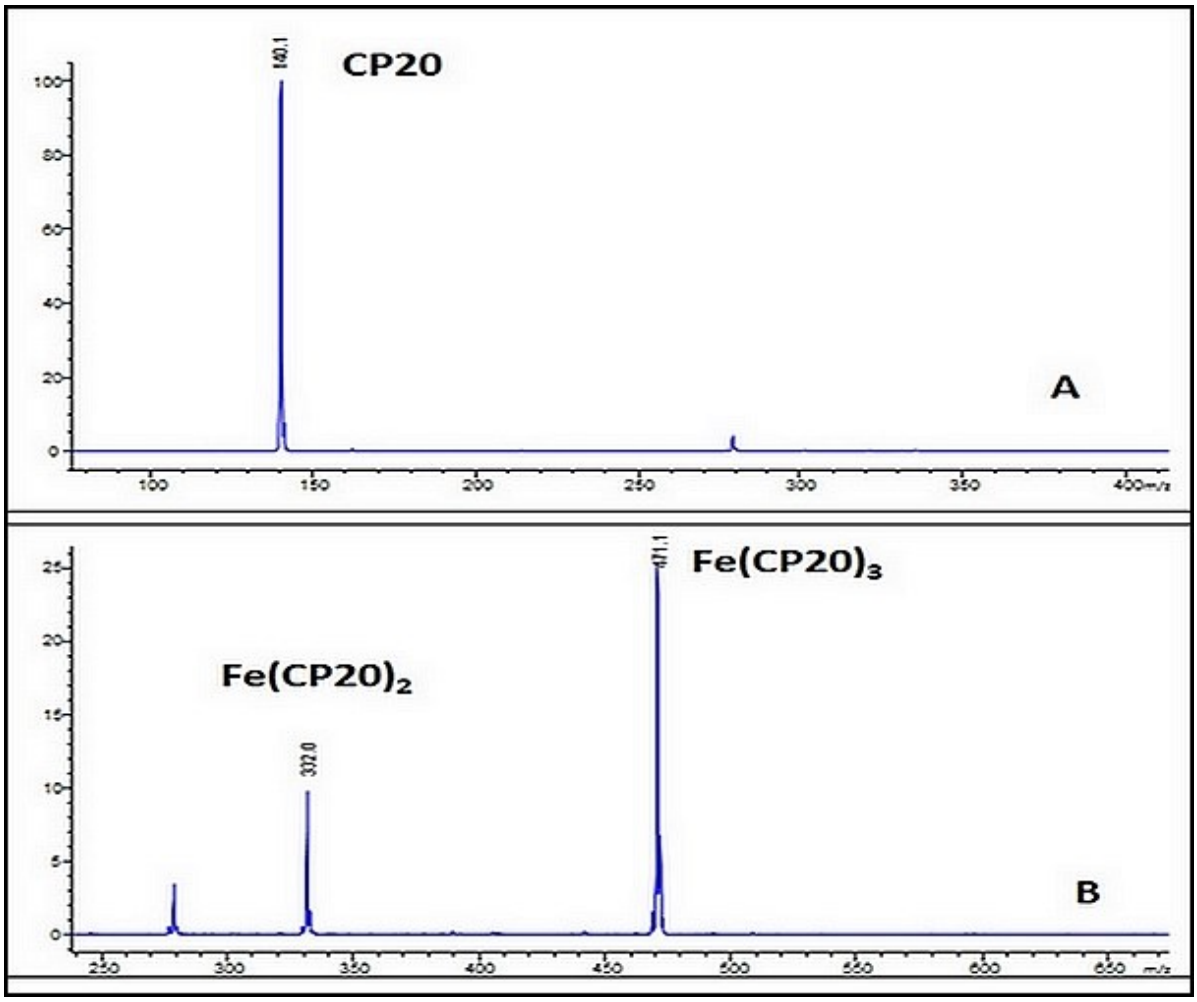

Fig. 29. MS spectra for free CP20 (A). MS spectra for $Fe(CP20)_2$ at m/z 332 and $Fe(CP20)_3$ at m/z 471 (B).

The divalent metal ions exhibited different interaction behaviors with CP20. Cu^{2+} (Fig. 28 blue) and Zn^{2+} (Fig. 28 brown) have similar affinities for CP20 under MST conditions with estimated EC_{50} values of 38.17 ± 3.39 and 39.51 ± 4.90 µM, respectively. In comparison to Fe^{3+}, a 2-fold excess was needed to achieve a half-maximal effect, reflecting the tendency of CP20 to more readily bind with Fe^{3+} than with Cu^{2+} and Zn^{2+}. However, the ESI-MS results for the Cu^{2+} and Zn^{2+} complexes illustrated that Cu^{2+} formed a stable $Cu(CP20)_2$ complex at m/z 340 with a relative abundance of 6% (Fig. 30 A), whereas the $Zn(CP20)_2$ complex was formed at m/a 341 with a 1.5% relative abundance (Fig. 30 B).

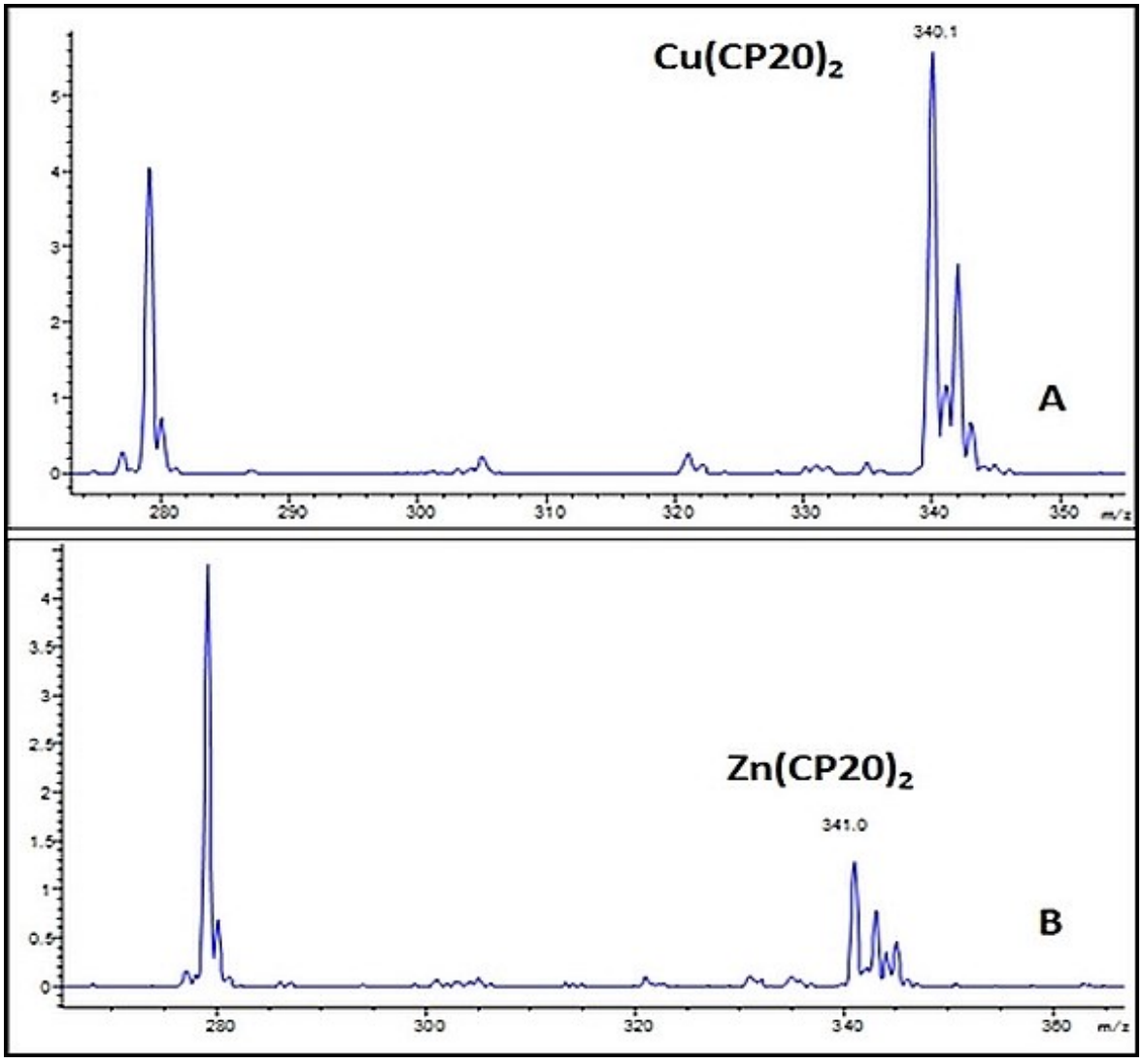

Fig. 30. MS spectra of the $Cu(CP20)_2$ complex at m/z 340 (A) and $Zn(CP20)_2$ complex at m/z 341 (B).

Indeed, the MST and ESI-MS results confirmed that Cu^{2+} and Zn^{2+} are more affected by CP20 chelation among divalent metal ions, and this finding is consistent with previous reports [9,12,133]. However, *in vivo* Zn^{2+} depletion is more obvious and clinically documented [38,134] than depletion of Cu^{2+}. Therefore, Zn^{2+} levels should be monitored, although Cu^{2+} is predicted to perturb Fe^{3+} speciation during CP20 treatment. On the contrary, Co^{2+} (Fig. 29 gray) and Ni^{2+} (Fig. 29 green) exhibited weak binding affinity for CP20 in comparison with the affinities of Cu^{2+} and Zn^{2+}. Although both metal ions displayed higher oxidation states and exhibited similar binding values as Zn^{2+} in a previous study [9], the MST results illustrated that a 2.5-fold excess of Co^{2+} was needed to achieve the Fe^{3+} EC_{50} (51.10 ± 6.86 µM), whereas a 5-fold excess was needed to achieve that of Ni^{2+} (101.09 ± 22.70 µM). Moreover, both Co^{2+} and Ni^{2+} formed weak complexes with CP20 with a relative abundance of <1.5% (Fig. 31 A and B). Therefore, the chelation effect of CP20 on Co^{2+} and Ni^{2+} is limited in comparison to that on Zn^{2+} and Cu^{2+}. This conclusion is consistent with a previous study that evaluated Co^{2+} and Ni^{2+} complex stability with CP20 and other synthesized hydroxypyridinones [135].

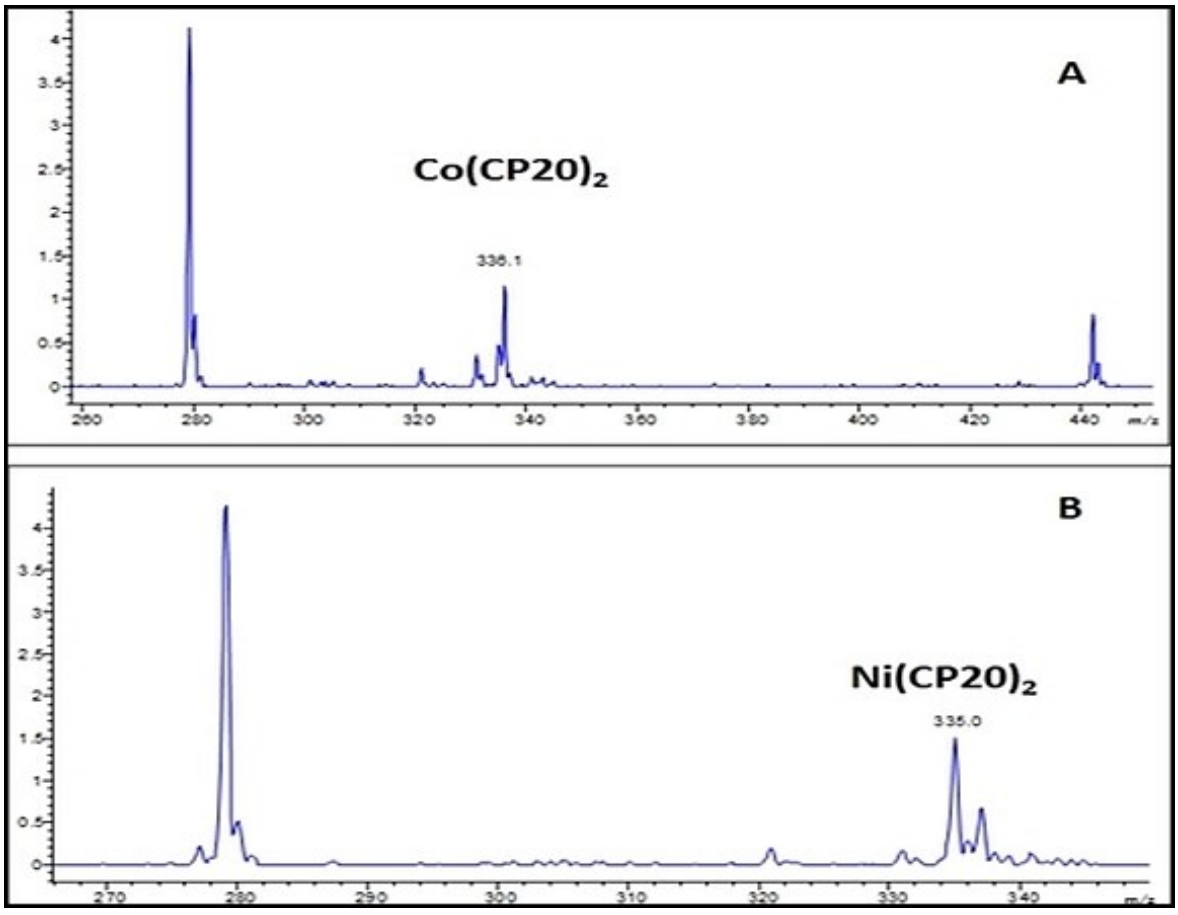

Fig. 31. MS spectra for the $Co(CP20)_2$ complex at m/z 336.1 (A) and $Ni(CP20)_2$ complex at m/z 335.0 (B).

Table 9 summarizes the m/z values for the investigated metal ion complexes based on positive ion mode scanning.

Table 9. ESI-MS data for CP20 and different essential metal ions

Metal ion	Molecular weight (g/mol)	Ligand	Molecular weight (g/mol)	m/z ratio
Ni^{2+}	58.69	CP20	139.1	335
Zn^{2+}	65.38			341
Cu^{2+}	63.54			340
Co^{2+}	58.93			336
Fe^{3+}	55.84			332, 471
Mn^{2+}	54.93			331
Mg^{2+}	24.30			300
Ca^{2+}	40.07			316

Mn^{2+} (Fig. 32 blue), Mg^{2+} (Fig. 32 brown), and Ca^{2+} (Fig. 32 green) did not exhibit any binding affinity for CP20 under the optimized MST conditions. Furthermore, the ESI-MS results confirmed that Mg^{2+} and Ca^{2+} do not form complexes with CP20.

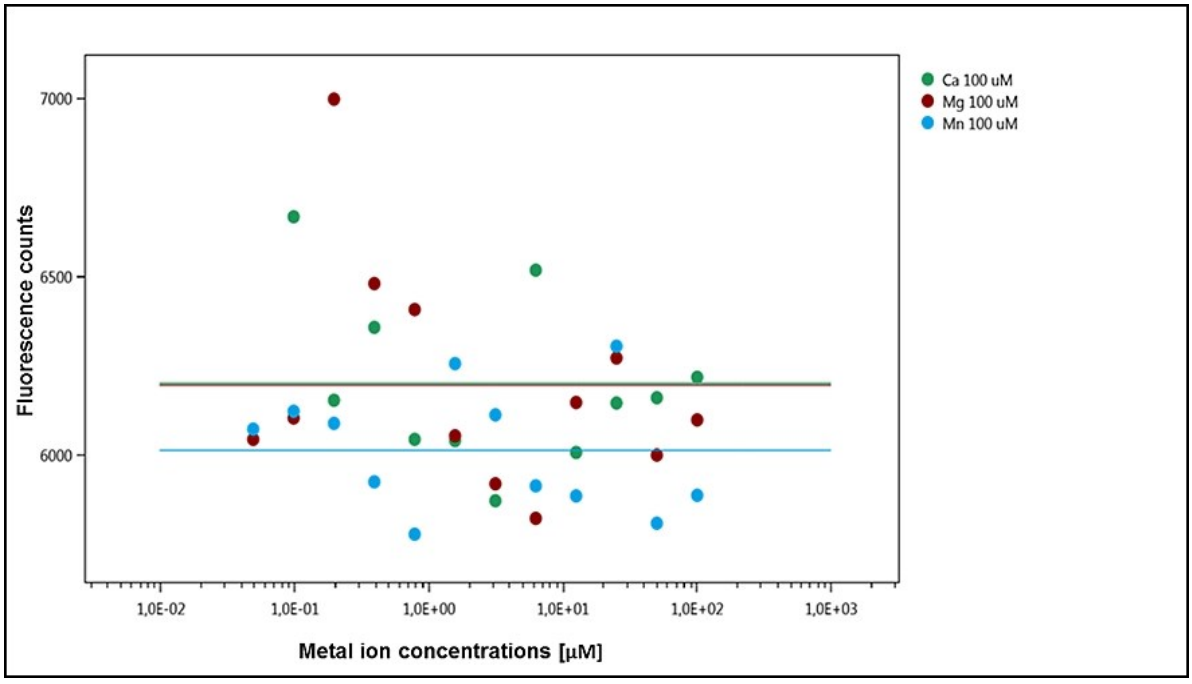

Fig. 32. Representative figure for nonbinding metal ions. Green dots represent Ca^{2+} ions, brown dots represent Mg^{2+} ions, and blue dots represent Mn^{2+} ions.

However, Mn^{2+} exhibited a different behavior in ESI-MS, producing a stable $Mn(CP20)_2$ complex at m/z 331 with a high relative abundance of 18% (Fig. 33). The different behavior of Mn^{2+} between MST and ESI-MS might be attributable to the experimental conditions of MST that prevent metal-ligand speciation in contrast with ESI-MS, which allowed CP20 to form a complex with Mn^{2+} the under gas phase state.

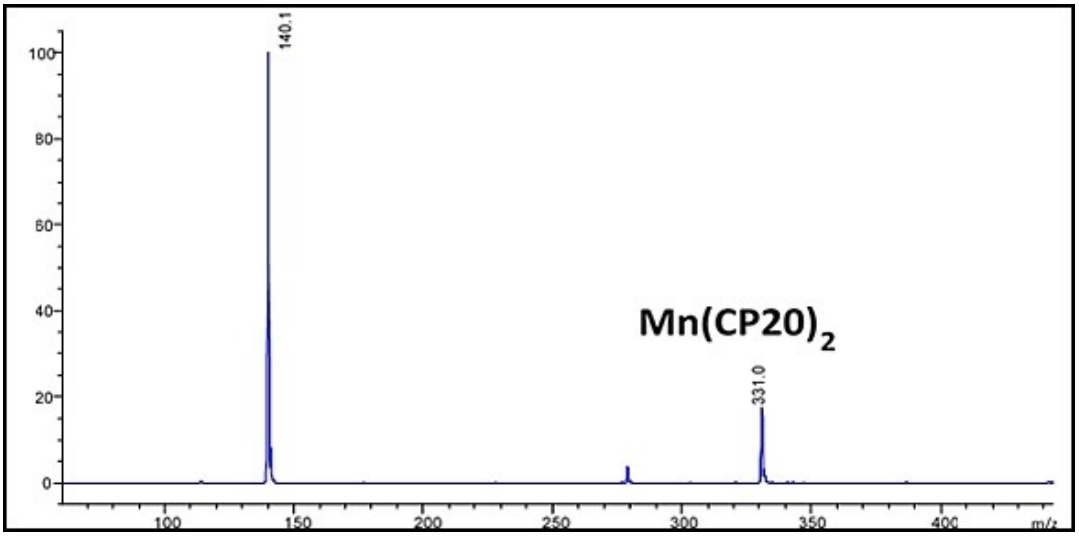

Fig. 33. MS spectra of the $Mn(CP20)_2$ complex at m/z 331.

4.3. Deferiprone-protein interaction studies

4.3.1. Deferiprone-human serum albumin interaction studies

4.3.1.1. MST method

In this study, the MST method was developed to quantify the binding events of CP20 with HSA. MST scanning was conducted for three different concentrations of CP20, HSA, H_2O, and phosphate buffer. Strong fluorescence signals were obtained for HSA depending on the intrinsic fluorophores present, such as tryptophan or tyrosine residues within the protein. MST measurements were recorded using a label-free MST system without the need for invasive procedures via protein labeling because the fluorescence signals obtained from CP20 and HSA are dissimilar. The signal obtained with 1 μM HSA was 10-fold larger than that obtained with 100 μM CP20. Thereafter, CP20 was serially diluted from 100 μM to 48 nM using a 1:1 dilution ratio titrated against a constant HSA concentration of 1 μM. Furthermore, no sample adsorption was indicated through capillary scan testing. The fluorescence intensity deviation for all measurements was within the limit of <10%.

The data were analyzed directly using Nanotemper software to obtain the binding curve. The obtained MST data was fit with the K_d calculation model (Fig. 34) and estimated as $LogK_a$ = 4.3 ± 0.59. The estimated binding constant using the MST method was in accordance with the previous published values [64]. The binding constants are summarized in Table 10 for all experiments concerning CP20-protein interactions.

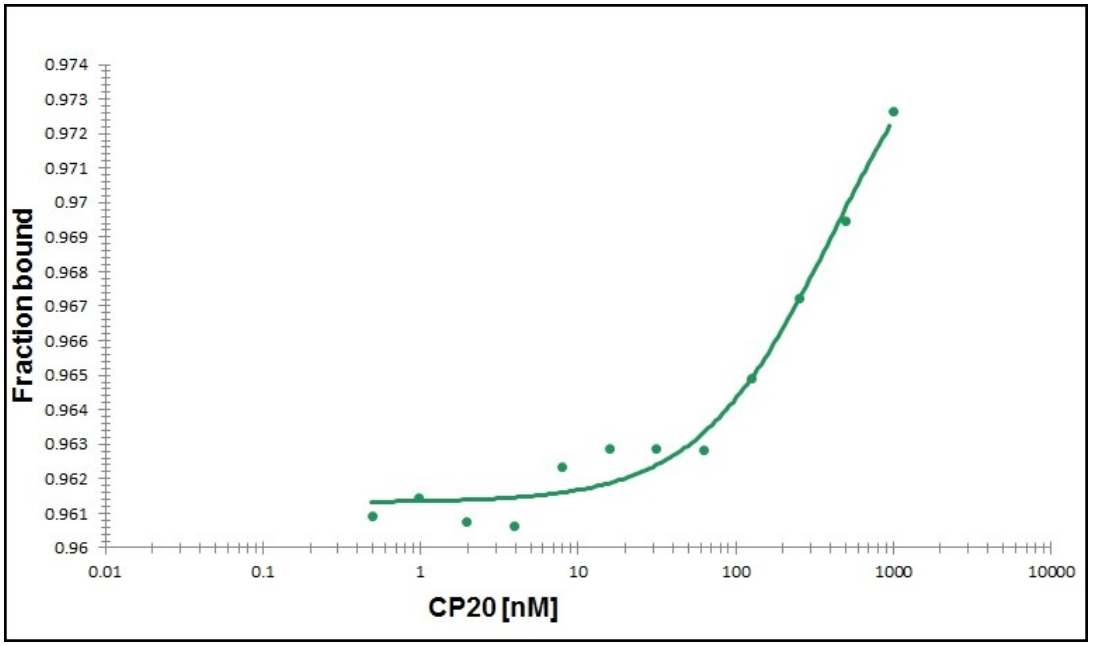

Fig. 34. The binding curve of CP20-HSA interaction using MST.

4.3.1.2. CE methods

The CE technique is characterized by the presence of several analytical modes for studying drug-protein interactions. This feature makes CE-based methods superior to all separative analytical techniques. In this approach, two CE modes were used to characterize the CP20-HSA interaction.

4.3.1.2.1. CE/FA mode

The CE/FA method was developed to characterize the CP20-HSA interaction. This mode was selected because it provided a highly stable system and it was robust CE mode for drug-protein interactions (see Table 1).

Under the optimal CE conditions as described in section 3.3.1.3, partial separation of CP20 from HSA was achieved through the formation of peak plateaus for CP20 and HSA as shown in Fig. 35. During the development of this method, the pre-equilibrated sample consisting of 150 µM HSA and 500 µM CP20 was injected for different time intervals (20–80 s) at 50 mbar. The frontal analysis system was obtained by injection a large plug sample for 80 s at 50 mbar. In this analysis, the binding equilibrium was maintained, and the binding events could be estimated.

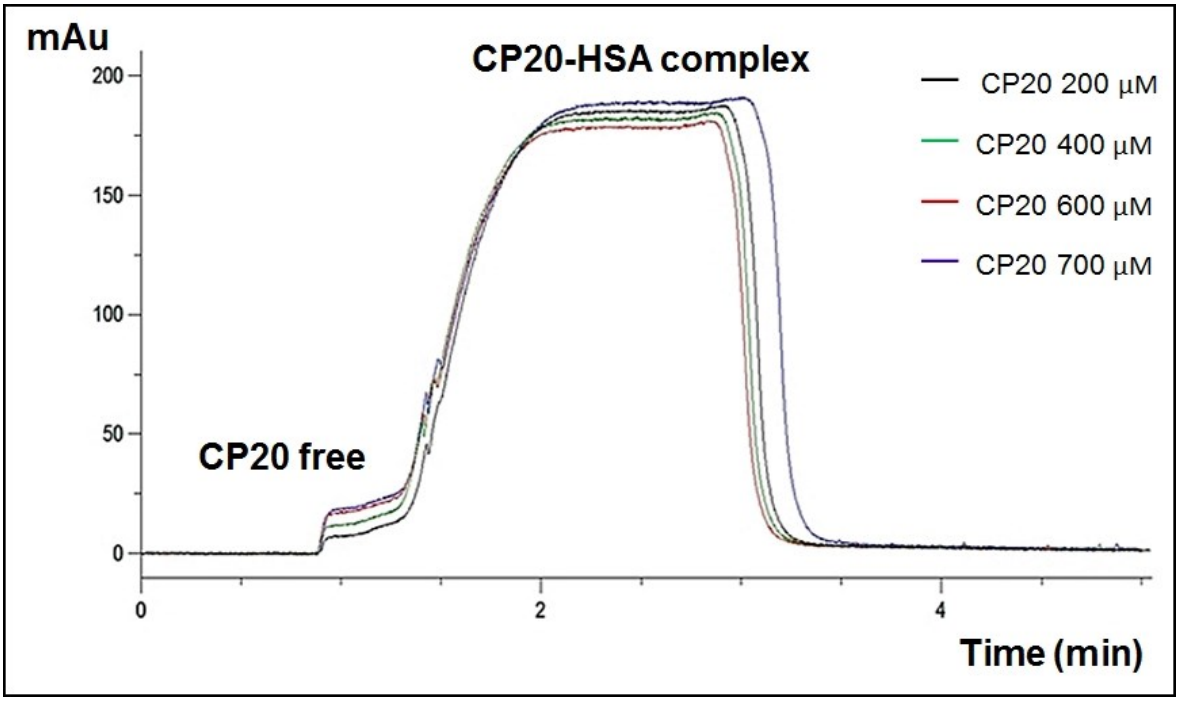

Fig. 35. Overlaid CE/FA electropherograms for CP20 and HSA, in which CP20 was injected at different concentrations (200, 400, 600, and 700 µM).

Meanwhile, CP20 at pH 7.4 is a neutral molecule; therefore, it is useful as an EOF marker for the CE system to monitor run-to-run variability. The binding events were estimated using an external CP20 calibration curve over a linear range (100–800 µM), and the drug-bound fraction was calculated by subtracting the free drug concentration that was obtained as an experimental response from the total drug concentration. The binding constant was estimated using nonlinear least-squares regression (see section 2.1.3), and a binding curve was obtained as presented in Fig 36. The binding constant was estimated as $LogK_a$ = 5.3 ± 0.28, and the number of binding sites was estimated as *ni* = 3.2 ± 2.0. All measurements were performed in triplicate.

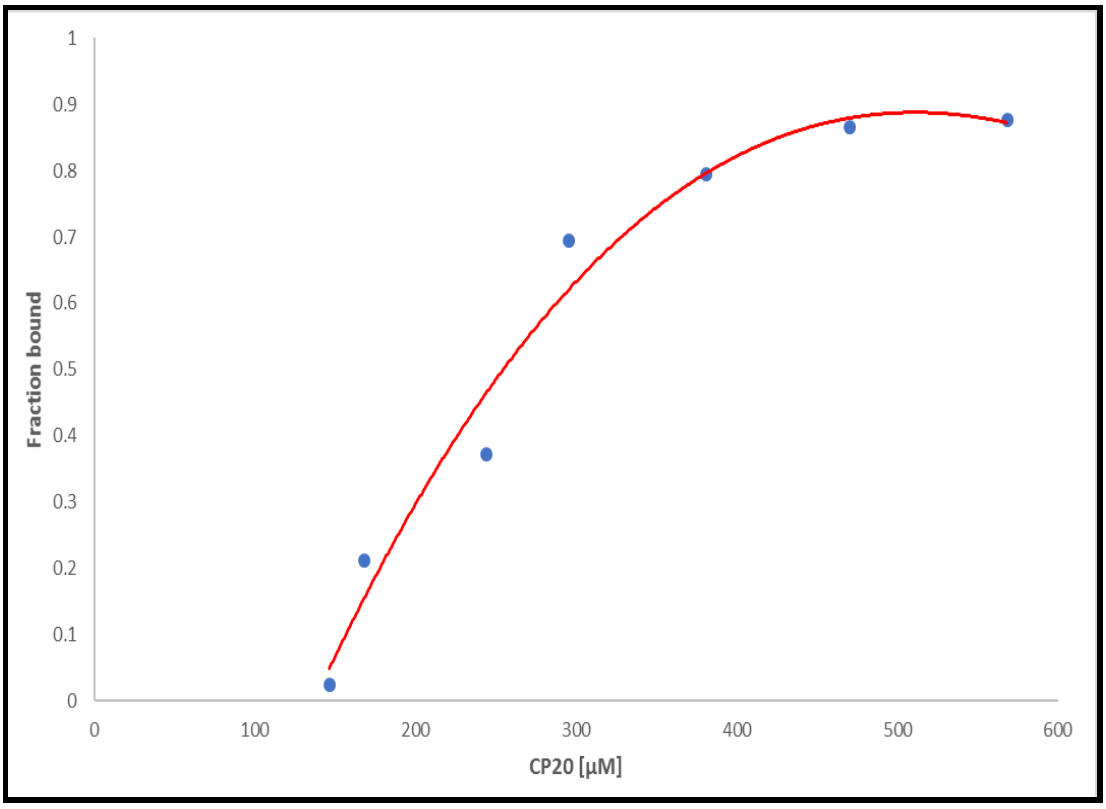

Fig 36. The binding curve of CP20-HSA using the CE/FA mode.

4.3.1.2.2. mACE mode

The mACE mode was selected in addition to the CE/FA mode as a comprehensive technique for studying the CP20-HSA interaction for several reasons as follows: (1) it has been widely and successfully used in the study of drug-protein interactions; (2) the instrumental response for estimating binding events was different from that of CE/FA, thereby presenting a different view of the binding system; and (3) it is extremely sensitive to weak interactions, and it can measure minute changes of the migration time up to 0.1 s [88,96,136]. In this approach, different CP20 concentrations were loaded into the capillary, and HSA was injected as the sample. This situation is opposite to the usual one because the mobility of CP20 is equal to that of the EOF marker, as both are neutral and have the same migration time. Moreover, HSA is charged at pH 7.4, and it could have been affected by its interaction with CP20 interactions because the mobility of HSA may have shifted. The capillary was pre-conditioned with different CP20 concentrations ranging from 50 to 400 µM and a fixed HSA concentration of 75 µM. The sample was mixed with 1 mM acetanilide acting as the EOF marker. The mobility of HSA shifted between 0.1 and 0.4 s in response to the macromolecular mobilities under the defined electrical field. This setup was sufficient to reveal the binding between CP20 and HSA as shown in Fig. 37.

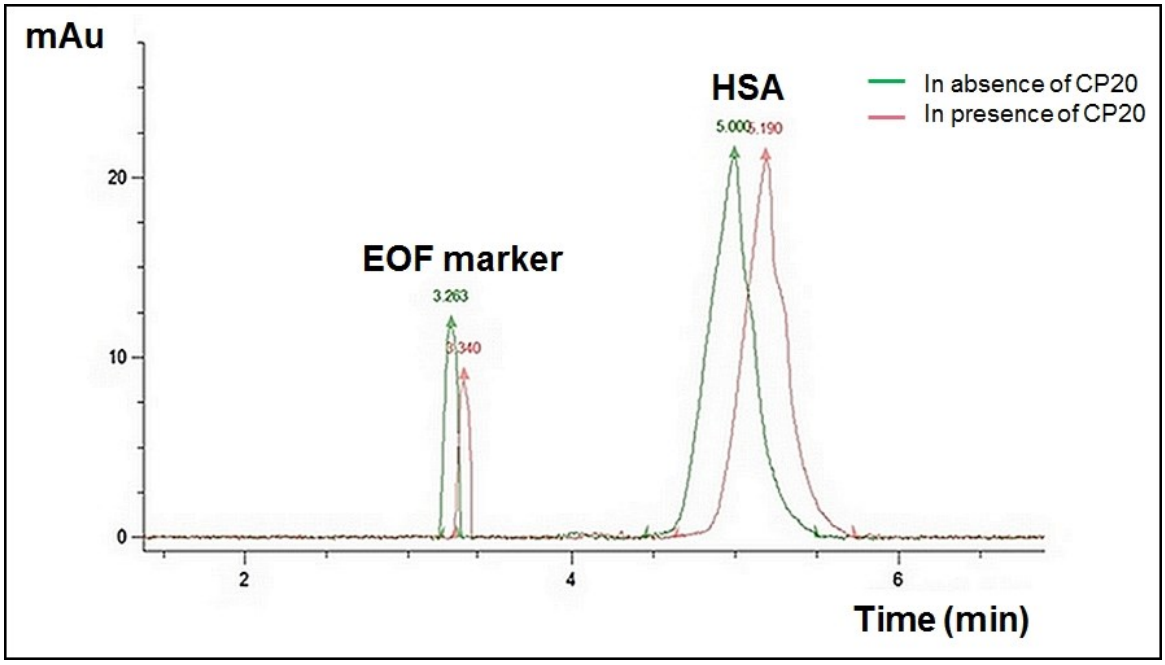

Fig. 37. mACE electropherogram for HSA and acetanilide (EOF marker) in the presence (green) and absence of CP20 (red).

The HSA mobility ratio (R) was calculated according to the relationship R = t_{eof}/t_{prot}, in which t_{eof} and t_{prot} were the migration times for the EOF marker (acetanilide) and HSA, respectively. These mobilities were calculated in the absence of CP20 and represented as R_f and R_i ratios. The binding constant was calculated using nonlinear regression as shown in Fig. 38. Moreover, R_c ratios were calculated at the saturated protein concentrations at which a protein's mobility did not change with an increase in the drug concentration. The binding constant was estimated as $LogK_a$ = 4.4 ± 0.54, and all measurements were obtained in triplicate.

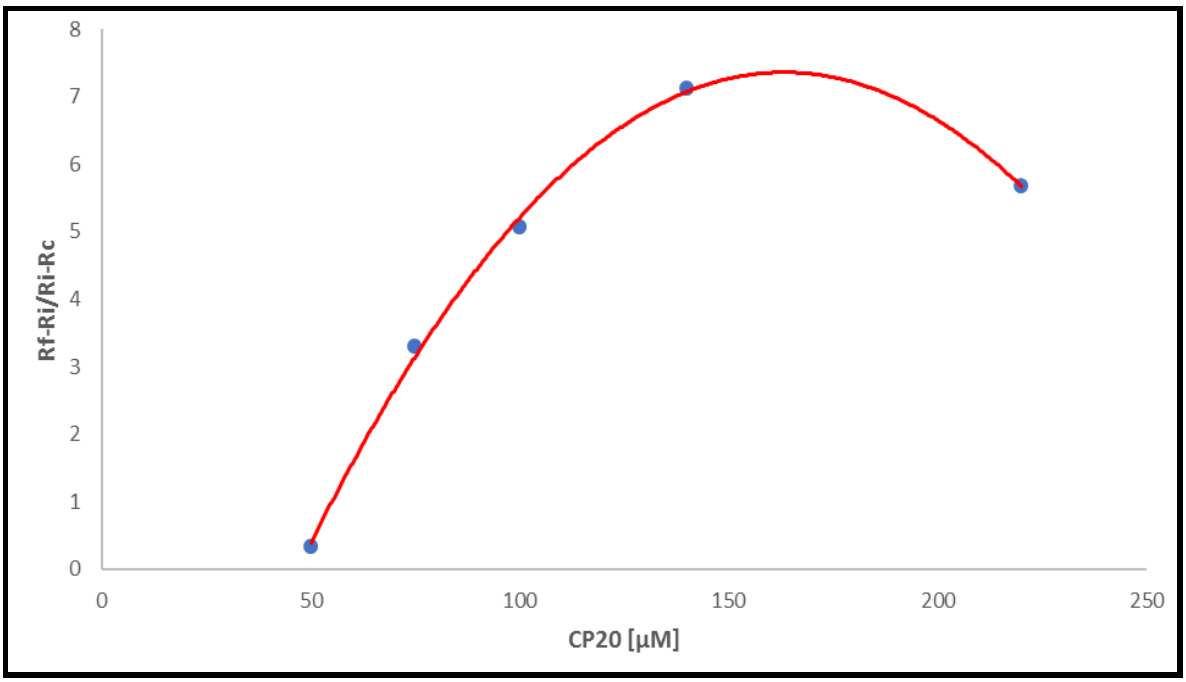

Fig. 38. Binding isotherm for the CP20-HSA interaction obtained in the mACE mode.

4.3.2. Deferiprone-human lactoferrin interaction studies

4.3.2.1. MST method

The MST method has been implemented successfully to quantify binding between CP20 and Lf. A challenging point for quantifying binding using CE-based methods was strong protein adsorption to the capillary wall. This problem has previously been reported [137]; therefore, Lf is usually separated under micellar electrokinetic chromatography (MECK) conditions. This method was conducted using surfactant additives. This approach could interfere with its interacting partners, especially Lf, because it is a highly positively charged molecule at physiological pH, at which nonspecific interactions could occur. The MST method is considered noninvasive and capable of quantifying the binding parameters under similar native conditions. During MST scanning, Lf exhibited extremely strong fluorescence signals in comparison to those of HSA, which might be attributable to the number of tryptophan residues because Lf contains nine tryptophans, versus only one in HSA. Therefore, the proper concentration for obtaining sufficient fluorescence signals was 120 nM, which was selected as the fixed Lf concentration in the role of the fluorescent partner. Conversely, CP20 was prepared at different concentrations in the range of 7 nM to 250 µM. The MST data was fit with the K_d model. The binding isotherm is shown in Fig. 39.

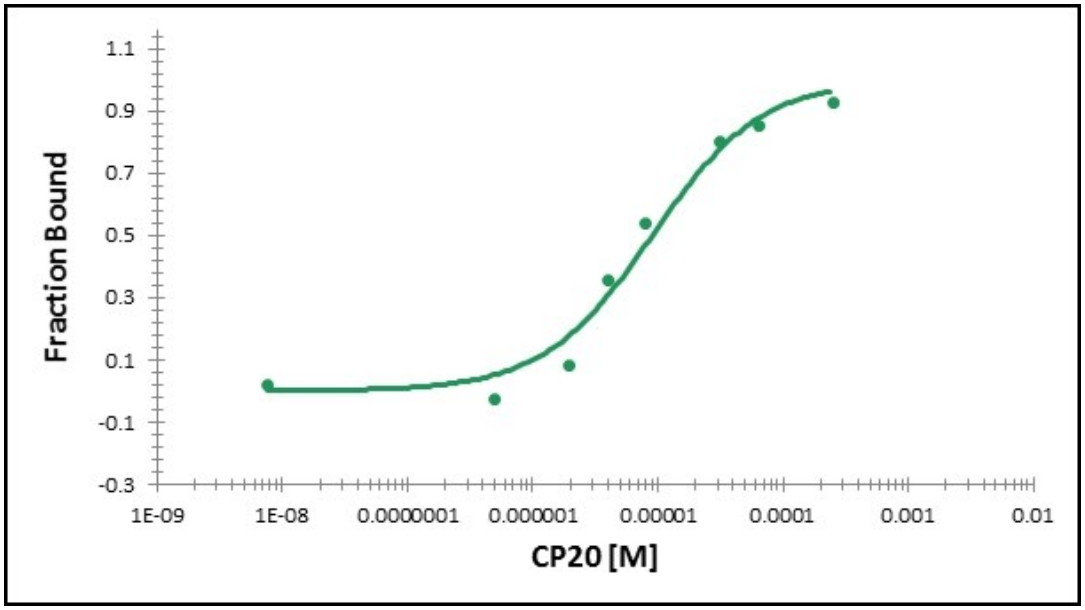

Fig. 39. The binding curve of the CP20-Lf interaction using the MST method.

4.3.3. Discussion of deferiprone-protein interactions

The CP20-HSA interaction was previously investigated via spectroscopic techniques aided by molecular docking software [64]. Affinity-based CE approaches are widely used in drug-protein interaction studies. In addition, the unique MST technique has gained popularity for use in characterizing biomolecular interactions. Therefore, the MST and CE techniques were used to investigate CP20-protein interactions, and the results were compared with those obtained using previously reported methods. Regarding the present approaches, MST is considered a noninvasive method, and its experimental procedures are easier to implement than those of CE because CE optimization is required before obtaining binding measurements to ensure good reproducibility. However, the CE technique remains a powerful technique for characterizing binding parameters because of the presence of several CE modes that can fit a wide range of binding systems. Moreover, more information, such as multi-equilibrium systems, binding stoichiometry, and equilibrium kinetics, could be obtained from affinity-based CE approaches.

In the first approach for characterizing CP20-HSA interactions, both methods were capable of estimating the binding constant. The MST-based result estimated the binding constant as $LogK_a$ = 4.3 ± 0.59, which is in greater agreement with the reported values obtained by Dorraji et al. ($LogK_a$ = 4.0 ± 0.004) than those obtained using CE approaches, which estimated the binding constants as $LogK_a$ = 5.3 ± 0.28 and 4.4 ± 0.54 for CE/FA and mACE modes, respectively. MST is superior to the CE technique with respect to analysis time, simple data processing, and simple optimization procedures, whereas CE/FA approaches introduce information about binding stoichiometry. In the CE approaches, the CE/FA and mACE modes are in agreement with each other, but the mACE value was closer to the reported value and the MST value. Repeatability was calculated as RSD% (<4.5) of the binding constant for three measurements (n = 3), whereas the repeatability of CE/FA expressed as the RSD% of the binding constant for the three measurements was <5.3%.

In the second approach, MST and CE were used to characterize the CP20-Lf interaction. CE approaches failed to determine Lf binding despite the use of several optimization procedures because of the high protein adsorption on the capillary wall. MST successfully determined the binding constant, which was estimated as $LogK_a$ = 5.0 ± 1.6. The success of the MST approach success might be attributable to its nature, which depends on the measurement of localized thermophoresis. MST is considered a good alternative technique for measuring binding events, especially under challenging conditions. The binding parameters for the CP20-protein interaction are summarized in Table 10.

Table 10. Binding parameters of CP20-protein interactions

Protein	Method	$LogK_a$	n_i	literature value
HSA	MST	4.3 ± 0.59	not possible	4.0 ± 0.004 [64]
	CE/FA	5.3 ± 0.28	3.2 ± 2.0	
	mACE	4.4 ± 0.54	not possible	
Lf	MST	5.0 ± 1.61	not possible	not reported

5. Summary

5.1. Deferiprone-metal ions separation and interaction studies

Once inside the human body, drugs can bind to several biomolecules, small molecules, or even metal ions. Therefore, the study of drug affinity for different targets have a key role in drug discovery and development. Moreover, all studies of drug pharmacokinetics/pharmacodynamics including drug transport, metabolism, excretion, and modulating biomolecular functions involve estimation of the binding properties of drug toward target biomolecules to improve the understanding to the behavior of drugs inside the body. In this context, CP20 remains an interesting therapeutic molecule that can be beneficial in several clinical situations in addition to β-thalassemia such as neurodegenerative diseases, cancers, and infectious diseases. In the past, the chromatographic profile of CP20 was extremely poor because of several technical challenges related to the characterization of drug separation. Moreover, previously developed chromatographic methods are inadequate for separating CP20 from its iron (III) complex. Conversely, CE-based methods were not described. Therefore, LC/MS and CE/FA methods were developed for the separation and concurrent determination of free CP20 and the $Fe(CP20)_3$ complex in one run as well as characterizing drug-metal interactions. In LC/MS approaches, the drug was determined and separated from the complex using a monolithic column and nonlinear gradient elution order, which are critical for the separation of two overlapping peaks. Moreover, the MS detector was used to study complex formation under the optimal conditions. Subsequently, the CE/FA method was developed to determine CP20 and separate free CP20 from the $Fe(CP20)_3$ complex. The developed CE/FA method depends on the formation of a stable peak plateau for the free drug that can be differentiated from the complex peak plateau, which moves as a bulk in the capillary to achieve binding equilibrium during the separation. The binding constant and binding stoichiometry were estimated after achieving good separation for free CP20 using nonlinear least square regression, after which the binding values were compared with the published values. In a comparison between LC/MS and CE/FA as separative methods, LC/MS gives direct information about the binding stoichiometry via MS screening; however, CE/FA is a more stable and accurate system for estimating binding parameters, in agreement with prior studies. Overall, both methods achieve good separation with satisfactory validity.

Furthermore, for the interactions of CP20 with other essential metal ions that cannot be investigated using separative techniques, MST and ESI-MS methods were used to investigate these types of weak interactions. MST is a new technique that has been developed for characterizing molecular and biomolecular interactions in free solution. The interaction between CP20 and different essential divalent metal ions, including Cu^{2+}, Zn^{2+}, Co^{2+}, Ni^{2+}, Mn^{2+}, Mg^{2+}, and Ca^{2+}, in

addition to Fe^{3+}, has been studied using a label-free MST system. Whereas CP20 produces sufficient fluorescence signals under MST conditions, which was reported for the first time. Indeed, Cu^{2+} and Zn^{2+} exhibited greater tendencies to interact with CP20 among divalent metal ions, not as strong as that of Fe^{3+}. Although Cu^{2+} and Zn^{2+} have similar interaction activity under the optimal MST conditions, Zn^{2+} should be monitored during CP20 treatment because the amount of Zn^{2+} are much larger than Cu^{2+} and Zn^{2+} deficiency is more observable.

Meanwhile, Co^{2+} and Ni^{2+} display weak binding affinity for CP20, and no chelation effect for CP20 against these ions. Contrarily, Mg^{2+} and Ca^{2+} are the most abundant divalent essential metal ions in the body, and they are not affected by CP20 chelation, as confirmed by the MST and ESI-MS results. The MST and ESI-MS results revealed the partial selectivity of CP20 to more readily bind with Fe^{3+} than with other divalent essential metal ions, whereas Zn^{2+} and Cu^{2+} are more likely to be depleted *in vivo* during CP20 treatment.

5.2. Deferiprone-protein interaction studies

The interactions of CP20 with proteins have rarely been studied. Only one study described the interaction of CP20 with HSA. Meanwhile, study of the binding affinity of CP20 to different target biomolecules may provide valuable information regarding the pharmacokinetic/dynamics, therapeutic effect, and toxicity of CP20. Primarily, HSA has been selected as a predominant carrier protein in plasma. MST- and CE-based methods have been developed to investigate the interaction of CP20 with HSA. MST was successfully used to assess drug-metal interactions and additionally used to estimate binding parameters in comparison with published literature values. The MST label-free system was used depending on the intrinsic fluorescence of HSA and then successfully applied to estimate binding parameters. Meanwhile, CE-based approaches enabled good comparability with MST. The CE/FA mode was used to investigate binding parameters via the discrimination between free CP20 as a peak plateau separated from the large bulk macromolecule. Therefore, the binding constant and stoichiometry have been easily estimated. Conversely, the mACE mode measures the mobility of HSA in the presence and absence of CP20, and the binding constant has been estimated directly based on the different mobilities of one partner. According to the obtained results, MST was superior because of the short analysis time, low sample consumption, and easy optimization procedures. Moreover, MST enabled automated scanning for system diagnosis. All of the developed methods were capable of estimating the binding constant; however, the results of MST were in greater agreement with the reported values from the literature.

Subsequently, human Lf was selected as a target protein, and an experiment was designed to estimate the CP20-Lf interaction and evaluate the impact on drug secretion in breast milk as a protein-bound molecule during lactation. MST technique proved to be valuable in binding studies realm. In this study, MST was superior to CE methods and was capable of estimating binding parameters, While CE methods have been failed to determine Lf protein because of strong protein adsorption to the capillary wall. The strong binding affinity between CP20 and Lf as shown in MST results reveals that CP20 secretion in breast milk can be predicted.

6. References

[1] V. Marina, G. Crisponi, J.I. Lachowicz, S. Medici, M. Peana, M. Antonietta, Chemical features of in use and in progress chelators for iron overload, J. Trace Elem. Med. Biol. 38 (2016) 10–18.

[2] W.O. Nelson, T.B. Karpishin, S.J. Rettig, C. Orvig, Physical and structural studies of N -substituted-3-hydroxy-2-methyl-4(1 H)-pyridinones, Can. J. Chem. 66 (1988) 123–131.

[3] P.S. Dobbin, R.C. Hider, Iron chelation therapy, Chem. Br. (1990) 565–568.

[4] G.J. Kontoghiorghes, M.B. Agarwal, P. Tondury, M.J. Kersten, M. Jaeger, G. Vreugdenhil, A. Vania, Y.E. Rahman, Future of oral iron chelator deferiprone (L1), TheLancet. 341 (1993) 1479–1480.

[5] E.M.A. Website, Ferriprox-EMEA/H/C/000236 - IB/0126/G, (2009). https://www.ema.europa.eu/en/medicines/human/EPAR/ferriprox#overview-section (accessed August 15, 2017).

[6] FDA website, Ferriprox, (2011). https://www.accessdata.fda.gov/drugsatfda_docs/label/2011/021825lbl.pdf (accessed August 15, 2017).

[7] C. Malaventura, L. Prossomariti, V. Caruso, M.C. Putti, P. Cianciulli, A. Meloni, L. Pitrolo, A. Pepe, M. Capra, A. Quarta, M.G. Bisconte, V. Positano, M. Lombardi, M. Missere, G. Rossi, A. Filosa, A. Maggio, M.A. Romeo, A. Lippi, M. Midiri, Deferasirox, deferiprone and desferrioxamine treatment in thalassemia major patients: cardiac iron and function comparison determined by quantitative magnetic resonance imaging, Haematologica. 96 (2010) 41–47.

[8] C. Vermylen, What is new in iron overload?, Eur. J. Pediatr. 167 (2008) 377–381.

[9] E.T. Clarke, A.E. Martell, Stabilities of 1,2-dimethyl-3-hydroxy-4-pyridinone chelates of divalent and trivalent metal ions, Inorganica Chim. Acta. 191 (1992) 57–63.

[10] I. Pashalidis, G.J. Kontoghiorghes, Competition studies of L1-deferiprone with copper and iron. Possible implications on efficacy, toxicity and new therapeutic applications, Transfus. Sci. 23 (2000) 259–261.

[11] M.A. Santos, S.M. Marques, S. Chaves, Hydroxypyridinones as “ privileged ” chelating structures for the design of medicinal drugs, 256 (2012) 240–259.

[12] V.M. Nurchi, G. Crisponi, T. Pivetta, M. Donatoni, M. Remelli, Potentiometric, spectrophotometric and calorimetric study on iron(III) and copper(II) complexes with 1,2-dimethyl-3-hydroxy-4-pyridinone, J. Inorg. Biochem. 102 (2008) 684–692.

[13] R.J. Motekaitis, A.E. Martell, Stabilities of the iron (III) chelates of 1 , 2-dimethyl-3-hydroxy-4-pyndinone and related ligands, 183 (1991) 71–80.

[14] C.N. Kontoghiorghe, A. Kolnagou, G.J. Kontoghiorghes, Potential clinical applications of chelating drugs in diseases targeting transferrin-bound iron and other metals, Expert Opin. Investig. Drugs. 22 (2013) 591–618.

[15] G. Crisponi, M. Remelli, Iron chelating agents for the treatment of iron overload, Coord. Chem. Rev. 252 (2008) 1225–1240.

[16] R. Hider, Recent developments centered on orally active iron chelators, Thalass. Reports. 4 (2014) 19–27.

[17] N. Birch, X. Wang, H.-S. Chong, Iron chelators as therapeutic iron depletion agents, Expert Opin. Ther. Pat. 16 (2006) 1533–1556.

[18] J.A.B. Balfour, R.H. Foster, D. Ematologia, C. Trapianti, M. Osseo, A. V Hoffbrand, R.F. Hospital, G. Koren, D. Clinical, A Review of its Clinical Potential in Iron Overload in β - Thalassaemia Major and Other Transfusion-Dependent Diseases, 58 (1999) 553–578.

[19] L.D. Devanur, H. Neubert, R.C. Hider, The Fenton Activity of Iron (III) in the Presence of Deferiprone, 97 (2008) 1454–1467.

[20] Y. Yu, E. Gutierrez, Z. Kovacevic, F. Saletta, P. Obeidy, Y. Suryo Rahmanto, D. R. Richardson, Iron Chelators for the Treatment of Cancer, Curr. Med. Chem. 19 (2012) 2689–2702.

[21] S. Veeraperumal, I.S. Serganova, R. V Simões, J. Varshavsky, R.G. Blasberg, E. Ackerstaff, J.A. Koutcher, Inhibition of prostate cancer proliferation by Deferiprone, NMR Biomed. 30 (2017) 1–11.
[22] M. Hoque, M.R. Jain, D.S. Heller, H. Li, B. Cracchiolo, M. Elisabeth, Blocking eIF5A Modi fi cation in Cervical Cancer Cells Alters the Expression of Cancer-Related Genes and Suppresses Cell Proliferation, 74 (2014) 552–563.
[23] C.E. Cicero, G. Mostile, R. Vasta, V. Rapisarda, S. Santo, M. Ferrante, M. Zappia, A. Nicoletti, Metals and neurodegenerative diseases . A systematic review, Environ. Res. 159 (2017) 82–94.
[24] G. Grolez, C. Moreau, B. Sablonnière, G. Garçon, J. Devedjian, S. Meguig, P. Gelé, C. Delmaire, R. Bordet, L. Defebvre, I.Z. Cabantchik, Ceruloplasmin activity and iron chelation treatment of patients with Parkinson ' s disease, BMC Neurol. 15 (2015) 2–7.
[25] A. Martin-bastida, R.J. Ward, R. Newbould, P. Piccini, C. Kabba, M.C. Patel, M. Spino, J. Connelly, R.R. Crichton, D.T. Dexter, Brain iron chelation by deferiprone in a phase 2 randomised double- blinded placebo controlled clinical trial in Parkinson ' s disease, Sci. Rep. 7 (2017) 1–9.
[26] N. Boddaert, K. Hanh, L. Quan, A. Leroy-willig, S. Gallet, F. Brunelle, D. Sidi, J. Thalabard, A. Munnich, Z.I. Cabantchik, Selective iron chelation in Friedreich ataxia : biologic and clinical implications, 110 (2019) 401–409.
[27] S. V Shah, ffect of deferiprone, an oral iron chelator, in diabetic and E non-diabetic glomerular disease, 23 (2013) 5–10.
[28] Y.W. Lai, L.T. Campbell, M.R. Wilkins, C.N.I. Pang, S. Chen, D.A. Carter, Synergy and antagonism between iron chelators and antifungal drugs in Cryptococcus, Int. J. Antimicrob. Agents. 48 (2016) 388–394.
[29] K.A. Zarember, A.R. Cruz, C.Y. Huang, J.I. Gallin, Antifungal activities of natural and synthetic iron chelators alone and in combination with azole and polyene antibiotics against Aspergillus fumigatus, Antimicrob. Agents Chemother. 53 (2009) 2654–2656.
[30] D. Saxena, M. Spino, F. Tricta, J. Connelly, B.M. Cracchiolo, A.R. Hanauske, D. D'Alliessi Gandolfi, M.B. Mathews, J. Karn, B. Holland, M.H. Park, T. Pe'ery, P.E. Palumbo, H.M. Hanauske-Abel, Drug-based lead discovery: The novel ablative antiretroviral profile of deferiprone in HIV-1-infected cells and in HIV-infected treatment-naive subjects of a double-blind, placebo-controlled, randomized exploratory trial, PLoS One. 11 (2016) 1–45.
[31] G.J. Kontoghiorghes, New concepts of iron and aluminium chelation therapy with Oral L1 (deferiprone) and other chelators: A review, Analyst. 120 (1995) 845–851.
[32] M. Blanuša, L. Prester, V.M. Varnai, D. Pavlović, K. Kostial, M.M. Jones, P.K. Singh, Chelation of aluminium by combining DFO and L1 in rats, Toxicology. 147 (2000) 151–156.
[33] R.A. Yokel, K.A. Meurer, C.B. Hong, K.M. Dickey, T.L. Skinner, A.M. Fredenburg, Short-term oral 3-hydroxypyridin-4-one dosing increases aluminum excretion and partially reverses aluminum-induced toxicity in the rabbit independent of chelator lipophilicity, Drug Metab. Dispos. 25 (1997) 182–190.
[34] M. Gómez, J.L. Esparza, J.L. Domingo, P.K. Singh, M.M. Jones, Comparative aluminium mobilizing actions of deferoxamine and four 3-hydroxypyrid-4-ones in aluminium-loaded rats, Toxicology. 130 (1998) 175–181.
[35] M. Gomez, J.L. Esparza, J.L. Domingo, J. Corbellal, P.K. Singh, M.M. Jones, Aluminium Distribution and Excretion: A Comparative study of a number of chelating agents in rats, Pharmacol. Toxicol. 82 (1998) 295–300.
[36] P. Liu, Y.N. Yao, S. De Wu, H.J. Dong, G.C. Feng, X.Y. Yuan, The efficacy of deferiprone on tissues aluminum removal and copper, zinc, manganese level in rabbits, J. Inorg. Biochem. 99 (2005) 1733–1737.
[37] K.H. Maclean, J.L. Cleveland, J.B. Porter, Cellular zinc content is a major determinant

of iron chelator-induced apoptosis of thymocytes, Blood. 98 (2001) 3831–3839.
[38] E. Erdoğan, D. Canatan, A.R. Örmeci, H. Vural, F. Aylak, The effects of chelators on zinc levels in patients with thalassemia major, J. Trace Elem. Med. Biol. 27 (2013) 109–111.
[39] S. Bartakke, S.B. Bavdekar, P. Kondurkar, M.N. Muranjan, M. V Manglani, R. Sharma, Effect of deferiprone on urinary zinc excretion in multiply transfused children with thalassemia major., Indian Pediatr. 42 (2005) 150–4.
[40] J.A. Barman Balfour, R.H. Foster, Deferiprone: a review of its clinical potential in iron overload in beta-thalassaemia major and other transfusion-dependent diseases, Drugs. 58 (1999) 553–578.
[41] S.S. Jamuar, A.H.M. Lai, Safety and efficacy of iron chelation therapy with deferiprone in patients with transfusion-dependent thalassemia, Ther. Adv. Hematol. 3 (2012) 299–307.
[42] M.A. Mashhadi, Copper status in patients with thalassemia major in Zahedan, Iran, Int. J. Hematol. Stem Cell Res. 7 (2013) 20–23.
[43] H. Haraguchi, Metallomics as integrated biometal science, 19 (2004) 5–14.
[44] G.J. Kontoghiorghes, Comparative efficacy and toxicity of desferrioxamine, deferiprone and other iron and aluminium chelating drugs, Toxicol. Lett. 80 (1995) 1–18.
[45] V. Eybl, D. Kotyzová, M. Kolek, J. Koutenský, P. Nielsen, The influence of deferiprone (L1) and deferoxamine on iron and essential element tissue level and parameters of oxidative status in dietary iron-loaded mice, Toxicol. Lett. 128 (2002) 169–175.
[46] A.S. Saljooghi, S.J.A. Fatemi, Clinical evaluation of Deferasirox for removal of cadmium ions in rat, BioMetals. 23 (2010) 707–712.
[47] S. Tubafard, S. Fatemi, Chelation of bismuth by combining desferrioxamine and deferiprone in rats, Toxicol. Ind. Health. 24 (2008) 235–240.
[48] M. Iranmanesh, S.J.A. Fatemi, M.R. Golbafan, F. Dahooee Balooch, Treatment of mercury vapor toxicity by combining deferasirox and deferiprone in rats, BioMetals. 26 (2013) 783–788.
[49] S. Tubafard, S.J. Fatemi, A.S. Saljooghi, M. Torkzadeh, Removal of vanadium by combining desferrioxamine and deferiprone chelators in rats, Med. Chem. Res. 19 (2010) 854–863.
[50] F.D. Balooch, S.J. Fatemi, M. Iranmanesh, Combined chelation of lead (II) by deferasirox and deferiprone in rats as biological model, BioMetals. 27 (2014) 89–95.
[51] M. Iranmanesh, S.J.A. Fatemi, R. Ebrahimpour, F. Dahooee Balooch, Chelation of chromium(VI) by combining deferasirox and deferiprone in rats, BioMetals. 26 (2013) 465–471.
[52] M. Sooriyaarachchi, J. Gailer, Removal of Fe3+ and Zn2+ from plasma metalloproteins by iron chelating therapeutics depicted with SEC-ICP-AES, Dalt. Trans. 39 (2010) 7466–7473.
[53] G.J. Kontoghiorghes, Iron mobilization from transferrin and non-transferrin-bound-iron by deferiprone. Implications in the treatment of thalassemia, anemia of chronic disease, cancer and other conditions., Hemoglobin. 30 (2006) 183–200.
[54] E.N. Baker, H.M. Baker, A structural framework for understanding the multifunctional character of lactoferrin, Biochimie. 91 (2009) 3–10. doi:10.1016/j.biochi.2008.05.006.
[55] H. Jenssen, R.E.W. Hancock, Antimicrobial properties of lactoferrin, Biochimie. 91 (2009) 19–29.
[56] P.P. Ward, E. Paz, O.M. Conneely, Multifunctional roles of lactoferrin: A critical overview, Cell. Mol. Life Sci. 62 (2005) 2540–2548.
[57] G. Kamalinia, F. Khodagholi, F. Atyabi, M. Amini, F. Shaerzadeh, M. Sharifzadeh, R. Dinarvand, Enhanced brain delivery of deferasirox-lactoferrin conjugates for iron chelation therapy in neurodegenerative disorders: In vitro and in vivo studies, Mol. Pharm. 10 (2013) 4418–4431.

[58] D. Chakraborty, M. Bhattacharyya, Deferiprone (L1) induced conformation change of hemoglobin: A fluorescence and CD spectroscopic study., Mol. Cell. Biochem. 204 (2000) 17–20.
[59] N. Sattarahmady, H. Heli, A.A. Moosavi-Movahedi, K. Karimian, Deferiprone: Structural and functional modulating agent of hemoglobin fructation, Mol. Biol. Rep. 41 (2014) 1723–1729.
[60] N. Sattarahmady, H. Heli, A.A. Moosavi-Movahedi, K. Karimian, N. Positioning, Nucleosome Positioning is to be released in Spring 2010 . The Effects of Deferiprone and Deferasirox on the Structure and Function of b -Thalassemia Hemoglobin, Mol. Biol. Rep. 41 (2014) 1723–1729.
[61] S. Agatonovic-Kustrin, D.W. Morton, L. Truong, S. Razic, Molecular Structural Characteristics Important in Drug-HSA Binding, Comb. Chem. High Throughput Screen. 17 (2015) 879–890.
[62] K. Vuignier, J. Schappler, J.-L. Veuthey, P.-A. Carrupt, S. Martel, Drug–protein binding: a critical review of analytical tools, Anal. Bioanal. Chem. 398 (2010) 53–66.
[63] G. Fanali, A. Di Masi, V. Trezza, M. Marino, M. Fasano, P. Ascenzi, Human serum albumin: From bench to bedside, Mol. Aspects Med. 33 (2012) 209–290.
[64] M.S.S. Dorraji, V.P. Azar, M.H. Rasoulifard, Interaction between deferiprone and human serum albumin : Multi-spectroscopic , electrochemical and molecular docking methods, Eur. J. Pharm. Sci. 64 (2014) 9–17.
[65] J.G. Goddard, G.J. Kontoghiorghes, Development of an HPLC method for measuring orally administered 1-substituted 2-alkyl-3hydroxypyrid-4-one iron chelators in biological fluids, Clin. Chem. 36 (1990) 5–8.
[66] J. Klein, L.A. Damani, D. Chung, O. Epemoulu, N. Olivieri, G. Koren, A High-performance liquid chromatographic method for the measurement of the Iron chelator 1,2-dimethyl-3-hydroxypyridin-4-one in human plasma, 13 (1991) 51–54.
[67] R.O. Epemolu, S. Singh, R.C. Hider, L.A. Damani, Chromatography of 3-hydroxypyridin-4-ones: novel orally active iron chelators, J. Chromatogr. A. 519 (1990) 171–178.
[68] A. El-Jammal, D.M. Templeton, Reversed-phase high-performance liquid chromatography of non-transferrin-bound iron and some hydroxypyridone and hydroxypyrone chelators, J. Chromatogr. B Biomed. Sci. Appl. 658 (1994) 121–127.
[69] B. Dresow, R. Fischer, G.E. Janka, E.E. Gabbc, M. Biochemie, P. Chemie, U. Eppendorf, HPLC-based measurement of the chelator 1,2-dimethyl-3-hydroxy-pyrid-4-one (L1) and Its Iron Complex for Pharmacokinetic Studies in Humans, 352 (1995) 562–564.
[70] T.S. Song, Y.W. Hsieh, C.T. Peng, C.H. Liu, T.L. Chen, M.J. Hour, Development of a fast LC-MS/MS assay for the determination of deferiprone in human plasma and application to pharmacokinetics, Biomed. Chromatogr. 26 (2012) 1575–1581.
[71] H.J. Lin, H.S. Kou, S.S. Chiou, S.M. Wu, Therapeutic deferoxamine and deferiprone monitoring in β-thalassemia patients' plasma by field-amplified sample injection and sweeping in capillary electrophoresis, Electrophoresis. 37 (2016) 2091–2096.
[72] M.J. Keith-Roach, A review of recent trends in electrospray ionisation-mass spectrometry for the analysis of metal-organic ligand complexes, Anal. Chim. Acta. 678 (2010) 140–148.
[73] S.H. Hansen, HPLC/UHPLC, in: T. Müllertz, A., Perrie, Y., & Rades (Ed.), Anal. Tech. Pharm. Sci. Adv. Deliv. Sci. Technol., 1st ed., Springer US, New York, 2016: pp. 413–437.
[74] P.R. Haddad, P.N. Nesterenko, W. Buchberger, Recent developments and emerging directions in ion chromatography, J. Chromatogr. A. 1184 (2008) 456–473.
[75] R.C.F. Cheung, J.H. Wong, T.B. Ng, Immobilized metal ion affinity chromatography: A review on its applications, Appl. Microbiol. Biotechnol. 96 (2012) 1411–1420.
[76] S. Fekete, J. Veuthey, D. Guillarme, Journal of Pharmaceutical and Biomedical Analysis

New trends in reversed-phase liquid chromatographic separations of therapeutic peptides and proteins : Theory and applications, J. Pharm. Biomed. Anal. 69 (2012) 9–27.
[77] V.R. Meyer, J. Wiley, Practical High-Performance Liquid Chromatography, 4th ed., John Wiley & Sons, 2004.
[78] J.J. Pitt, Principles and Applications of Liquid Chromatography- Mass Spectrometry in Clinical Biochemistry, Clin. Biochem. Rev. 30 (2009) 19–34.
[79] W.A. Korfmacher, Principles and applications of LC – MS in new drug discovery, Drug Discov. Today. 10 (2005) 1357–1367.
[80] U. Leurs, U.H. Mistarz, K.D. Rand, Applications of mass spectrometry in drug development science, in: T. (Eds.). Müllertz, A., Perrie, Y., & Rades (Ed.), Anal. Tech. Pharm. Sci., 1st ed., Springer US, New York, 2016: pp. 253–288.
[81] M. Holˇ, R. Jirásko, M. Lísa, Recent developments in liquid chromatography – mass spectrometry and related techniques, J. Chromatogr. A. 1259 (2012) 3–15.
[82] L. Suntornsuk, Recent advances of capillary electrophoresis in pharmaceutical analysis, Anal. Bioanal. Chem. 398 (2010) 29–52.
[83] J. Østergaard, S.W. Larsen, H. Jensen, Capillary-Based Techniques for Physical-Chemical Characterization of Drug Substances and Drug Delivery Systems, in: T. (Eds. . Müllertz, A., Perrie, Y., & Rades (Ed.), Anal. Tech. Pharm. Sci. Adv. Deliv. Sci. Technol., 1st ed., Springer US, New York, 2016: pp. 439–465.
[84] A. Weston, P.R. Brown, Separations in Capillary electrophoresis, in: HPLC CE, Elsevier, 1997: pp. 154–184.
[85] H. Whatley, Basic Principles and Modes of Capillary Electrophoresis, in: H. Petersen, J. R., Mohammad, A. A., & Whatley (Ed.), Clin. Forensic Appl. Capill. Electrophor., 1st ed., Humana Press, Totowa, NJ, 2003: pp. 21–58.
[86] N.W. Frost, M. Jing, M.T. Bowser, Capillary Electrophoresis, Anal. Chem. 82 (2010) 4682–4698.
[87] P.R. Haddad, Joule heating effects and the experimental determination of temperature during CE, Electrophoresis. 30 (2009) 897–909.
[88] N.H.H. Heegaard, Review Applications of affinity interactions in capillary electrophoresis, Electrophoresis. 24 (2003) 3879–3891.
[89] L. Michalcová, Z. Glatz, Comparison of various capillary electrophoretic approaches for the study of drug–protein interaction with emphasis on minimal consumption of protein sample and possibility of automation†, J. Sep. Sci. 38 (2015) 325–331.
[90] L. Michalcová, Z. Glatz, Study on the interactions of sulfonylurea antidiabetic drugs with normal and glycated human serum albumin by capillary electrophoresis-frontal analysis, J. Sep. Sci. 39 (2016) 3631–3637.
[91] H. Olabi, Mais, Stein Matthias, Wätzig, Affinity capillary electrophoresis for studying interactions in life sciences, Methods. 146 (2018) 76–92.
[92] J. Østergaard, S.H. Hansen, H. Jensen, A.E. Thomsen, Pre-equilibrium capillary zone electrophoresis or frontal analysis : Advantages of plateau peak conditions in affinity capillary electrophoresis, Electrophoresis. 26 (2005) 4050–4054.
[93] J. Østergaard, N.H.H. Heegaard, Review Capillary electrophoresis frontal analysis : Principles and applications for the study of drug-plasma protein binding, 24 (2003) 2903–2913.
[94] D.W. Armstrong, Use of CE for the determination of binding constants, Electrophoresis. 31 (2010) 17–27.
[95] K.L. Rundlett, D.W. Armstrong, Review Methods for the determination of binding constants by capillary electrophoresis, 22 (2001) 1419–1427.
[96] D. El-Hady, S. Kühne, N. Abo El Maali, H. Wätzig, Precision in affinity capillary electrophoresis for drug-protein binding studies, J. Pharm. Biomed. Anal. 52 (2010) 232–241.

[97] C. Qian, K.A. Kovalchik, M.S. Maclennan, X. Huang, D.D.Y. Chen, Mobility-based correction for accurate determination of binding constants by capillary electrophoresis-frontal analysis, Electrophoresis. 38 (2017) 1572–1581.
[98] K. Vuignier, J. Schappler, J. Veuthey, P. Carrupt, S. Martel, Improvement of a capillary electrophoresis / frontal analysis (CE / FA) method for determining binding constants : Discussion on relevant parameters, J. Pharm. Biomed. Anal. 53 (2010) 1288–1297.
[99] S. Ohlson, M.-D. Duong-Thi, Emerging Technologies for Fragment Screening, in: D.A.E. and W. Jahnke (Ed.), Fragm. Drug Discov. Lessons Outlook, 1st ed., Wiley-VCH Verlag, kGaA, 2016: pp. 173–195.
[100] S.A.I. Seidel, P.M. Dijkman, W.A. Lea, G. van den Bogaart, M. Jerabek-Willemsen, A. Lazic, J.S. Joseph, P. Srinivasan, P. Baaske, A. Simeonov, I. Katritch, F.A. Melo, J.E. Ladbury, G. Schreiber, A. Watts, D. Braun, S. Duhr, Microscale thermophoresis quantifies biomolecular interactions under previously challenging conditions, Methods. 59 (2013) 301–315.
[101] H.J. Keh, S.H. Chen, Particle interactions in thermophoresis, Chem. Eng. Sci. 50 (1995) 3395–3407.
[102] E.E. Michaelides, Brownian movement and thermophoresis of nanoparticles in liquids, Int. J. Heat Mass Transf. 81 (2015) 179–187.
[103] J. Anderson, Colloid Transport By Interfacial Forces, Annu. Rev. Fluid Mech. 21 (1989) 61–99.
[104] J. Stejskal, M. Trchová, I.A. Ananieva, J. Janča, J. Prokeš, S. Fedorova, I. Sapurina, Poly(aniline-co-pyrrole): Powders, films, and colloids. Thermophoretic mobility of colloidal particles, Synth. Met. 146 (2004) 29–36.
[105] D. Braun, A. Libchaber, Trapping of DNA by Thermophoretic Depletion and Convection, Phys. Rev. Lett. 89 (2002) 1881031–4.
[106] S. Duhr, D. Braun, Optothermal Molecule Trapping by Opposing Fluid Flow with Thermophoretic Drift, 038103 (2006) 1–4.
[107] R. Piazza, B. Triulzi, D. Fisica, Thermophoresis as a probe of particle-solvent interactions: The case of protein solutions, Phys. Chem. Chem. Phys. 6 (2004) 1616–1622.
[108] S. Iacopini, R. Piazza, Thermophoresis in protein solutions, Europhys. Lett. 63 (2007) 247–253.
[109] S. Duhr, D. Braun, Why molecules move along a temperature gradient, Proc. Natl. Acad. Sci. 103 (2006) 19678–19682.
[110] P. Reineck, C.J. Wienken, D. Braun, Thermophoresis of single stranded DNA, Electrophoresis. 31 (2010) 279–286.
[111] C.J. Wienken, P. Baaske, U. Rothbauer, D. Braun, S. Duhr, Protein-binding assays in biological liquids using microscale thermophoresis, Nat Commun. 1093 (2010) 1–7.
[112] S. Lippok, S.A.I. Seidel, S. Duhr, K. Uhland, H.-P. Holthoff, D. Jenne, D. Braun, Direct detection of antibody concentration and affinity in human serum using microscale thermophoresis., Anal. Chem. 84 (2012) 3523–30.
[113] C.C. Lin, F.A. Melo, R. Ghosh, K.M. Suen, L.J. Stagg, J. Kirkpatrick, S.T. Arold, Z. Ahmed, J.E. Ladbury, Inhibition of basal FGF receptor signaling by dimeric Grb2, Cell. 149 (2012) 1514–1524.
[114] A. Löf, J.P. Müller, M. Benoit, M.A. Brehm, Biophysical approaches promote advances in the understanding of von Willebrand factor processing and function, Adv. Biol. Regul. 63 (2017) 81–91.
[115] K. Zillner, M. Filarsky, K. Rachow, M. Weinberger, G. Längst, A. Németh, Large-scale organization of ribosomal DNA chromatin is regulated by Tip5, Nucleic Acids Res. 41 (2013) 5251–5262.
[116] T. Schubert, M.C. Pusch, S. Diermeier, V. Benes, E. Kremmer, A. Imhof, G. Längst, Df31 Protein and snoRNAs Maintain Accessible Higher-Order Structures of Chromatin,

Mol. Cell. 48 (2012) 434–444.
[117] M.E. Welsch, A. Kaplan, J.M. Chambers, M.E. Stokes, P.H. Bos, A. Zask, Y. Zhang, M. Sanchez-Martin, M.A. Badgley, C.S. Huang, T.H. Tran, H. Akkiraju, L.M. Brown, R. Nandakumar, S. Cremers, W.S. Yang, L. Tong, K.P. Olive, A. Ferrando, B.R. Stockwell, Multivalent Small-Molecule Pan-RAS Inhibitors, Cell. 168 (2017) 878-889.e29.
[118] M. Winiewska, E. Bugajska, J. Poznański, ITC-derived binding affinity may be biased due to titrant (nano)-aggregation. Binding of halogenated benzotriazoles to the catalytic domain of human protein kinase CK2, PLoS One. 0173260 (2017) 1–15.
[119] K.-E. Lillsunde, T. Tomašič, D. Kikelj, P. Tammela, Marine alkaloid oroidin analogues with antiviral potential: A novel class of synthetic compounds targeting the cellular chaperone Hsp90, Chem. Biol. Drug Des. 90 (2017) 1147–1154.
[120] G. Den Van Bogaart, K. Meyenberg, U. Diederichsen, R. Jahn, Phosphatidylinositol 4,5-bisphosphate increases Ca2+ affinity of synaptotagmin-1 by 40-fold, J. Biol. Chem. 287 (2012) 16447–16453.
[121] Y. Pang, W. Lan, X. Huang, G. Zuo, H. Liu, J. Zhang, Inhibition of ferric ion to oxalate oxidase shed light on the substrate binding site, BioMetals. 28 (2015) 861–868.
[122] M. Jerabek-Willemsen, C.J. Wienken, D. Braun, P. Baaske, S. Duhr, Molecular interaction studies using microscale thermophoresis., Assay Drug Dev. Technol. 9 (2011) 342–353.
[123] M. Jerabek-Willemsen, T. André, R. Wanner, H.M. Roth, S. Duhr, P. Baaske, D. Breitsprecher, MicroScale Thermophoresis: Interaction analysis and beyond, J. Mol. Struct. 1077 (2014) 101–113.
[124] J.M. Rainard, G.C. Pandarakalam, S.P. Mcelroy, Using Microscale Thermophoresis to Characterize Hits from High-Throughput Screening : A European Lead Factory Perspective, SLAS Discov. 23 (2018) 225–241.
[125] H. Wätzig, I. Oltmann-Norden, F. Steinicke, H.A. Alhazmi, M. Nachbar, D.A. El-Hady, H.M. Albishri, K. Baumann, T. Exner, F.M. Böckler, S. El Deeb, Data quality in drug discovery: The role of analytical performance in ligand binding assays, J. Comput. Aided. Mol. Des. 29 (2015) 847–865.
[126] E.C. Gaffarogullari, A. Krause, J. Balbo, D.-P. Herten, A. Jäschke, Microscale thermophoresis provides insights into mechanism and thermodynamics of ribozyme catalysis, RNA Biol. 10 (2013) 1815–1821.
[127] C. Entzian, T. Schubert, Studying small molecule-aptamer interactions using MicroScale Thermophoresis (MST), Methods. 97 (2016) 27–34.
[128] F. Syntia, R. Nehmé, B. Claude, P. Morin, Human neutrophil elastase inhibition studied by capillary electrophoresis with laser induced fluorescence detection and microscale thermophoresis, J. Chromatogr. A. 1431 (2016) 215–223.
[129] E. Fisher, Y. Zhao, R. Richardson, A.K. Buell, F.I. Aigbirhio, G. Toth, Detection and Characterization of Small Molecule Interactions with Fibrillar Protein Aggregates using Microscale Thermophoresis Detection and Characterization of Small Molecule Interactions with Fibrillar Protein Aggregates Using Microscale Thermophoresis, ACS Chem. Neurosci. 8 (2017) 2088–2095.
[130] T. Rogez-Florent, C. Foulon, A.S. Drucbert, N. Schifano, P. Six, S. Devassine, P. Depreux, P.M. Danzé, L. Goossens, C. Danel, J.F. Goossens, Chiral separation of new sulfonamide derivatives and evaluation of their enantioselective affinity for human carbonic anhydrase II by microscale thermophoresis and surface plasmon resonance, J. Pharm. Biomed. Anal. 137 (2017) 113–122.
[131] F. Immekus, L.J. Barandun, M. Betz, F. Debaene, S. Petiot, S. Sanglier-Cianferani, K. Reuter, F. Diederich, G. Klebe, Launching spiking ligands into a protein-protein interface: A promising strategy to destabilize and break interface formation in a tRNA modifying enzyme, ACS Chem. Biol. 8 (2013) 1163–1178.
[132] X. Wang, K. Corin, P. Baaske, C.J. Wienken, M. Jerabek-Willemsen, S. Duhr, D. Braun,

S. Zhang, Peptide surfactants for cell-free production of functional G protein-coupled receptors., Proc. Natl. Acad. Sci. U. S. A. 108 (2011) 9049–9054.
[133] G. Crisponi, V.M. Nurchi, M. Crespo-Alonso, G. Sanna, M.A. Zoroddu, G. Alberti, R. Biesuz, A speciation study on the perturbing effects of iron chelators on the homeostasis of essential metal ions, PLoS One. 10 (2015) 1–14.
[134] F.N. Al-Refaie, B. Wonke, D.G. Wickens, Y. Aydinok, A. Fielding, A. V. Hoffbrand, Zinc concentration in patients with iron overload receiving oral iron chelator 1,2-dimethyl-3-hydroxypyrid-4-one or desferrioxamine, J. Clin. Pathol. 47 (1994) 657–660.
[135] C. Queiros, M.J. Amorim, A. Leite, M. Ferreira, P. Gameiro, B. De Castro, K. Biernacki, A. Magalhães, J. Burgess, M. Rangel, Nickel(II) and cobalt(II) 3-hydroxy-4-pyridinone complexes: Synthesis, characterization and speciation studies in aqueous solution, Eur. J. Inorg. Chem. (2011) 131–140.
[136] Y. Xu, S. Redweik, D.A. El-Hady, H.M. Albishri, L. Preu, H. Wätzig, Precise, fast, and flexible determination of protein interactions by affinity capillary electrophoresis: Part 3: Anions, Electrophoresis. 35 (2014) 2203–2212.
[137] J. Li, X. Ding, Y. Chen, B. Song, S. Zhao, Z. Wang, Determination of bovine lactoferrin in infant formula by capillary electrophoresis with ultraviolet detection, J. Chromatogr. A. 1244 (2012) 178–183.

Curriculum Vitae

MUFARREH MOHAMMED M. ASMARI

nmufarreh@hotmail.com

20.11.1979

SAUDI ARABIA

Mobile: +966530189891

Work Address

Institute of Medicinal and Pharmaceutical chemistry
Technical University of Braunschweig
Beethoven Strasse, 55
38106 Braunschweig
Germany
Tel: 05313912273
m.asmari@tu-bs.de

Home Address

Rebenring 61, Zi. 413
38106 Braunschweig
Germany
Mobile: 017622574800

Permanent Address

King Khalid University
P.O.Box 4536
ABHA, 61412
Saudi Arabia
Tel: +966172417110

Education

2015 - 2019	PhD student at Institute of Medicinal and Pharmaceutical Chemistry, Technical University of Braunschweig, Germany.
2008-2012	M.Sc. (Pharmaceutical Analysis), Faculty of Pharmacy, King Saud University, Riyadh, Saudi Arabia.
1998-2003	B.Sc. (pharmaceutical sciences), Faculty of Pharmacy, King Saud University, Riyadh, Saudi Arabia

Academic career

2013 -2015	Vice dean at College of applied medical sciences/khamis mushait (King Khalid University)
2012-2013	Department head of basic medical science in College of applied medical sciences/khamis mushait (King Khalid University)
2007-2009	Clinical instructor at college of health science in ABHA (Ministry of Health)

Membership in professional associations

2006-present	Membership of Saudi pharmaceutical society
2010-2015	Membership of American society of mass spectrometry
2009-2014	Membership of International pharmaceutical federation

Professional honors & fellowships

2007	Fellowship program for the clinical instructors, (Ministry of Health), Saudi Araibia
2003	Honored as ideal student (Faculty of Pharmacy candidate) from King Saud University
2003	Honored as a leader for non-academic activities in Faculty of Pharmacy, King Saud University

Training courses & workshops

- Effective meeting workshop, Grade life program, 6th and 7th November 2017, Braunschweig
- Scientific integrity workshop, Grade life program, 18th and 19th December 2017, Braunschweig
- Basic chemometrics course, Euroanalysis 2017, 28th August 2017, Stockholm
- Robust CE method Course, Euroanalysis 2017, 28th August 2017, Stockholm
- Targeted metabolomics for biomarker discovery workshop, MHH, 2nd November 2016, Hannover
- Bioanalytics meeting, NanoTemper Technologies, 27th and 28th October 2016, Muncih
- Bioanalytics meeting, NanoTemper Technologies, 16th and 17th June 2016, Muncih
- Fundamentals of mass spectrometry course, ISC2014, 13 Septemper 2014, Salzburg
- Bases of chemical safety workshop, chemical safety program, 5th and 6th May 2013, Riyadh
- Strategic planning for the colleges workshop, Knig Khalid University, 13th Febreuary 2013, ABHA
- Cardiopulmonary resuscitation as BLS provider, training course, Saudi Hear Association, 2012, Saudi Arabia

List of Publications

Articles in Journals

1. Asmari M., Ratih R., Alhazmia H., El Deeb S., Thermophoresis for characterizing biomolecular interaction, ***Methods*** **(2018)**, *146*, 107-119.

   DOI: org/10.1016/j.ymeth.2018.02.003

2. Asmari M., Michalcova L., Alhazmi H., Zdenek G., El Deeb S., Investigation of deferiprone binding to different essential metal ions using microscale thermophoresis and electrospray ionization mass spectrometry, ***Michrochemical Journal*** **(2018)**, *137*, 98-104.

   DOI: org/10.1016/j.microc.2017.10.004

3. Al Bratty M., Alhazmi A. H., Javed A. S., Lalitha G. K., Asmari M., Wölker J., El Deeb S., Development and Validation of LC–MS/MS Method for Simultaneous Determination of Metformin and Four Gliptins in Human Plasma, ***Chromatographia*** **(2017)**, *80*, 891- 899.

   DOI: 10.1007/s10337-017-3288-0

Poster presentation

1. Asmari M., Ratih R., El Deeb S., Label-free microscale thermophoresis for the study of lactoferrin-drug interaction, Euroanalysis 2017 in Stockholm, 28 August -1 Septemper, 2017 **(Sweden)**.
2. Ratih R., Asmari M., Oner S., El Deeb S., Immobilization of Chondroitin Sulfate A into Monolithic Epoxy Column for Chiral Separation, HPLC 2017 in Prague, June 18-22, 2017 **(Czech Republic)**.
3. Michalcová L., Asmari M., Glatz Z., El Deeb S., Capillary Electrophoresis-Frontal Analysis for the characterization of drug-metal binding, CE-2016 in Berno, October 16-19, 2016 **(Czech Republic)**.
4. Asmari M., Kleusch C., El Deeb S., MicroScale thermophoretic investigation of deferiprone interaction with selected biometals, DPhG (German Association of Pharmacists) in Munich, October 4-7, 2016 **(in Germany)**.
5. Uzlu Z., Ule J., Ahmed F., Balaiev I., Asmari M., Eldeeb S., Investigation of deferiprone binding to zinc (II) and copper (II) ions for potential chelation effect using capillary zone electrophoresis, Internship scientific day TU Braunschweig, 10th May, 2016 **(Germany)**.
6. Asmari M., Alhazmi H., El Deeb S., LC-ESI-MS Study of Iron (III) Complexes with Deferiprone, Analytical Technology Europe in Vienna, March 15-18, 2016 **(Austria)**.
7. Asmari M., Alhazmi H., Wölker J., El Deeb S., LC-ESI-MS method development and validation for determination of five hypoglycemic agents in mixture using monolithic silica column, DPhG (German Association of Pharmacists) in Dusseldorf, September 23-25, 2015 **(Germany)**.